2016-12-01

Development of a Performance-Based Procedure for Assessment of Liquefaction-Induced Free-Field Settlements

Brian David Peterson
Brigham Young University

Development of a Performance-Based Procedure for Assessment of Liquefaction-Induced Free-Field Settlements

Brian David Peterson

A thesis submitted to the faculty of
Brigham Young University
in partial fulfillment of the requirements for the degree of

Master of Science

Kevin W. Franke, Chair
Kyle M. Rollins
W. Spencer Guthrie

Department of Civil and Environmental Engineering

Brigham Young University

ABSTRACT

Development of a Performance-Based Procedure for Assessment of
Liquefaction-Induced Free-Field Settlements

Brian David Peterson
Department of Civil and Environmental Engineering, BYU
Master of Science

Liquefaction-induced settlement can cause significant damage to structures and infrastructure in the wake of a seismic event. Predicting settlement is an essential component of a comprehensive seismic design. The inherent uncertainty associated with seismic events makes the accurate prediction of settlement difficult. While several methods of assessing seismic hazards exist, perhaps the most promising is performance-based earthquake engineering, a framework presented by the Pacific Earthquake Engineering Research (PEER) Center. The PEER framework incorporates probability theory to generate a comprehensive seismic hazard analysis. Two settlement estimation methods are incorporated into the PEER framework to create a fully probabilistic settlement estimation procedure. A seismic hazard analysis tool known as *PBLiquefY* was updated to include the fully probabilistic method described above. The goal of the additions to *PBLiquefY* is to facilitate the development of a simplified performance-based procedure for the prediction of liquefaction-induced free-field settlements.

Settlement estimations are computed using conventional deterministic methods and the fully probabilistic procedure for five theoretical soil profiles in 10 cities of varying seismicity levels. A comparison of these results suggests that deterministic methods are adequate when considering events of low seismicity but may result in a considerable under-estimation of seismic hazard when considering events of mid to high seismicity.

Key words: liquefaction, *PBLiquefY*, PEER, performance-based earthquake engineering, probabilistic, seismic hazard, settlement

ACKNOWLEDGEMENTS

I thank my advisor, Dr. Kevin Franke, for his encouragement and patience. He helped me to recognize my potential and introduced me to a field that I have grown to love dearly. Without his guidance and support, I would not be who I am today. I thank the members of my graduate committee, Dr. Kyle M. Rollins and Dr. W. Spencer Guthrie. They encouraged me to push myself beyond my comfort zone and provided valuable knowledge and suggestions during the completion of this work. I thank Dr. Norman L. Jones, who volunteered hours of tutoring and provided me with the necessary skills to complete my research.

I thank my fellow graduate students, bonded together by the confines of a closet office. Thank you, Levi Ekstrom and Kristin Ulmer. Thank you, Braden Error, Lucy Astorga, Jasmyn Harper, and Alex Arndt. Your friendship, support, and humor provided the relief I needed to endure the grind of graduate research.

Most of all, I thank my wife, Macey. You have supported me tirelessly throughout my graduate work and you have sacrificed so much to help me get here. You never wavered in your dedication to helping me accomplish my goals. You are my rock, and I love you.

TABLE OF CONTENTS

LIST OF TABLES

LIST OF FIGURES

1 INTRODUCTION

The settlement of soils resulting from seismically-induced liquefaction can cause devastation in the wake of an earthquake event. The most obvious potential danger of differential settlement is the severing of lifelines and utilities, resulting in large populations left without power and running water during a crisis. The 1906 San Francisco earthquake demonstrated this danger when, after the water lines were severed due to liquefaction effects, fires raged through the city for days, destroying homes and lives. Aside from the potential loss of life, settlement can have a devastating economic impact. Settlement can cause severe cracking in structures, rendering them uninhabitable. Roadways and railways can be damaged or destroyed, preventing the shipment of supplies and goods. In short, settlement poses a serious threat to the economic stability of a region affected by seismic activity.

Accurate prediction of seismic activity and its effects is essential to prevent the scenarios described above. The methods used to characterize seismic hazard and quantify the effects of seismic events (i.e., liquefaction) are constantly being improved and refined. Engineers most commonly use deterministic seismic hazard analysis (DSHA) (often through the use of pseudo-probabilistic methods) to predict seismic hazard. However, deterministic analyses can be insufficient in accounting for the inherent uncertainty associated with seismic events. Probabilistic seismic hazard analysis (PSHA) is able to account for the uncertainty associated with strong ground motions and provide a more complete understanding of seismic hazard.

Performance-based earthquake engineering (PBEE) methods allow engineers to incorporate probabilistic ground motions in the analysis of various seismic-related effects, and it provides significant advantages to seismic hazard prediction. Probabilistic or performance-based methods are not commonly used, however, because they are less familiar and more complicated to perform than conventional deterministic methods. In many cases, practicing engineers simply can not afford to take the time necessary to learn the complexities of probability theory. It has become evident that probabilistic methods must be simplified to be generally accepted in practice. This is accomplished through the creation of tools that make probabilistic methods accessible to all practicing professionals, regardless of their understanding of probability theory.

The quantification of the differences between deterministic and probabilistic methods is a key step in understanding the importance of transitioning to fully-probabilistic seismic hazard analysis (SHA). While studies have focused on performing quantified comparisons of different liquefaction effects (i.e., liquefaction triggering, lateral spread, etc.), no study has performed a quantified comparison of settlement.

There are two purposes of this study: first, to create a new performance-based procedure for the prediction of post-liquefaction free-field settlements and create an analysis tool to be used in the simplification process mentioned above; and, second, to explicitly quantify the discrepancies between the pseudo-probabilistic and fully-probabilistic methods of settlement estimation. This research is an important stepping stone in the process of the simplification of probabilistic post-liquefaction settlement estimations.

2 UNDERSTANDING LIQUEFACTION

2.1 Introduction

While settlement at the ground surface does not usually directly result in the loss of life, it can have significant economic repercussions. Settlement can cause considerable damage to structures with shallow foundations, utilities, and lifelines, especially those buried at shallow depths. The severing of lifelines (e.g., water, power, etc.) can result in increased damage and loss of life from aftermaths like fire, as seen in the 1906 San Francisco earthquake. Because the settlements under consideration in this study are the result of seismically-induced liquefaction, a review of liquefaction is provided in this chapter.

2.2 Liquefaction

Liquefaction is a complex effect of earthquake events. One of the reasons liquefaction is so difficult to understand is that it only first captured the attention of geotechnical engineers in 1964, when the Good Friday earthquake in Alaska (M_W=9.2) was followed closely by the Niigata earthquake (M_S=7.5) in Japan, with both earthquakes exhibiting significant liquefaction-induced damage including slope failures, bridge and building foundation failures, and flotation of buried structures (Kramer 1996). These two events became the genesis for a new branch of geotechnical earthquake engineering dedicated to studying the causes and effects of seismically-

induced liquefaction. Because the study of liquefaction and its associated hazards is still a relatively new topic, many differences of opinion still exist over the correct analysis approach.

The term liquefaction, coined by Mogami and Kubo (1953), has been used to refer to a number of related phenomena, all of which involve the repeated disturbance of saturated, cohesionless soils under undrained conditions (Kramer 1996). When loose cohesionless soils experience static or cyclic loading, they tend to contract. This contraction of the soil under saturated conditions results in a generation of excess positive pore pressure as pore water is pushed from the pore space, lowering the effective stress of the soil. In this weakened condition the soil softens considerably and is susceptible to a variety of deformations or failures, which generally manifest in themselves in one of two ways: flow liquefaction and cyclic mobility. While flow liquefaction tends to have the most devastating consequences, it occurs much less frequently. Cyclic mobility can occur under a broad range of soil and site conditions, with consequences ranging from insignificant to severe. Both of these phenomena are discussed in more detail in later sections. In this study, the term liquefaction refers to both flow liquefaction and cyclic mobility, with clarification provided when necessary.

2.3 **Liquefaction Susceptibility**

Liquefaction does not occur in all soils. Furthermore, a soil that would normally be susceptible to liquefaction may, under certain circumstances, exhibit a resiliency to liquefaction initiation. Therefore, the first step in characterizing liquefaction hazard is usually the determination of susceptibility to liquefaction. There are several factors contributing to liquefaction susceptibility, including historical, geologic, compositional, and state criteria.

2.3.1 Historical Criteria

Understanding how a site has performed under seismic loading in the past can play an important role in predicting future behavior. For example, post-earthquake investigations have shown that liquefaction often recurs at the same location when soil and groundwater conditions have remained unchanged (Youd 1984). These investigations result in the development of case histories that can be used to identify sites and, more generally, conditions that may be especially susceptible to liquefaction. Youd (1991) has shown the utility of this approach in mapping liquefaction susceptibility.

Case histories have shown that liquefaction effects are usually confined to a certain maximum radial distance from the epicenter of the earthquake. Ambraseys (1988) observed a correlation between moment magnitude and maximum epicentral distance with observed liquefaction, where the distance increased with increasing moment magnitude. These criteria serve to provide a rough estimate of expected liquefaction potential at a site.

2.3.2 Geologic Criteria

The depositional environment of a soil plays a significant role in defining its susceptibility to liquefaction. Soils that exhibit high susceptibility are usually deposited in environments that produce loose, uniformly graded material. Fluvial, colluvial, and aeolian deposits are, when saturated, good examples of material with high potential susceptibility to liquefaction. Other depositional environments such as alluvial-fan and estuarine deposits can produce similar material. It should be noted that, in some instances, man-made soil deposits can also experience high susceptibility. For example, non-compacted fill and hydraulic fill result in loosely deposited material that have traditionally exhibited significant liquefaction hazard. The age of the soil can also contribute to liquefaction susceptibility. In general, older soils

demonstrate less susceptibility to liquefaction than younger soils (Youd and Perkins 1978). One potential source of this change in behavior is the conditioning of a soil from previous seismic loads.

Because liquefaction requires the generation of positive excess pore pressure, a soil must be saturated to be susceptible. Soils experience the greatest susceptibility when the groundwater table is within a few meters of the ground surface. Liquefaction susceptibility decreases as the depth of the groundwater increases. As might be expected, in areas where the depth of groundwater is variable, the liquefaction susceptibility of a soil may also be variable.

2.3.3 Compositional Criteria

The physical characteristics of the individual soil particles, including size, shape, and gradation, also play an important role in liquefaction susceptibility. Liquefaction involves the generation of excess pore pressures through the densification of a soil. If a soil is difficult to densify, or is unable to sustain elevated pore pressures, liquefaction is unlikely to occur. When a saturated soil is loaded and begins to densify, the void space in the soil decreases, and water is essentially "squeezed" out of the soil. If the water cannot escape from the soil fast enough, it begins to push back, resulting in the generation of excess pore pressure. The ease with which water is able to move through a soil is called permeability and is generally governed by the size of the individual soil particles and the amount of fine-grained soils in the pore space between the soil particles. Large, bulky soil particles (e.g., gravel) have large voids between them and are generally very permeable. As a result, excess pore pressures are usually not sustained as the water is easily forced out of the void space. When impermeable layers are present around the permeable material, however, the water is unable to escape, and pore

pressures can develop. If the soil is well-graded, smaller particles fill the void space between larger particles, and the permeability of the soil decreases.

Fine-grained material with thin, plate-like particles exhibit a phenomenon called cohesion, where particles are attracted to each other by significant electrical and chemical interactions. These forces created by these interactions are very large relative to the particle size and tend to govern behavior of the soil. Sufficient cohesion will generally inhibit the initiation of liquefaction.

Pore pressures can only develop if a soil is able to undergo volumetric change when loaded. Soils that have smooth, rounded particles, such as those found in fluvial and alluvial environments, densify more easily than particles that have a jagged, angular exterior. The rough exteriors of angular particles tend to interlock, resisting volumetric change. Another soil characteristic that can restrict volumetric change is the gradation of the soil. In a well-graded soil, the void spaces between large particles are filled with smaller particles. This reduces the overall void space and consequently the potential for volumetric change. Generally, well-graded soils are less susceptible to liquefaction than poorly-graded soils.

2.3.4 State Criteria

Even if a soil fulfills all of the preceding criteria for liquefaction potential, it may still not be susceptible to liquefaction. Susceptibility to liquefaction also depends on the initial state of the soil. In other words, susceptibility is affected by both the density and initial stress conditions of the soil at the time of an earthquake. This may be considered fairly intuitive, given that looser soils are more likely to densify and are therefore more likely to generate the excess pore pressures necessary to trigger liquefaction.

Casagrande (1936) laid the foundation for understanding the contractive and dilatant behavior of soils under shear. He found that all soils tested at the same effective confining pressure approached the same density when sheared to large strains. Loose soils densified during shearing and dense soils dilated. Once the soils reached the same density, they continued to shear with constant shearing resistance. Casagrande called the void ratio associated with this density the critical void ratio, e_c. He found that the critical void ratio was unique to the effective confining pressure and after plotting the relationship between effective confining pressure and critical void ratio, named the resulting line the critical void ratio (CVR) line. The CVR line was thought to be the boundary between contractive and dilative soils and, equivalently, between soils that are susceptible and not susceptible to liquefaction. A plot showing the behavior observed by Casagrande is shown in Figure 2-1, and a plot of the CVR line is shown in Figure 2-2.

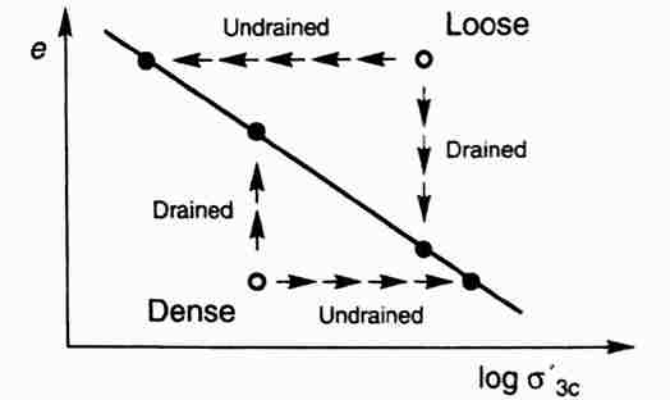

Figure 2-1: Behavior of loose and dense specimens under drained and undrained loading, as observed by Casagrande (after Kramer, 1996)

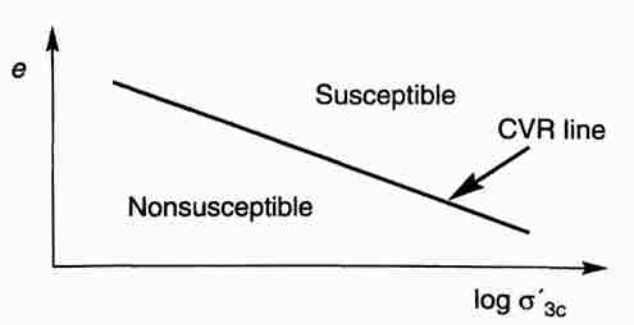

Figure 2-2: Casagrande's CVR line (after Kramer, 1996)

The CVR line was proven to be insufficient in predicting liquefaction susceptibility after the Fort Peck Dam suffered a flow liquefaction failure during construction in 1938 (Middlebrooks 1942). Investigation showed that the initial state of the liquefied material plotted below the CVR line, in the nonsusceptible region. The discrepancy was attributed to the fact that strain-controlled laboratory tests could not reproduce all of the phenomena that contribute to liquefaction in an actual stress-controlled failure. New criteria for defining liquefaction susceptibility needed to be established.

In 1969, Castro, who was one of Casagrande's students, performed various stress-controlled triaxial tests that led to the discovery of what was later termed the steady state of deformation (Castro and Poulos 1977, Poulos 1981), which describes the state in which a soil flows continuously under constant shear stress and constant effective confining pressure at constant volume and constant velocity. The relationship of void ratio and effective confining pressure in the steady state of deformation is called the steady-state line (SSL). The SSL is a three dimensional curve in $e-\sigma'-\tau$ or $e-p'-q$ space and is presented in Figure 2-3. The SSL can be projected onto a plane of constant shear stress (τ) and in this case can be represented by Figure 2-4. Because the shearing resistance of a soil is proportional to the effective confining

stress, the strength-based SSL is parallel to the effective confining pressure-based SSL when both are plotted logarithmically. Soils that plot below the SSL are not susceptible to flow liquefaction, while soils that plot above the SSL are susceptible if the static shear stress exceeds its steady-state (i.e., residual) strength. It should be noted that the SSL is useful for identifying conditions under which a soil may be susceptible to flow liquefaction but not necessarily for predicting susceptibility to cyclic mobility (Kramer 1996).

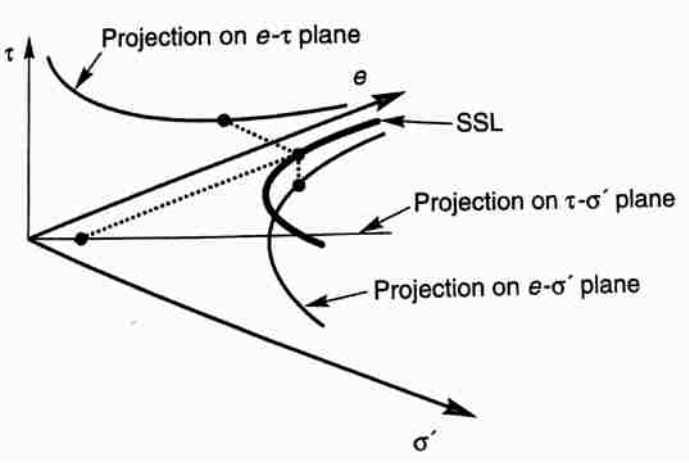

Figure 2-3: Three-dimensional steady-state line (after Kramer, 1996)

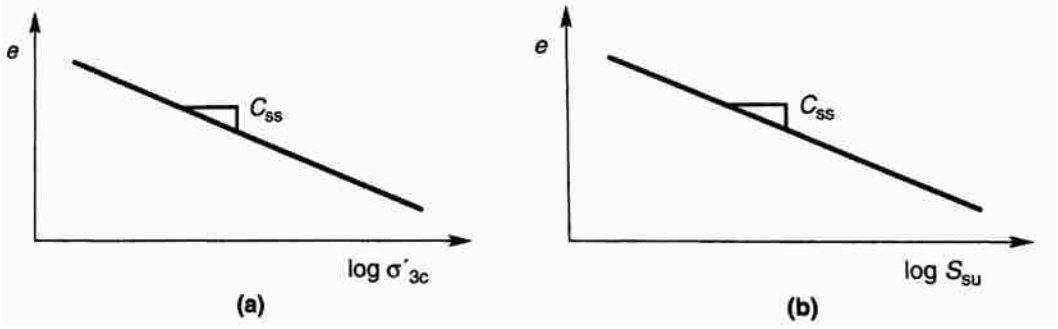

Figure 2-4: Strength-based and effective confining pressure-based steady-state lines with identical slopes (after Kramer, 1996)

One of the limitations of the steady-state line is that is uses absolute measures of density (e.g., void ratio, relative density, etc.) as an indicator of liquefaction susceptibility. As can be

seen in Figure 2-4, a soil with a specific void ratio may or may not be susceptible to liquefaction, depending on the initial confining stress of the soil. The need for a more complete measure of liquefaction potential is made clear in this discrepancy. Roscoe and Pooroshasb (1963) showed that the susceptibility of a cohesionless soil is better represented by the distance of its initial state from the steady-state line than by a measure of absolute density. These findings suggest that soils whose initial states are similarly distanced from the steady-state line should behave similarly. Therefore, a new measure of determining liquefaction susceptibility was created and called the state parameter (Been and Jeffries 1985). The state parameter (ψ) is defined as the difference between the initial void ratio of the soil and the steady-state void ratio of the soil at the confining pressure of interest. If the state parameter is positive, the soil will exhibit contractive behavior and is likely susceptible to liquefaction. If the state parameter is negative, the soil will exhibit dilative behavior and is not susceptible to liquefaction. It is important to remember that the state parameter can only be determined with the accuracy to which the steady-state line can be determined.

2.4 **Liquefaction Initiation**

A soil that has been found to be susceptible to liquefaction using the criteria given above is not guaranteed to experience liquefaction in an earthquake. The earthquake must create disturbances that are large enough to initiate a liquefaction event in the soil. The process of determining the type of disturbance required to trigger liquefaction is an essential part of the liquefaction hazard evaluation of a soil. The mechanics of both flow liquefaction and cyclic mobility are briefly discussed below. The mechanics of flow liquefaction and cyclic mobility are most easily described using stress path space (Hanzawa et al. 1979) and the following explanations are given in that context.

2.4.1 Flow Liquefaction Surface

Figure 2-5 demonstrates the stress path behavior of a sample of loose, saturated sand under monotonic loading. Because the soil is initially well above the SSL (point A), it will exhibit contractive behavior. Before loading, the soil exhibits no strain and no excess pore pressure. During loading, the soil demonstrates an increase in shear strength until it reaches a peak strength, at some small strain (point B). If the loading continues past this point, the shear stress exceeds the peak shear strength and the soil matrix becomes unstable and begins to collapse. This collapse results in rapid increases in excess pore pressure and strain and the soil reaches a steady-state residual strength that is much smaller than the peak strength (point C). The effective confining pressure of the soil at this point of residual strength is a fraction of the initial confining pressure. The soil has experienced flow liquefaction, which was initiated exactly at the point when the soil became irreversibly unstable.

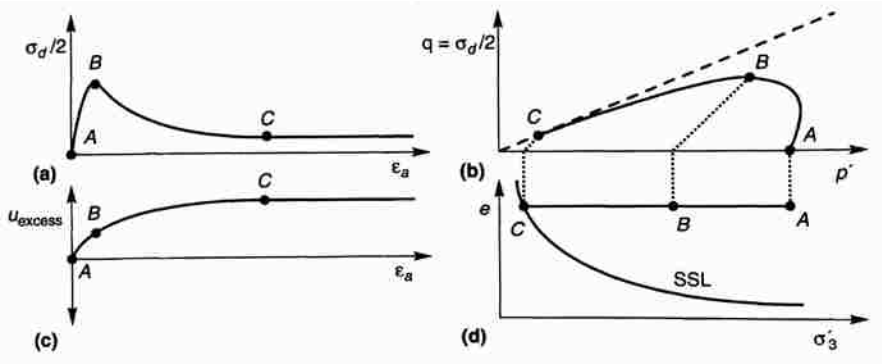

Figure 2-5: Response of isotropically consolidated specimen of loose, saturated sand: (a) stress-strain curve, (b) effective stress path, (c) excess pore pressure, and (d) effective confining pressure (after Kramer, 1996)

Now consider a group of soil specimens isotropically consolidated to the same void ratio but with varying initial confining stress. The response of each specimen to monotonic loading

can be seen in Figure 2-6. Specimens A and B are below the SSL and exhibit dilation as they approach the steady-state point. Specimens C, D, and E are above the SSL and experience the behavior explained above. The shear strength increases with strain to the peak shear strength and then collapses to the residual shear strength as the soil becomes unstable. The point at which the soil becomes unstable is marked with an x. Vaid and Chern (1983) showed that a straight line, originating at the origin of the stress path, can be drawn through the points on each specimen at the point of flow liquefaction initiation. This straight line defines the flow liquefaction surface (FLS). The FLS defines the boundary of stable and unstable conditions in undrained shear. If the stress state of an element reaches the FLS in undrained shear, the soil will experience flow liquefaction and the shear resistance will be rapidly reduced to the steady-state strength. In other words, the FLS defines the conditions that will cause flow liquefaction. Figure 2-7 shows the orientation of the FLS in stress path space.

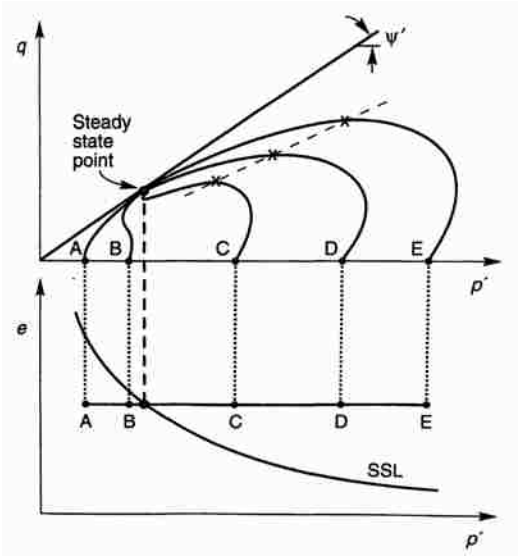

Figure 2-6: Response of five specimens isotropically consolidated to the same initial void ratio at different initial effective confining pressures with flow liquefaction in specimens C, D, and E initiated at the points marked with an x (after Kramer, 1996)

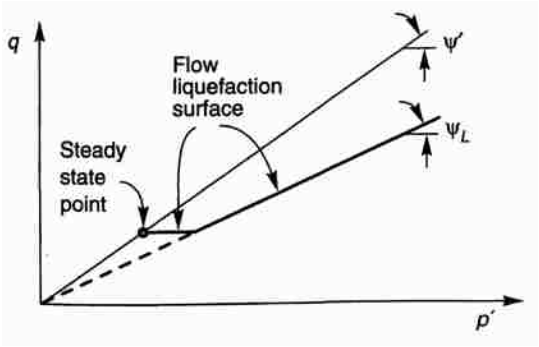

Figure 2-7: Orientation of the flow liquefaction surface in stress path space (after Kramer, 1996)

It is important to note that monotonic loading is not the only way to drive a soil to the FLS. A soil can also reach the FLS under cyclic loading. Consider Figure 2-8, which shows the initiation of flow liquefaction for a soil under monotonic and cyclic loading. The soil under monotonic loading (path ABC) demonstrates the phenomenon that was explained previously. The effective stress path of the cyclically loaded soil (path ADC) moves to the left as positive excess pore pressures develop under each additional cycle. When the effective stress path reaches the FLS, flow liquefaction is initiated.

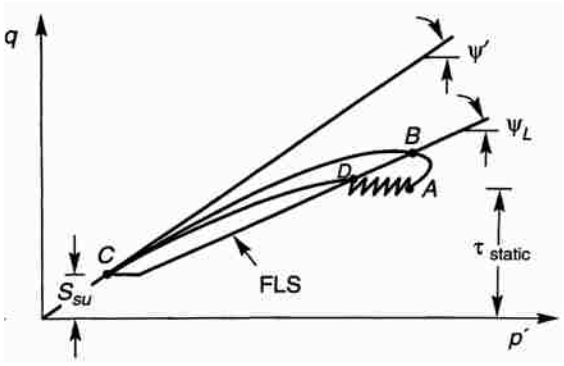

Figure 2-8: Initiation of flow liquefaction by cyclic and monotonic loading (after Kramer, 1996)

Despite the fact that the stress states of point B and D are different, they both lead to flow liquefaction initiation. This example demonstrates that the FLS marks the boundary of soil instability. Lade (1992) provides a more detailed explanation of the nature of this instability,

In summary, flow liquefaction occurs in two stages. The first stage involves the generation of pore pressures under small strains, from either monotonic or cyclic loading, that move the effective stress of the soil to the FLS. The second stage involves strain-softening driven by the soil approaching the steady-state condition, resulting in the development of large strains. If the soil reaches the FLS during the first stage, the second stage is automatically triggered.

2.4.2 Flow Liquefaction

Flow liquefaction can be initiated when the shear stress required for static equilibrium is greater than the steady-state strength. These stresses are mainly caused by gravity in the field and are constant until large deformations occur and stabilize the driving forces. Therefore, only soils with initial states that fall within the shaded region of Figure 2-9 are susceptible to flow liquefaction. If the initial state of the soil is close to the FLS, small levels of excess pore pressure will trigger flow liquefaction. The further away the initial state is from the FLS, the greater the excess pore pressure necessary to drive the stress state to the FLS.

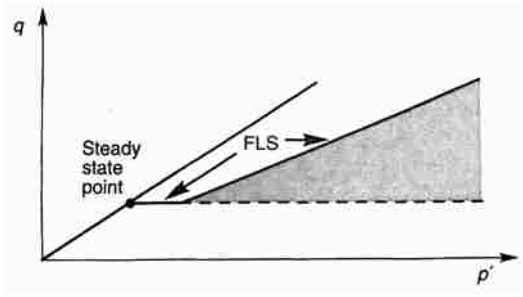

Figure 2-9: Zone of susceptibility to flow liquefaction (after Kramer, 1996)

2.4.3 Cyclic Mobility

When the static shear strength is less than the steady-state strength, flow liquefaction cannot occur. However, cyclic mobility can still occur. The zone of initial stresses susceptible to cyclic mobility is shown in Figure 2-10. It should be noted that soils to the left and below the steady-state point would need to dilate (i.e., move the stress path to the right) to reach the steady-state point. This demonstrates that cyclic mobility can occur in both loose and dense soils (i.e., soils that would plot both above and below the SSL).

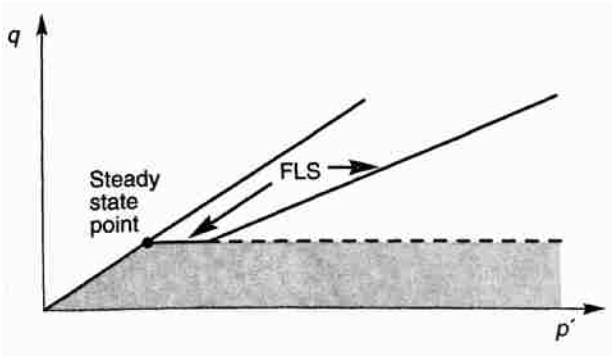

Figure 2-10: Zone of susceptibility to cyclic mobility (after Kramer, 1996)

Three possible conditions generally lead to cyclic mobility. The first condition involves cyclic loading with no stress reversal and no exceedance of steady-state strength (Figure 2-11(a)). In this case, the effective stress path moves to the left until it reaches the failure envelope. Any additional loading cycles after this will simply cause the stress state to move along the failure envelope. The effective stress of the soil has been reduced significantly, and the low stiffness associated with the decreased effective stress allows large, permanent strains to occur. The second case involves cyclic loading with no stress reversal and momentary exceedance of steady-state strength (Figure 2-11(b)). In this case, the effective stress path moves

to the left until it reaches the FLS, at which time the soil will experience momentary periods of instability. This instability causes large permanent strains to develop, but the straining stops once the stress state drops below the FLS. The final case involves cyclic loading with stress reversal and no exceedance of steady-state strength (Figure 2-11(c)). This case involves both compressional and extensional loading within each cycle. The rate of pore pressure generation increases significantly as the degree of stress reversal increases. Because of this phenomenon, the effective stress path moves quickly to the left. Once it reaches the failure envelope, it moves along the compression and extension portions of the failure envelope. Large permanent strains can develop as the soil experiences moments of zero effective stress at the point of stress reversal.

Unlike flow liquefaction, cyclic mobility does not have a clear point of initiation. Rather, the strains caused by cyclic mobility accumulate with each loading cycle. The magnitude of the strains is dependent on both the levels of static shear stress and the duration of the ground motions. Therefore, a ground surface that is relatively flat (i.e., low initial shear stress) and/or that undergoes short periods of ground shaking will generally exhibit smaller deformations, while a ground surface that is sloped (i.e., high initial shear stress) and/or experiences longer periods of ground shaking will exhibit larger soil deformations.

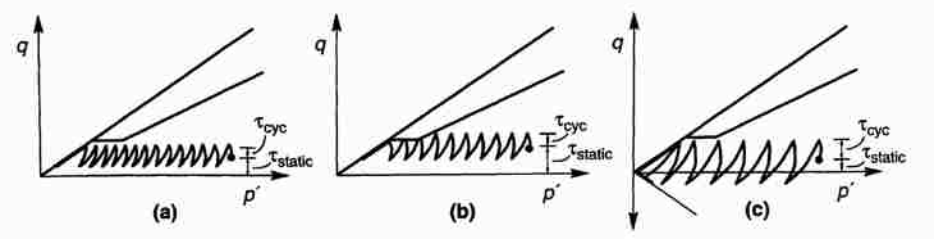

Figure 2-11: Three cases of cyclic mobility (a) no stress reversal and no exceedance of steady-state strength; (b) no stress reversal with momentary periods of steady-state strength exceedance; (c) stress reversal with no exceedance of steady-state strength

2.5 Liquefaction Effects

Liquefied soil can cause considerable damage to buildings, infrastructure, utilities, dams, and other structures. One of the main purposes of the study of liquefaction is to be able to predict the magnitude of the damage caused by its effects. Some of the most serious effects of liquefaction are described below.

2.5.1 Settlement Due to Free-field Reconsolidation of the Soil

When loose sand is loaded, it has a tendency to densify. The densification of a profile of sand is manifested by settlement at the ground surface. This settlement can cause serious damage to lifelines, utilities, and structures supported by shallow foundations. The damage is increased when the surface settles non-uniformly, a phenomenon called differential settlement. Free-field post-liquefaction settlement is the focus of this work and is discussed in greater detail in later sections.

2.5.2 Lateral Spread

Lateral spread is a phenomenon in which blocks of the ground surface break apart and are incrementally carried by the liquefied soil down a slope or towards a free face. These blocks can move irregularly, and movements can vary from a few centimeters to several meters or more, depending on the severity of the ground motions. Lateral spread can cause severe damage to lifelines and structures alike.

2.5.3 Loss of Bearing Capacity

When a soil liquefies, it experiences a rapid and significant decrease in shear strength. Structures supported by liquefied soil can often rotate or punch through the soil. Buried

structures are also affected by this phenomenon. Gas tanks, sewage pipes, and other utilities can float to the surface because the buoyant force acting on the structure is greater than the shear strength of the soil.

2.5.4 Other Effects

Other effects of liquefaction include alteration of ground motions during earthquake loading, the development of sand boils, and general flow failure. These effects are explained in greater detail in Kramer (1996).

2.6 Chapter Summary

Liquefaction is a phenomenon where a loose, saturated soil is loaded and experiences rapid generation of excess pore pressures and a dramatic decrease in effective stress and shear strength. For a soil to be susceptible to liquefaction, it must meet a variety of criteria including historical, geologic, compositional, and state conditions. Liquefaction is manifested as either flow liquefaction or cyclic mobility and can cause significant damage to structures and utilities through a variety of phenomena including free-field settlement and lateral spread.

3 CHARACTERIZATION OF SEISMIC LOADING

Liquefaction is primarily triggered by seismic loading. Understanding earthquakes and the ground motions they create provides a necessary background for understanding liquefaction but is insufficient. The ability to characterize and quantify the ground motions created by earthquakes is what makes the prediction of liquefaction effects possible. Earthquake engineering is a relatively young science, and the ability of the engineering community to characterize earthquakes is constantly improving with the development and proliferation of improved instrumentation, the improved understanding of the physics and mechanics behind the ground motions, and the development of more sophisticated ground motion prediction equations.

3.1 Earthquakes

Earthquakes consistently pose one of the greatest natural threats to civilization. The loss of life, destruction of property, and damage to infrastructure resulting from a large-scale seismic event can cripple a region. In an attempt to mitigate the effects of such an event, engineers try to prepare for these events by designing structures to withstand a certain level of seismic loading. For this to be possible, a metric must exist to quantify the level of seismic loading generated by an earthquake.

Several scales have been established to describe the size of earthquakes. Qualitative scales (e.g., the Mercalli and Rossi-Forel scales) were the first attempts to quantify earthquake shaking.

These scales were created before the technology for earthquake instrumentation existed and relied heavily on eye-witness accounts and subjective interpretations of the earthquake. To apply these methods, data were often acquired through a survey sent to residents in the mail or through door-to-door visits. The consistency and objectivity of the data, however, were questionable. The need for a better and more consistent method of ground motion characterization was universally recognized.

Quantitative measures were developed as ground motion instrumentation became more readily available. This instrumentation provided objective records of earthquake ground motions in the form of acceleration, velocity, and/or displacement. These records became known as earthquake time histories and led to the development of many of the earthquake engineering design practices applied today.

Early ground motion instruments led to the development of various magnitude scales intended to quantify the "size" of the earthquake. Several such scales have been proposed and a few of the most common are explained briefly. The Richter magnitude scale is one of the most commonly known earthquake scales (Boore 1989). The Richter magnitude scale was created for shallow, local earthquakes and is not a valid metric in many instances. It is not often used in earthquake design. Magnitude scales based on surface waves and body waves were later developed (Kanamori 1983) and are more widely applicable than the Richter magnitude scale, but they are generally less reliable when distinguishing between large earthquakes. The seismic intensity generated by large earthquakes tends to produce constant readings in many of the ground motion instruments used to define various scales of magnitude (a phenomenon known as saturation), resulting in an inability to accurately characterize the size of large earthquakes. The most common magnitude scale for quantifying earthquake size today is the moment magnitude

scale. The moment magnitude is independent of local intensity and is not directly measured by any ground motion instrument. Instead, the instrument recordings are used to back-calculate the seismic moment of the earthquake, which is a measure of the amount of energy released by the earthquake and is not subject to saturation. Therefore, the moment magnitude scale is applicable to all earthquake events and is widely considered the best metric for measuring earthquake strength. All references to earthquake magnitude in this study use the moment magnitude scale.

3.2 Ground Motion Parameters

The strong ground motions created during a seismic event are often difficult to characterize. It is considered impossible to accurately describe all the important ground motion characteristics with a single parameter (Jennings 1985, Joyner and Boore 1988). The most common method of describing ground motions is through the use of time histories. A time history is a record of a given quantity (usually acceleration) over the duration of an earthquake. From a time history, multiple ground motion parameters (GMPs) can be obtained. Some of the most useful parameters are briefly described below.

3.2.1 Amplitude Parameters

Amplitude is a measure of the maximum value of a designated type of ground motion. Amplitude can be expressed in terms of maximum acceleration, velocity, or displacement. A common measure of amplitude is the peak ground acceleration (PGA) or peak ground surface acceleration (a_{max}).

The PGA is often used because it is fairly indicative of the largest dynamic forces induced in stiff structures during a seismic event. However, using the PGA or another amplitude-based GMP as the sole means of characterizing the strong ground motions of an earthquake is

considered by many to be inadequate. Two hypothetical time histories are presented in Figure 3-1. The time histories in this example have similar PGA values, but using amplitude as the only GMP to describe these two events would be misleading. It is clear that time history (b) releases more energy than time history (a). This example demonstrates clearly that additional GMPs must be used to provide a more complete understanding of the characteristics of a recorded strong ground motion.

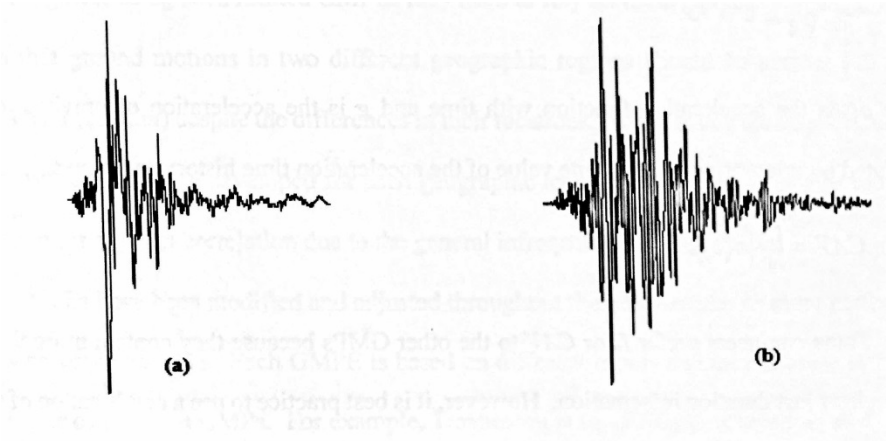

Figure 3-1: Two hypothetical time histories (after Kramer 1996)

3.2.2 Frequency Parameters

Frequency content describes how rapidly a ground motion is repeated in a given amount of time. The rate of load repetition can have a significant effect on the response to loading of a structure or object. All structures exhibit a natural frequency, which is an inherent rate of oscillation or elastic response that occurs when loaded. If the frequency of loading matches the natural rate of oscillation of a structure, the magnitude of oscillation is compounded through the

phenomenon of resonance. Larger displacements in a stiff structure result in increased deformations and damage, generally reducing the natural rate of oscillation of the structure.

Understanding the frequency content of a ground motion and how that frequency content compares to the natural frequency of the structure plays an important role in predicting the potential damage to a structure. However, describing the frequency content of a ground motion can be difficult. Earthquakes produce complicated ground motions that span a wide range of frequencies. One of the most common metrics used to describe the frequency content of a ground motion is a mathematical function known as the Fourier series. The Fourier series is a sum of simple harmonic terms with varying frequency, amplitude, and phase. When the Fourier amplitude is plotted versus the frequency (known as the Fourier amplitude spectrum), the frequency of the ground motion can be clearly observed. An example of two Fourier spectra is provided in Figure 3-2. The frequency of the first spectrum is strongest at low periods (i.e., high frequencies), while the second is strongest at high periods (i.e., low frequencies). This information assists in the analysis of potential hazard to structures affected by these ground motions. If a structure has a natural frequency similar to the frequencies most strongly represented by the ground motion, it is more likely to experience significant damage and must be designed accordingly. Kramer (1996) provides further explanation of the Fourier series and the derivation of the various spectra used in earthquake design. It should be noted that, while a Fourier spectrum focuses on the amplitudes and frequency content of a time history, many engineers prefer a spectrum related to the structural response instead. A more detailed explanation of the response spectrum is given by Hudson (1956).

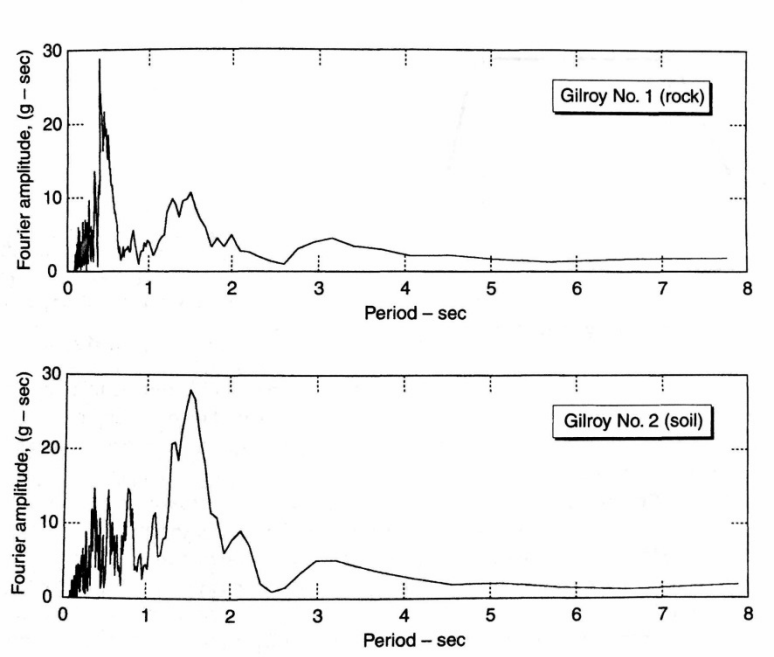

Figure 3-2: Fourier amplitude spectra for the E-W components of the Gilroy No. 1 (rock) and Gilroy No. 2 (soil) strong motion records (after Kramer, 1996)

3.2.3 Duration Parameters

Damages incurred during an earthquake are largely dependent on the duration of the ground motions. An extended duration of loading allows the effects to compound over time, resulting in more significant distresses. For example, liquefaction is triggered by the generation of excess pore water pressure in loose, granular soil. Repeated cyclical loading is the driving force in the generation of excess pore pressure. The risk of liquefaction triggering and its resultant effects increase with every additional loading cycle. One example of a duration parameter is bracketed duration, defined as the time between the first and last occurrence of some threshold acceleration (Kawashima and Aizawa 1989).

3.2.4 Ground Motion Parameters That Describe Multiple Characteristics of the Ground Motion

Because all of the GMPs described in the previous sections are important to the characterization of seismic loading, there have been many attempts to create GMPs that describe multiple characteristics of ground motions. Examples of these combined GMPs included the Arias intensity (I_a) (Arias 1970), the cumulative absolute velocity (CAV) (Benjamin 1988), and the response spectrum intensity (Housner 1959). Use of such GMPs allows engineers to simultaneously characterize multiple attributes of a ground motion. Therefore, they are more efficient than applying multiple GMPs that only characterize one aspect of a ground motion. It is no surprise, therefore, that many researchers are searching for ways to incorporate these types of GMPs in their newly developed response models to predict the effects of earthquakes.

3.3 Ground Motion Prediction Equations

Time histories provide understanding of past seismic events, but engineers base their designs on events that have not yet occurred. To do this, they must estimate the GMPs they use in their design. Predictive relationships have been developed that estimate a GMP based on the variables that affect it most. Some of the factors that can affect a GMP include magnitude, distance, and modifying effects that are described in more detail in section 3.4. Predictive equations that are used for parameters that decrease with increasing distance (e.g. peak acceleration or peak velocity), are called attenuation relationships. Extensive effort has been exerted in the development of attenuation relationships. For peak acceleration, Campbell (1981) developed attenuation relationships for areas within 50 km of earthquakes with magnitudes between 5.0 and 7.7. Campbell and Bozorgnia (1994) widened the scope of those relationships to

areas within 60 km of earthquakes with magnitudes between 4.7 and 8.1. Boore et al. (1993) developed relationships for western North America within 100 km of events with magnitudes between 5.0 and 7.7. Toro et al. (1995) developed relationships for the midcontinental eastern United States. Youngs et al. (1988) did similar work for areas subject to subduction zones. Regarding peak velocity, Joyner and Boore (1988) developed relationships for earthquakes with magnitudes between 5.0 and 7.7. As more data became available from earthquake events, updates to these attenuation relationships were necessary. Research teams were assembled to develop new equations known as the Next Generation Attenuation (NGA) Relationships (Abrahamson and Silva 2008, Boore and Atkinson 2008, Chiou and Youngs 2008, Campbell and Bozorgnia 2008, Idriss 2008). Each of these teams developed GMP prediction equations using the same database of ground motion data. The NGA equations were updated in 2013 to the NGA West 2 relationships (Ancheta et al. 2014). It should be noted that each of these attenuation relationships is very specific in scope and applies to certain areas and/or seismic events. Care should be taken to avoid extrapolation when using these relationships to predict GMPs.

3.4 **Local Site Effects**

The relationships described above rely heavily on magnitude and distance to predict GMPs. However, other factors can significantly affect the ground motions measured at a site. These factors are site-specific, and, while their effects are easily observed, they can be difficult to predict. An important step of SHA is to identify these potential sources of ground motion alterations.

The energy waves created by an earthquake propagate outwards through the surrounding soil and rock. The density and stiffness of this material plays an important role in the attenuation of these waves (Kramer 1996). Generally, stiff soil/rock amplifies waves with high frequencies,

while softer material has the opposite effect, amplifying waves of low frequency (Seed et al. 1976, Seed et al. 1990). One of the most prominent examples of these effects is provided in the 1985 Michoacan ($M_s = 8.1$) earthquake. While the Michoacan caused only moderate damage in the area surrounding its epicenter, it caused severe damage in Mexico City (some 350 km away) (Kramer 1996). Mexico City is constructed above deep, soft lake deposits that are surrounded by basaltic bedrock. The accelerations measured in the bedrock were very low. The soft lake deposits, however, amplified the low frequency waves of the earthquake and caused significant damage. It should also be noted that the damage was selective, affecting only those structures with a natural period approaching that of the amplified frequency. Amplification is not the only result of soil density. As waves move between materials of varying density, they are refracted (Kramer 1996). This refraction leads to wave interaction, causing "peaks" and "valleys" in wave intensity. Stratified soil often exhibits this behavior, especially in areas where the depositional mechanism varies between layers.

Site topography can play an important role in ground motion alterations. Crests and ridges have a tendency to amplify waves as they propagate upwards to the peak. This phenomenon was clearly demonstrated by Jibson (1987) and can be observed in Figure 3-3. The average peak acceleration in the crest of the ridge was about 2.5 times that of the base. These amplifications can become complex with irregularities in site geometry and wave type and angle (Sanchez-Sesma and Campillo 1993). However, because few important structures are built on peaks, these effects are somewhat less important to seismic design. For critical structures, finite element analysis can be used to approximate these effects.

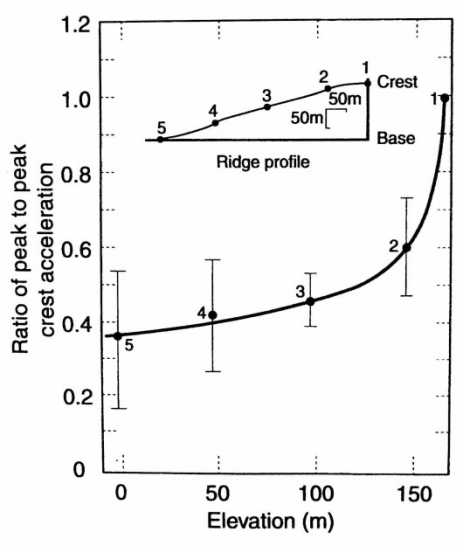

Figure 3-3: Normalized peak accelerations recorded on mountain ridge at Matsuzaki, Japan (After Jibson, 1987)

Basin effects describe the result of the natural curvature that occurs in alluvial deposits. This curvature can trap body waves and cause propagation of increased surface waves, resulting in stronger shaking and longer durations than would normally be predicted (Vidale and Helmberger 1988). These effects are of noted importance, considering that many large cities are built on alluvial valleys. Basin effects are relatively easy to predict in the center of the basin but become complex near the edges.

Directivity is another site-specific source of alteration of ground motions. Directivity refers to the direction of fault rupture with respect to the site. If a fault ruptures towards the site, observable spikes in velocity and displacement occur (Somerville et al. 1997). This pulse of energy can lead to excessive damage, as demonstrated by the Kobe, Japan (1995), earthquake.

3.5 Chapter Summary

Characterizing the ground motions generated by seismic events is an essential step in the process of evaluating liquefaction hazard. Using a combination of amplitude, frequency, and duration, GMPs provide the most complete characterization of an earthquake. These parameters can be significantly affected by local site effects, and these effects should be considered when evaluating seismic hazard.

4 PERFORMANCE-BASED EARTHQUAKE ENGINEERING

The standards of building design evolve as engineers learn about structural response to loading. This is especially true within the realm of earthquake engineering, a relatively young science. Because recorded data of seismic events are still in relatively limited supply, each new earthquake provides valuable data sets that lead to increased understanding of structural response to seismic loading. This improved understanding is then reflected in updates to standard practices and building codes. The goal of this process is to produce structures that perform better under seismic loading. Current codes, however, usually stipulate processes (e.g. acceptable design methods, building materials, etc.) instead of focusing on the desired end result, the performance of the structure (Mayfield 2007).

The goal of earthquake engineering is to design a structure that will withstand a reasonable level of seismic loading while performing at or above a predetermined standard. To accomplish this, engineers must attempt to predict the ground motions that are most likely to occur at a given site. However, predicting the magnitude, location, and ground motions of a future earthquake is extremely difficult. In early earthquake engineering practice, engineers often chose to bypass the difficulty of predicting earthquakes by using a worst-case scenario as the basis for design. One of the problems with using this approach (DSHA) is that no consideration is given to the probability of occurrence of the design event. This approach can result in structures that are over-designed relative to the importance and/or design life of the structure.

In an attempt to address the problems with current standard practice described above, a new seismic design approach, known as performance-based earthquake engineering (PBEE) , has been developed by the Pacific Earthquake Engineering Research (PEER) Center (Cornell and Krawinkler 2000, Deierlein et al. 2003). This chapter will provide a review of basic SHA principles and outline the PEER framework for PBEE.

4.1 Seismic Hazard Analysis

SHA is the process of quantitative estimation of ground shaking hazards at a particular site. There are two basic types of analyses. The first, known as deterministic analysis, involves assuming an earthquake scenario (usually worst-case) and designing the structure based on the ground motions associated with that scenario. The second method, known as probabilistic analysis, takes into account every possible scenario and its accompanied probability of occurrence when determining the design ground motions and parameters. Each method is explained in more detail below.

4.1.1 Deterministic Seismic Hazard Analysis

DSHA is a method that was created early in the development of earthquake engineering. It involves the speculation of an earthquake of a specific size occurring at a specific location. This theoretical scenario is then used as the basis for the ground motions used during the design of a structure. It should be noted that some of the decisions made during a DSHA, like the selection of the appropriate design scenario is relatively subjective and potentially results in excessively conservative design.

Kramer (1996) explains the process of completing a DSHA as follows. Performing a DSHA involves four steps, shown in Figure 4-1. First, all potential significant seismic sources

are identified and characterized. This characterization includes spatial and temporal descriptions of the seismic source. Second, a source-to-site distance must be defined. Depending on the predictive relationship used in the following step, different types of distance metrics can be used (e.g. epicentral, hypocentral, etc.). The closest distance for a given metric along the distribution of source-to-site distances of a seismic source usually produces the most critical scenario. Third, a controlling earthquake is selected from among the potential sources. This decision is often based on which source generates the "worst-case" earthquake scenario. Fourth, the seismic hazard produced at the site is defined through the ground motions created by the controlling earthquake. This hazard is expressed as one or more ground motion parameters, calculated using predictive relationships like those described in Chapter 3.

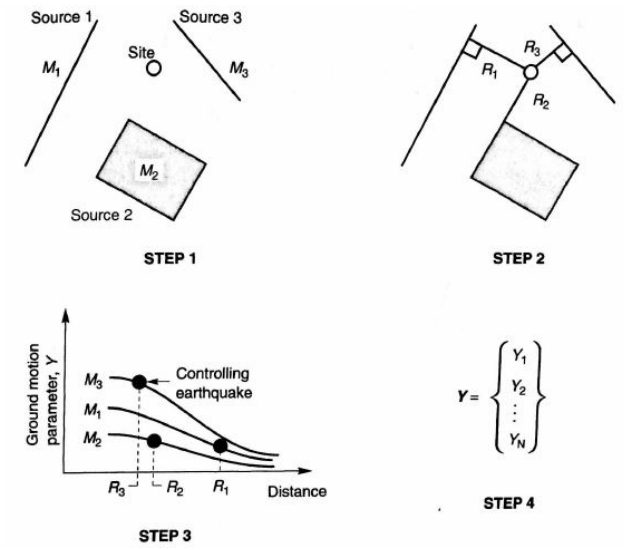

Figure 4-1: Steps of DSHA (after Kramer, 1996)

Performing a DSHA provides a simple, straightforward procedure for estimating seismic hazard when designing critical structures, such as dams, nuclear power plants, etc. The use of a

worst-case scenario provides confidence in the integrity of these structures in a variety of seismic scenarios. However, DSHA does not consider the inherent uncertainty of seismic events. For example, when choosing a controlling earthquake, no consideration is given to the probability of occurrence of that earthquake. This can lead to structures that are designed to resist ground motions that are unrealistically large, especially in the case of non-critical structures.

4.1.2 Probabilistic Seismic Hazard Analysis

Using concepts of probability, the uncertainties mentioned above (e.g. uncertainty in size, location, and recurrence of earthquakes, uncertainty in ground motion characteristics) can be addressed and a more complete characterization of seismic hazard can be created using a PSHA (Cornell 1968). Kramer (1996) said that PSHA "…provides a framework in which these uncertainties can be identified, quantified, and combined in a rational manner to provide a more complete picture of the seismic hazard."

Understanding PSHA requires a basic understanding of probabilistic concepts, which are beyond the scope of this study. For background information on probabilistic methods, see Kramer (1996). PSHA can be summarized in four steps, which are somewhat similar to the steps of the DSHA method. These steps are illustrated in Figure 4-2. First, the earthquake sources must be identified and characterized. This step is identical to the first step of the DSHA, except that the sources are further characterized by the probability distribution of potential rupture within the source. Usually, uniform probability distributions are assigned to every point within the source, implying that rupture is equally likely to occur at any point within the source. If enough data exist to provide evidence that the probability of rupture is not uniform across a source, a different distribution may be applied to provide a more realistic representation of the source. Second, the seismicity of the earthquake source must be characterized. This is usually done through a

recurrence relationship, which describes the temporal distribution of earthquake recurrence. In other words, it describes the average rate at which an earthquake of a certain size occurs. In a DSHA, this rate of recurrence is limited to the maximum size earthquake, but a PSHA is able to account for all possible earthquakes created by a given source. Third, the ground motions created at the site by earthquakes of any size produced at any location must be determined using predictive relationships. The uncertainty of these predictive relationships is included in the analysis. Fourth, the uncertainties of location, size, and ground motion parameter prediction are compiled to calculate the probability that the ground motion parameter will be exceeded during a particular time period.

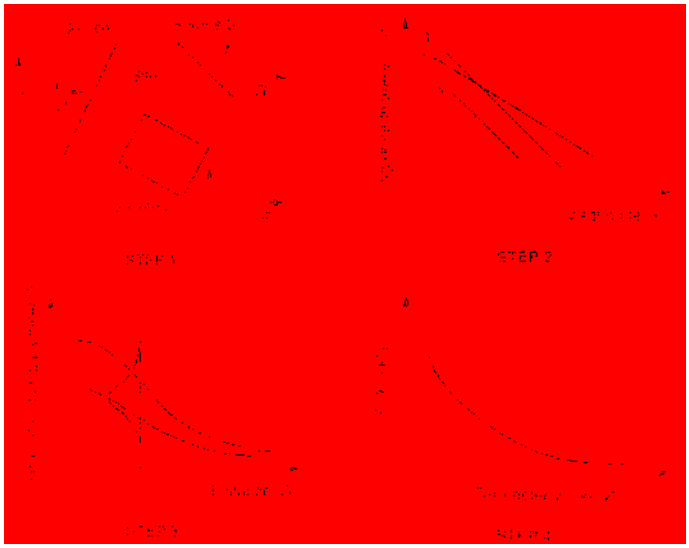

Figure 4-2: Steps of PSHA

When performing a DSHA, the result is usually a factor of safety for a specific seismic event. In a PSHA, because every possible seismic scenario is considered, a single value, such as a factor of safety, is not computed. Rather, the annual rate of exceedance (λ), the likelihood that

a given event will occur in any given year, of each event is calculated. These probabilities are often presented in seismic hazard curves, which are described in the next section.

4.1.3 Seismic Hazard Curves

A seismic hazard curve is a graphical representation of the probability of exceeding a given ground motion at a particular location. They can be created for individual earthquake sources or combined to create a complete understanding of hazard at a site. Seismic hazard curves are computed by determining the probability of exceeding a given ground motion for one possible earthquake at one possible location. This probability is then multiplied by the probability of that earthquake occurring at that location. This process is then repeated for all possible earthquakes at all possible locations. The result of the sum of these probabilities is λ of the given ground motion parameter. The ground motion parameter is then incremented and the process is repeated until a full seismic hazard curve is created. If λ communicates the likelihood of occurrence of a given event within a year, then the inverse of λ is the number of years between occurrences of the given event, also known as the return period (T_R).

The probability of exceeding a ground motion parameter is usually computed by considering two variables, the magnitude of the earthquake and the distance of the earthquake from the site. Using these inputs, with the assumption that they are independent of one another, the probability of exceedance for a given source can be computed as

$$P\left[Y > y^*\right] = \int\int P\left[Y > y^* \middle| m, r\right] f_M(m) f_R(r)\, dm\, dr \tag{4.1}$$

where $P\left[Y > y^* \middle| m, r\right]$ is obtained from the chosen predictive relationship and $f_M(m)$ and $f_R(r)$ are the probability density functions for magnitude and distance, respectively. If a site is exposed to N_s sources, the total average exceedance rate for the site is given by

$$\lambda_{y^*} = \sum_{i=1}^{N_s} v_i \int\int P\left[Y > y^* \middle| m, r\right] f_M(m) f_R(r)\, dm\, dr \tag{4.2}$$

where v_i is the average rate of threshold magnitude exceedance, given by

$$v_i = \exp(\alpha_i - \beta_i m_o) \tag{4.3}$$

where $\alpha = 2.303a$ and $\beta = 2.303b$, where a and b are Gutenberg-Richter coefficients. The average rate of threshold magnitude exceedance is used to limit the considered earthquakes to some range of significant magnitude. Because earthquakes of low magnitude (e.g. below 4.0-5.0) cause very little significant damage, they are often ignored in SHA. The components of equation (4.2) are usually too complicated to be computed explicitly, necessitating the use of numerical integration. While there are many ways to perform numerical integration, one of the simplest is to divide the possible ranges of magnitude and distance into a number of equal segments of N_M and N_R. Using this approach, the average rate of exceedance can be estimated by

$$\lambda_{y^*} = \sum_{i=1}^{N_S} \sum_{j=1}^{N_M} \sum_{k=1}^{N_R} v_i P[Y > y^* \left| m_j, r_k \right] f_{Mi}(m_j) f_{Ri}(r_k) \Delta m \Delta r \tag{4.4}$$

where $m_j = m_0 + (j - 0.5)(m_{\max} - m_0) / N_M$, $r_k = r_{\min} + (k - 0.5)(r_{\max} - r_{\min}) / N_R$, $\Delta m = (m_{\max} - m_0) / N_m$, and $\Delta r = (r_{\max} - r_{\min}) / N_R$. This method assumes that each source is only capable of generating N_M earthquakes of different magnitude at only N_R different source-to-site distances. This assumption is equivalent to

$$\lambda_{y^*} = \sum_{i=1}^{N_S} \sum_{j=1}^{N_M} \sum_{k=1}^{N_R} v_i P[Y > y^* \,|\, m_j, r_k] P[M = m_j] P[R = r_k] \tag{4.5}$$

The result of equation (4.5) is a single point on the hazard curve. The process is repeated for all increments of y^*. This method becomes more accurate as the number of intervals of N_M and N_R increase. It should be noted that this method is one of the simplest forms of numerical integration; more refined methods will produce more accurate results.

4.2 Introduction to Performance-based Earthquake Engineering

Historically, the main focus of earthquake engineering has been to protect life. Structures are designed to perform well enough to ensure that all occupants survive. After the earthquake event, structures are often found to be in poor condition, resulting in wide scale repair or even demolition and reconstruction. The economic toll of this process can be devastating to public and private entities alike, as demonstrated by the 1995 Kobe earthquake. It was noted that while many structures survived without collapse, the cost of damage repair was often excessive and uneconomic (Fajfar and Krawinkler 1997). Events like the Kobe earthquake highlight the need to establish design standards with a broader scope than life safety alone. The methods introduced in PBEE, described in detail in this section, accomplish this goal. The full development of PBEE will allow performance to be expressed in terms of "risk". In other words, performance will be expressed in terms that reflect both the direct and indirect losses associated with the occurrence of earthquakes. Such losses can be expressed in terms of casualties, economic losses, and lost time (Kramer 2008).

Another problem presented within conventional design methods is the inability to accurately communicate between stakeholders. Engineers report the results of their assessment in terms of a factor of safety against failure for a design earthquake, but usually omit the likelihood of occurrence of that earthquake. Decision makers are often unsure of how to interpret the factor of safety, resulting in confusion and frustration. Performance-Based Earthquake Engineering (PBEE) seeks to improve seismic risk decision-making through assessment and design methods that are more transparent, scientific, and informative to stakeholders than current prescriptive approaches (Deierlein et al. 2003). As mentioned previously, the goal of PBEE is to present seismic hazard in terms of risk, a vernacular to which many decision makers are accustomed. By communicating risk in understandable terms, engineers empower stakeholders to make informed decisions during the design process.

The various stakeholders in the design process think of risk and performance differently. For example, seismologists usually think in terms of ground motions, geotechnical engineers think of effects (e.g. settlement, lateral spread, etc.), structural engineers think of structural deformation or damage, owners are concerned about cost, and regulating agencies focus on life safety. Figure 4-3 illustrates some of the metrics used to weigh risk and measure performance. While conventional design methods struggle to connect these ideas explicitly, PBEE combines them into a successive "cause and effect" framework, facilitating communication between all parties.

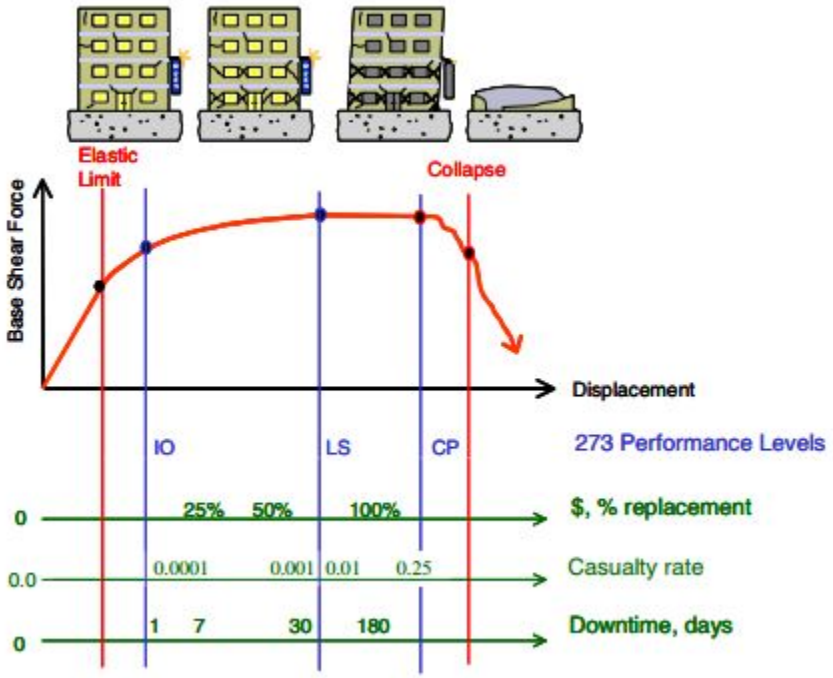

Figure 4-3: Static pushover visualization of seismic performance assessment (after Moehle and Deierlein, 2004)

PBEE is centered on the idea that the uncertainty inherent in predicting seismic events and building response can be quantified and structure performance can be reliably predicted. Once uncertainty has been quantified, it can be used to help stakeholders define a satisfactory performance level with an acceptable amount of risk. An illustration of balance between performance and risk is provided in Figure 4-4. Critical structures (e.g. hospitals, power plants, emergency response structures, etc.) must be designed to remain operational after even a rare seismic event. A higher minimum allowable performance level results in an acceptable level of risk that is much lower than that of non-critical structures (e.g. office buildings, shopping centers, residences, etc.). An understanding of the desired performance level of a structure and the associated allowable risk enables stakeholders to make more informed decisions.

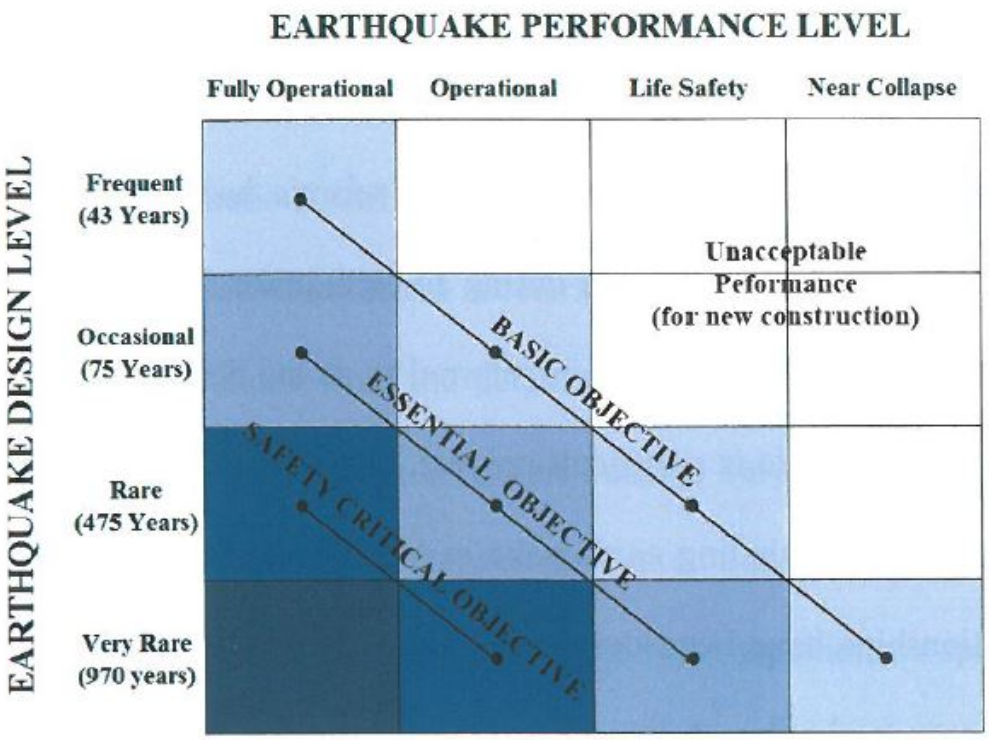

Figure 4-4: Minimum design objectives for various risk levels (after Bertero and Bertero, 2002)

4.3 PBEE Framework

The PBEE framework consists of the following components (see Figure 4-5):

- *Intensity Measure (IM)*: a quantity that captures attributes of the ground motion hazard at a site. Usually defined as a scalar value, determined probabilistically after considering nearby faults and geological characteristics of the surrounding region. *IM* values are usually determined by seismologists.
- *Engineering Demand Parameter (EDP)*: a characterization of the response of a system to the *IM*. The definition of the *EDP* depends on the system of interest and is commonly related to either the structural system (e.g. story drift, strength deterioration, etc.) or, as is

the case with this study, the soil matrix below the structure (e.g. settlement, lateral spread, slope stability, etc.).

- *Damage Measure (DM)*: a description of the physical condition of the system and its components as a function of the *EDP*. Defined in terms of the consequences of the damage (e.g. necessary repairs, degradation of expected performance under future earthquakes, etc.)
- *Decision Variable (DV)*: a characterization of the risk associated with the *DM*. The *DV* translates damage measures into quantities that relate to risk management decisions concerning economic loss and life safety (e.g. casualties, down time, repair costs, etc.)

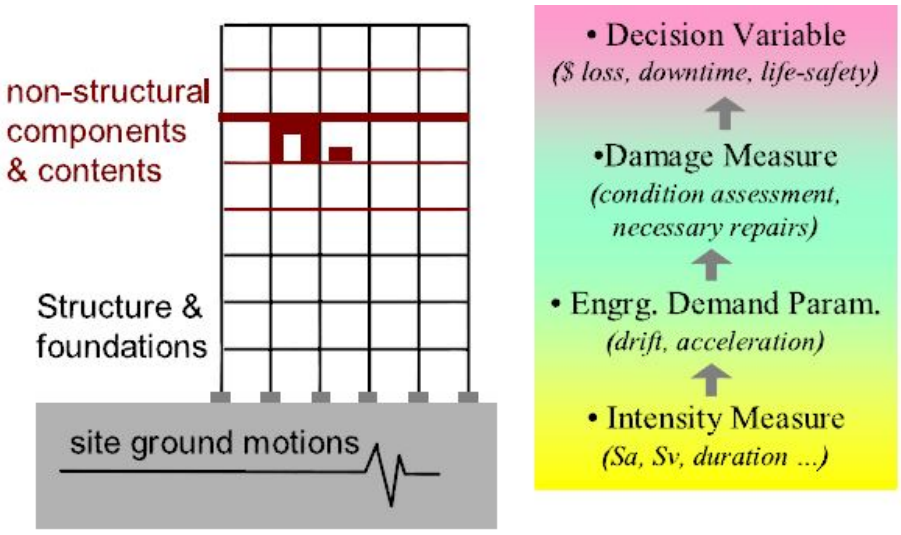

Figure 4-5: Components of performance-based earthquake assessment methodology (after Deierlein et al., 2003)

The PBEE framework is structured similarly to a PSHA, in that the mean annual rate of exceedance (λ) of a certain outcome is computed for a given range of input scenarios. For

example, the mean annual rate of exceedance of a certain *EDP* is computed from the possible ranges of a certain *IM*. The equation used to compute λ_{EDP} is given as:

$$\lambda_{EDP} = \int P\left[EDP > edp \middle| IM = im_j \right] \Delta\lambda_{IM} \tag{4.6}$$

where $P\left[a \middle| b \right]$ represents the conditional probability of a given b and $\Delta\lambda_{IM}$ is the incremental mean annual rate of exceedance of the *IM*. This process is repeated sequentially for each component until the mean annual rate of exceedance of a *DV* (λ_{DV}) is determined. The complete process of the PBEE framework can be summarized as:

$$\lambda_{DV} = \iiint P\left[DV \middle| DM \right] dP\left[DM \middle| EDP \right] dP\left[EDP \middle| IM \right] d\lambda_{IM} \tag{4.7}$$

and can be estimated numerically as:

$$\begin{aligned} \lambda_{DV} = \sum_{k=1}^{N_{DM}} \sum_{j=1}^{N_{EDP}} \sum_{i=1}^{N_{IM}} & P\left[DV > dv \middle| DM = dm_k \right] \times \\ & P\left[DM = dm_k \middle| EDP = edp_j \right] P\left[EDP = edp_j \middle| IM = im_i \right] \Delta\lambda_{im_i} \end{aligned} \tag{4.8}$$

where N_{DM}, N_{EDP}, and N_{IM} are the number of increments of *DM*, *EDP*, and *IM*, respectively. If equation (4.8) is iterated for a range of *DV*s, a hazard curve is obtained that clearly communicates the likelihood of exceeding various levels of the defined *DV* (see Figure 4-6). Once λ_{DV} has been estimated, decision makers can begin the decision making process for seismic risk mitigation. Another benefit of the PBEE framework is that λ values are established for each component while calculating λ_{DV}, providing engineers with a clear understanding of the seismic hazard for a given *EDP*.

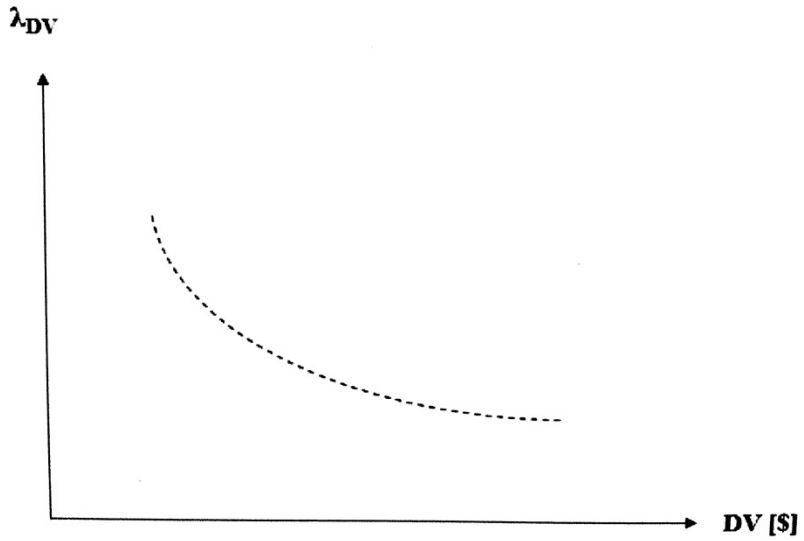

Figure 4-6: Example hazard curve for a given *DV*

4.4 Chapter Summary

The goal of earthquake engineering is to design a structure that will perform at or above a predetermined standard in a given seismic event. Predicting the seismic even that is most likely to occur at a site can be difficult. DSHA, the process of selecting a "worst case" scenario, has traditionally been used to determine seismic hazard. However, the use of DSHA can lead to problems like poor communication between stakeholders or over-design due to the selection of unrealistically high seismic hazards. PSHA, the process of evaluating the likelihood of all possible seismic scenarios, is slowly beginning to replace deterministic methods, but has not yet been widely embraced by engineers due to the complex nature of the analysis. The PBEE framework, developed by PEER, seeks to improve seismic risk decision-making through assessment and design methods that are more transparent, scientific, and informative to stakeholders than current prescriptive approaches (Deierlein et al. 2003). The PBEE framework empowers decision makers to have more control over the design process and provides transparency between stakehold

5 FREE-FIELD POST LIQUEFACTION SETTLEMENT

The densification of soil following a seismically induced liquefaction event can result in serious consequences for both the safety and economic stability of the affected region. Differential settlement in the ground beneath a structure, while rarely life-threatening, can lead to structural and architectural damages that result in costly repairs (Bray et al. 2013). Settlement can cause utility lines to shear, creating power outages and disruption in water supply. Limited access to power and fresh water can significantly increase the risk of illness and affect proper functioning of health facilities (Watson, Gayer, and Connolly 2007). The prediction of settlement effects, leading to adequate design of structures and infrastructure, is a key component of preventing damage and facilitating recovery from a seismic event.

5.1 Understanding Settlement

The in-situ state of a soil matrix is a function of the depositional environment in which it was placed. Some depositional mechanisms (e.g. Alluvial, Aeolian, Colluvial, etc.) result in loosely placed material with large void spaces between soil particles. Seismic loading induces large strains that act as a compaction mechanism, causing the soil particles to realign themselves in a denser, more stable configuration. As the soil densifies, the reduction in void space can cause large volumetric strains (see Figure 5-1). This change in volume resulting from soil densification is called settlement and is usually manifested at the ground surface by a change in

ground surface elevation (see Figure 5-2). As is described in greater detail below, the total settlement manifested at the ground surface is a function of the thickness of the loose soil layer and the strain incurred by the seismic loading. In areas where the thicknesses of loose soil layers are variable, as is often the case for the depositional environments mentioned above, differential settlement (i.e., variable changes in ground surface elevation across a site) can occur. Differences in total settlement can be large and pose a serious threat to structures and infrastructure. When a building, utility line, or other structure with shallow foundations spans a zone of differential settlement, damage can occur. Mild cases result in architectural cracking, while more severe cases can result in damage to structural members, tilting, severed utilities, and other similar damages (see Figure 5-3 and Figure 5-4).

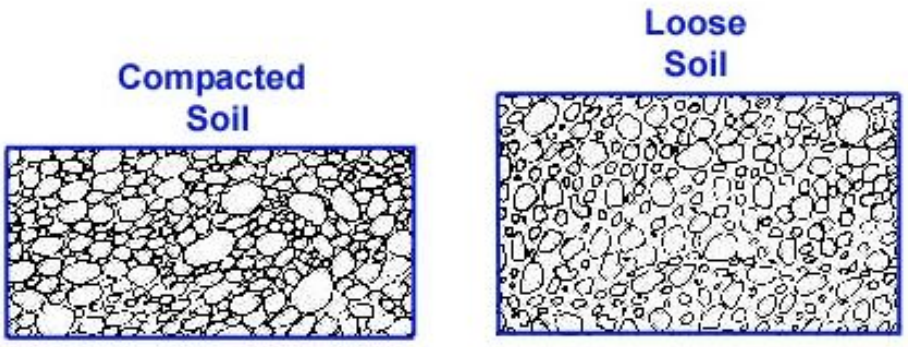

Figure 5-1: Example of volumetric change resulting from soil densification

Figure 5-2: Example of ground elevation change from settlement (after Tsukamoto and Ishihara 2010)

Figure 5-3: Collapsed stairway resulting from settlement (after Tsukamoto and Ishihara 2010)

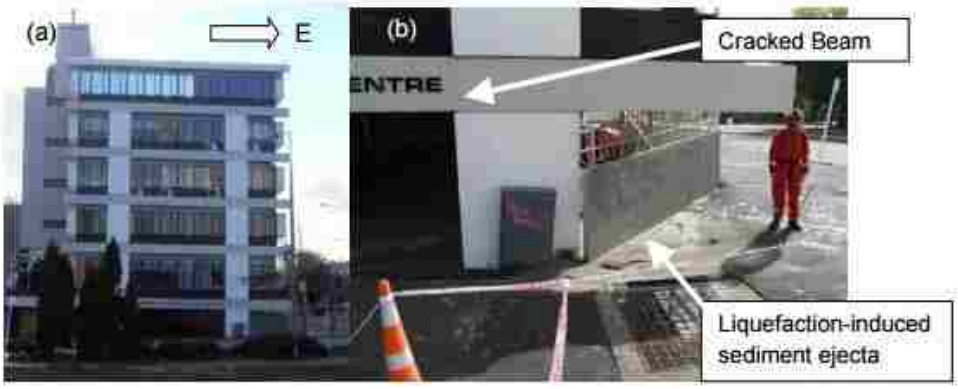

Figure 5-4: (a) Building tilt and (b) structural damage resulting from differential settlement (after Bray et al. 2013)

The risk associated with differential settlement should not be underestimated. Although rarely posing a serious risk to life safety (with the possible exception of the consequences of severed utilities, as mentioned previously), even mild cases of settlement can result in expensive repairs. In severe cases, widespread cracking, tilting, and damage to structural members can result in total economic loss. Mitigating the effects of differential settlement through proper design is an essential step to controlling the economic risk associated with seismic events.

It should be noted that soil deformations commonly occur beneath structures during earthquakes due to other mechanisms related to soil-foundations-structure interaction (SFSI) and loss of soil through piping, also known as liquefaction ejecta (Bray and Dashti 2014). All post-liquefaction settlement discussed in this study refers to free-field settlement from soil reconsolidation and does not consider SFSI mechanisms or volume change due to liquefaction ejecta.

Deep foundation structures are also subjected to significant risk during a liquefaction-induced settlement event. As soil moves downward relative to a pile, load is transferred from the soil to the pile. This load is known as pile downdrag (Lambe, Garlanger, and Leifer 1974).

Downdrag forces can lead to overloading of the foundation system, possibly resulting in pile failure.

5.2 Computing Settlement

The accurate estimation of the risk of settlement is the first step of providing an adequate design. The PBEE framework, explained in the previous chapter, provides the necessary context to complete this step. Many settlement estimation methods have been presented, with some more generally accepted than others. There are two predominant types of models: numerical and semiempirical. Numerical models usually take the form of finite element or finite difference analyses, while semiempirical models are developed based on laboratory tests, field tests, and performance data (case histories). Numerical models can be problematic to perform due to the difficulty of determining appropriate input model parameters. Resultantly, semiempirical models constitute the current state of practice for settlement assessments (Cetin et al. 2009).

Two semiempirical methods that have been generally accepted are the Cetin et al. (2009) and the Ishihara and Yoshimine (1992) methods, which are the focus of this study. Each method, including its incorporation into the PBEE framework, is described in this section. It should be noted that these methods predict free-field settlements only. In other words, these methods do not apply to soils experiencing additional loading from structures or other elements. Each method is incorporated using numerical estimation to simplify computations, as discussed in the previous chapter.

5.2.1 Cetin et al. Method

The derivation of the Cetin et al. (2009) method stemmed from a desire to create a more reliable and accurate semiempirical model, considering that some of the predictions by currently existing models were documented to exhibit error exceeding a factor of 2 (Bilge and Cetin 2007). To address the lack of accuracy demonstrated by existing semiempirical models, Cetin et al. (2009) derived a new semiempirical model by compiling the data of 49 high-quality, cyclically induced ground settlement case histories from seven different earthquakes. These case histories were chosen from a pool of over 200, filtered to exclude cases exhibiting poor data quality or completeness. Examples of filtering criteria include: poor site soil profile definitions, inconsistently reported ground deformations, sites with piles or improved soil layers, sites with sloping ground (gradient > 5%), soil profiles consisting of exclusively cohesive material, and sites with large reported lateral deformations (>1.5 m).

The result of the Cetin et al. (2009) study was a new semiempirical model for the assessment of cyclically induced straining of saturated cohesionless soils using either a chart solution, shown in Figure 5-5, or the closed-form solution presented in Equation (5.10). The closed-form solution will be explained in detail below. Cetin compared the predictions of this new semiempirical model with those of existing models (Tokimatsu and Seed 1984, Ishihara and Yoshimine 1992, Shamoto et al. 1998, and Wu and Seed 2004) and found that the new model correlated better to measured settlements (in some cases almost 100% better), was characterized by a smaller standard deviation, and demonstrated a model error of just 15% (Cetin et al. 2009).

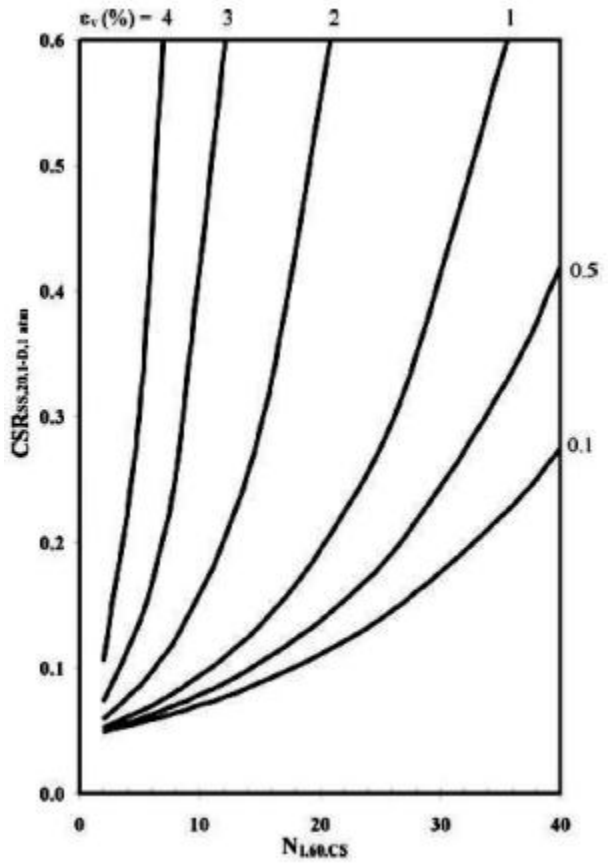

Figure 5-5: Cetin et al. (2009) method for predicting volumetric strain

The incorporation of the Cetin et al. (2009) model into the PBEE framework involves creating hazard curves of strain and, subsequently, settlement for each sublayer in a soil profile. First, a cyclic stress ratio (CSR) is computed for N_{req} values from 1 to 49 using the following relationship provided by Mayfield et al. (2010):

$$CSR = CRR(N_{req}) \tag{5.1}$$

where CRR is the cyclic resistance ratio (the soil's resistance to liquefaction initiation). It should be noted that the factor of safety against liquefaction (FS_{liq}) is defined as the ratio of CRR to CSR. Therefore, solving for CSR as a function of the CRR value required to prevent liquefaction

is an appropriate replacement for FS_{liq}. Mayfield (2010) showed that the CRR for a given soil layer can be computed as

$$CRR = \exp\left[\frac{N_{req}^{Cetin} - 29.06\ln M_w - 3.82\ln\left(\frac{\sigma_{vo}^{'}}{p_a}\right) + 15.25 + \sigma_e \Phi^{-1}(P_L)}{13.79}\right] \tag{5.2}$$

where M_w is earthquake moment magnitude, $\sigma_{vo}^{'}$ is initial vertical effective stress, p_a is atmospheric pressure (in same units as $\sigma_{vo}^{'}$), σ_e is the estimated model and parameter uncertainty (standard deviation), and $\Phi^{-1}(P_L)$ is the inverse standard cumulative normal distribution of the probability of liquefaction (P_L). Cetin et al. (2004) used the simplifying assumptions of $M_w = 7.5$, $\sigma_{vo}^{'} = 1$ atm. If these assumptions are combined with the assumption that P_L = 50% (focusing solely on the median liquefaction triggering curve), then Equation (5.2) can be simplified as

$$CRR = \exp\left[\frac{N_{req}^{Cetin} - 29.06 * \ln(7.5) + 15.25}{13.79}\right] \tag{5.3}$$

Cetin et al. (2004) showed that if parametric uncertainty is excluded, the coefficients 29.06, 15.25, and 13.79 change to 29.53, 16.85, and 13.32, respectively. Once the CSR has been computed, it is adjusted to account for multidirectional shaking effects. This adjustment was shown by Cetin et al. (2009) to be computed as

$$CSR_{SS,20,1D,1atm} = \frac{CSR_{field}}{K_{md} K_{M_W} K_{\sigma}} \tag{5.4}$$

where CSR_{field} is the CSR computed in Equation (5.1), K_{md} is the correction factor to convert the multidirectionally applied CSR_{field} value to the value of a unidirectionally applied laboratory CSR, K_{M_W} is the correction factor to convert the CSR to a value corresponding to a $M_w = 7.5$ earthquake, and K_σ is the correction factor used to account for the nonlinear increase in cyclic resistance to shear stresses with increasing confining effective stresses. Because the assumptions $M_w = 7.5$ and $\sigma'_{vo} = 1$ atm were used, the last two correction factors can be ignored, and Equation (5.4) can be simplified as

$$CSR_{SS,20,1D,1atm} = \frac{CSR_{field}}{K_{md}} \tag{5.5}$$

where K_{md} is computed as

$$K_{md} = 0.361\ln(D_R) - 0.579 \tag{5.6}$$

where D_R is the relative density (in percent) of the soil layer. Once the $CSR_{SS,20,1D,1atm}$ values for each N_{req} have been obtained for each sublayer in the soil profile, the strain hazard curves for each sublayer can be calculated.

The methodology used to compute the strain hazard curves is that of the PEER framework, which computes the mean annual rate of exceeding some engineering design parameter (EDP) given some intensity measure(s) (IM). Kramer et al. (2014) showed that the mean annual rate of exceeding some value of EDP = edp is given by

$$\lambda_{EDP}(edp) = \sum_{i=1}^{N_{IM}} P\left[EDP > edp \middle| IM = im_i\right] \Delta\lambda_{IM}(im_i) \tag{5.7}$$

Kramer et al. (2008) and Kramer et al. (2014) demonstrated that applying the PEER framework to the analysis of liquefaction-induced settlement yields

$$\lambda_{\varepsilon_{vi}} = \sum_{m=1}^{N_{CSR}} P\left[\varepsilon_{vi} > \varepsilon_{vi}^{*} \middle| CSR_i, N_i\right] \Delta\lambda_{CSR} \tag{5.8}$$

where ε_{vi} is the strain of a given sublayer, CSR_i is the $CSR_{SS,20,1D,1atm}$ computed in Equation (5.5), N_i is the $N_{1,60,CS}$ computed from the blow count of a standard penetration test (SPT), and $\Delta\lambda_{CSR}$ is the incremental joint mean annual rate of exceedance for the given CSR. Furthermore, Kramer et al. (2008) and Kramer et al. (2014) explained that

$$P\left[\varepsilon_v > \varepsilon_v^{*} \middle| CSR, N\right] = \Phi\left[\frac{\mu_{\ln\varepsilon_v} - \ln\varepsilon_v^{*}}{\sigma_{\ln\varepsilon_v}}\right] \tag{5.9}$$

where $\Phi(\cdot)$ is the standard normal cumulative distribution function, $\mu_{\ln\varepsilon_v}$ is the mean value of $\ln\varepsilon_v$, and $\sigma_{\ln\varepsilon_v}$ is the standard deviation of the probability function that was found to be 0.61 by Cetin et al. (2009). Cetin et al. (2009) showed that the mean value of $\ln\varepsilon_v$ can be computed as

$$\ln(\varepsilon_v) = \ln\left[1.879\ln\left[\frac{780.416\ln(CSR_{SS,20,1D,1atm}) - N_{1,60,CS} + 2,442.465}{636.613N_{1,60,CS} + 306.732}\right] + 5.583\right] \pm 0.689 \tag{5.10}$$

$$\lim: 5 \le N_{1,60,CS} \le 40, \quad 0.05 \le \mathrm{CSR}_{SS,20,1D,1atm} \le 0.60$$

This process is repeated for strains ranging from 0.1% to 15%, creating a hazard curve of strains with their associated mean annual rate of exceedance. After comparing the predicted strains to those observed in case histories, Cetin et al. (2009) introduced calibration coefficients to improve the accuracy of model predictions. It was observed that the Cetin et al. (2009) model underestimates settlements and should be corrected by a factor of 1.15.

The strains computed in Equation (5.10) do not consider the uncertainty in the soil response, (i.e., the likelihood that the soil will liquefy given some level of ground shaking). This uncertainty is represented by the probability of liquefaction (P_L) that was shown by Ulmer et al. (2015) to be computed as

$$P_L = \Phi\left[-\frac{N_{site} - N_{req}}{4.21}\right] \tag{5.11}$$

If parametric uncertainty is ignored, the denominator of Equation (5.11) becomes 2.7. To account for P_L the mean value of $\ln \varepsilon_v$ computed in Equation (5.10) is multiplied by the P_L computed in Equation (5.11). The analysis in this study was performed without considering P_L for simplicity.

Kramer et al. (2008) explained that direct computation of vertical strain distributions from the relationship provided in Equation (5.9) has been found to produce significant probabilities of unrealistically large strain values and that this was caused by the assumption of lognormally distributed vertical strains. For low values of $N_{1,60,CS}$, the slope of the lognormal function increased dramatically, resulting in infinitely increasing values of strain with decreasing values of $N_{1,60,CS}$. Extensive experimentation, however, has shown that soil has a limited ability to densify and must be governed by some limiting maximum strain. Huang (2008) performed a study to find the maximum limiting value of vertical strain using the deterministic soil models of Tokimatsu and Seed (1987), Ishihara and Yoshimine (1992), Shamoto et al. (1998), and Wu and Seed (2004). A weighted average of the four relationships was used to create a relationship for mean limiting strain as shown in Figure 5-6.

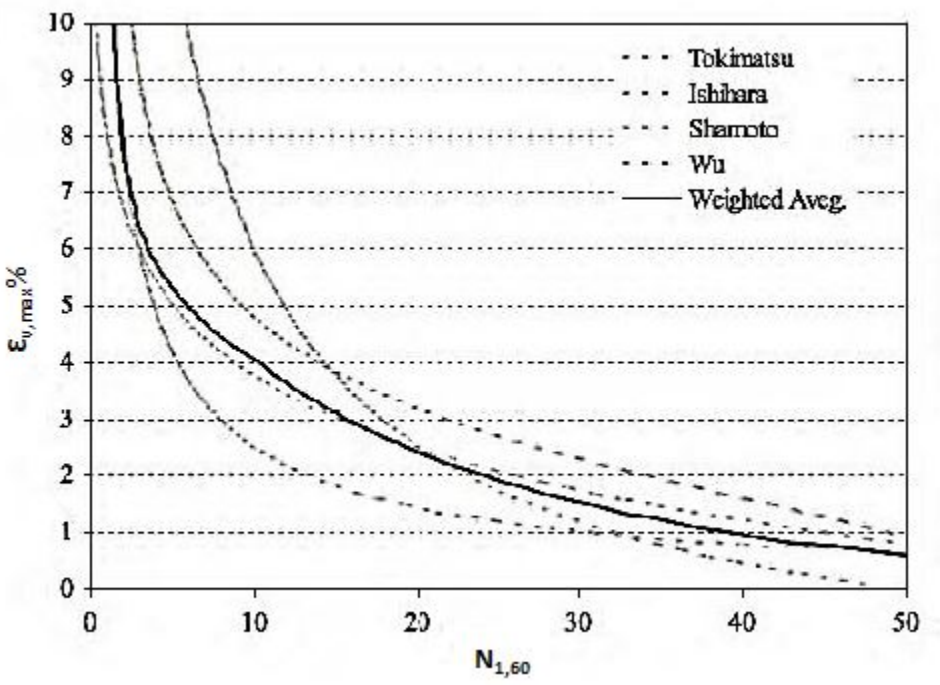

Figure 5-6 Mean limiting strain relationship derived from deterministic vertical strain models (after Huang, 2008)

Kramer et al. (2014) showed that this relationship can be approximated by

$$\overline{\varepsilon}_{v,\max}(\%) = 9.765 - 2.427 \ln\left[(N_1)_{60,CS}\right] \tag{5.12}$$

The approximation found in Equation (5.12) was used for this study. Huang (2008) suggested that, because the maximum strain relationship is approximate, $\overline{\varepsilon}_{v,\max}$ be uniformly distributed over a range of $0.5^* \overline{\varepsilon}_{v,\max}$ to $1.5^* \overline{\varepsilon}_{v,\max}$. This is done to account for the scatter observed in the relationships presented in Figure 5-6. In this study, $\overline{\varepsilon}_{v,\max}$ was distributed by increments of $0.02^* \overline{\varepsilon}_{v,\max}$.

Once the hazard curves are computed and weighted according to the recommendations of Huang (2008), settlement hazard curves are computed. An explanation of the settlement computation is provided later in this section.

5.2.2 Ishihara and Yoshimine Method

Extensive laboratory testing of the volume change characteristics of sand under undrained cyclic loading (Lee and Albaisa 1974, Tatsuoka et al. 1984, and Nagase and Ishihara 1988) demonstrated that maximum shear strain is a key parameter affecting post-liquefaction volumetric strain. Ishihara and Yoshimine (1992) developed a procedure for estimating ground settlements based on the maximum shear strain, which is a function of FS_{liq}. Extensive simple shear tests on sand samples subjected to horizontal, undrained shear stresses with irregular time histories were performed at the University of Tokyo, the results of which were combined with the data provided by Nagase and Ishihara (1988) to create the database used as the basis for the derivation of the Ishihara and Yoshimine (1992) method. Examination of this data resulted in the establishment of a family of relationships, presented in Figure 5-7, in which the volumetric strain can be computed as a function of FS_{liq}. The numerical approximations of these relationships, as presented by Idriss and Boulanger (2008) is provided in Equations (5.15) through (5.20).

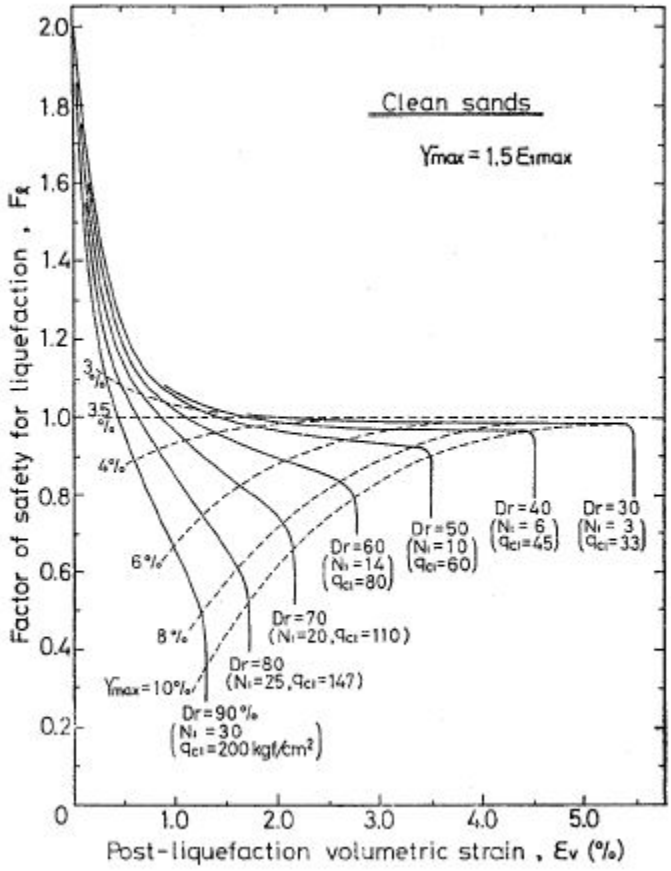

Figure 5-7: Ishihara and Yoshimine method for predicting volumetric strain (Ishihara and Yoshimine 1992)

The incorporation of the Ishihara and Yoshimine (1992) method into the PBEE framework is similar to the Cetin et al. (2009) method, except that instead of computing strains as a function of CSR, strains are computed as a function of FS_{liq}. Hazard curves of strain and settlement are computed for each sublayer in a soil profile. The FS_{liq} is computed for N_{req} values from 1 to 49 using the following relationship provided by Ulmer et al. (2015):

$$FS_{liq} = \exp\left[\left(\frac{N_{1,60,CS} - N_{req}}{14.1}\right) + \left(\frac{N_{1,60,CS}{}^2 - N_{req}{}^2}{126^2}\right) - \left(\frac{N_{1,60,CS}{}^3 - N_{req}{}^3}{23.6^3}\right) + \left(\frac{N_{1,60,CS}{}^4 - N_{req}{}^4}{25.4^4}\right)\right] \quad (5.13)$$

Once the FS_{liq} values for each N_{req} have been obtained for each sublayer in the soil profile, the strain hazard curves for each sublayer can be computed. This is done using the PEER framework as explained in the Cetin et al. (2009) method. Equation (5.8) can be adjusted to account for the change in intensity measure (from CSR to FS_{liq}) as expressed by

$$\lambda_{\varepsilon_{vi}} = \sum_{m=1}^{N_{FSliq}} P\left[\varepsilon_{vi} > \varepsilon_{vi}^{*} \left| FS_{liq_i}, N_i \right.\right] \Delta\Lambda FS_{liq} \tag{5.14}$$

where Λ is the mean annual rate of non-exceedance.

Equation (5.9) is utilized again, with $\sigma_{\ln \varepsilon_v} = 1.12$. Ishihara and Yoshimine (1992) compute the mean value of ε_v as

$$\varepsilon_v = 1.5 \cdot \exp\left(-0.369\sqrt{(N_1)_{60,CS}}\right) \cdot \min\left(0.08, \gamma_{\max}\right) \tag{5.15}$$

where $\min(\cdot)$ signifies the use of the minimum value found within the parenthesis, and $\gamma_{\max}$ is the maximum shear strain. The maximum shear strain is used because of the asymptotic nature of the strain curves and is computed as

$$\gamma_{\max} = 0 \text{ if } FS_{liq} \geq 2 \tag{5.16}$$

$$\gamma_{\max} = \min\left(\gamma_{\lim}, 0.035(2-FS_{liq})\left(\frac{1-F_\alpha}{FS_{liq}-F_\alpha}\right)\right) \quad \text{if } 2 > FS_{liq} > F_\alpha \tag{5.17}$$

$$\gamma_{\max} = \gamma_{\lim} \text{ if } FS_{liq} \leq F_\alpha \tag{5.18}$$

where $\gamma_{\lim}$ is computed as

$$\gamma_{\lim} = 1.859\left(1.1 - \sqrt{\frac{N_{1,60,CS}}{46}}\right)^3 \geq 0 \tag{5.19}$$

and F_α is computed as

$$F_\alpha = .032 + 4.7D_R - 6.0(D_R)^2 \tag{5.20}$$

where D_R is the relative density of the sublayer as a decimal.

This process is repeated for strains ranging from 0.1% to 15%, creating a hazard curve of strains with their associated mean annual rate of exceedance. The strains computed in Equation (5.15) are adjusted by a correction coefficient of 0.9 according to the recommendations provided by Cetin et al. (2009).

It should be mentioned that the strains computed in Equation(5.15) do not consider P_L. To account for P_L, the following equation can be applied as demonstrated by Ulmer et al. (2015):

$$P_L = \Phi\left[\ln\left(FS_L^{-3.61}\right)\right] \tag{5.21}$$

If parametric uncertainty is ignored, the exponent in Equation (5.21) becomes -7.69. To account for P_L, the mean value of $\ln \varepsilon_v$ computed in Equation (5.15) is multiplied by the P_L computed in Equation (5.21). The analysis in this study was performed without considering P_L for simplicity.

The maximum strain considerations introduced by Huang (2008) are also considered, with $\overline{\varepsilon}_{v,\max}$ uniformly distributed over a range of $0.5*\overline{\varepsilon}_{v,\max}$ to $1.5*\overline{\varepsilon}_{v,\max}$. In this study, $\overline{\varepsilon}_{v,\max}$ was distributed by increments of $0.02*\overline{\varepsilon}_{v,\max}$.

Once the hazard curves are computed and weighted as outlined above, settlement hazard curves are computed. An explanation of the settlement computation is provided below.

5.2.3 Settlement Computation

The method used to compute the settlement from the strain hazard curves is the method proposed by Cetin et al. (2009). Because settlement is a function of strain, depth, and thickness of the soil layer, it is compatible with the Cetin et al. (2009) and Ishihara and Yoshimine (1992) methods. Cetin et al. (2009) introduced an equivalent strain for the entire soil profile, defined as

$$\varepsilon_{v,\text{eqv.}} = \frac{\sum \varepsilon_{v,i} t_i DF_i}{\sum t_i DF_i} \tag{5.22}$$

where $\varepsilon_{v,eqv.}$ is the equivalent strain for the soil profile, $\varepsilon_{v,i}$ is the strain for a given sublayer in the soil profile, t_i is the thickness of the given sublayer, and DF_i is the depth weighting factor of the given sublayer and is computed by

$$DF_i = 1 - \frac{d_i}{z_{cr} = 18m} \tag{5.23}$$

where d_i is the depth of the given sublayer. Cetin (2009) provides 3 reasons for applying a depth weighting factor: (1) unfavorably higher void ratios in shallower sublayers of soil due to upward seepage; (2) reduced shear stresses and number of shear stress cycles in deeper soil layers due to initial liquefaction of surficial layers; and (3) possible bridging effects due to nonliquefied soil layers. Once the equivalent strain has been computed using Equation (5.22), the settlement for the soil profile is then computed as

$$s_{estimated} = \varepsilon_{v,eqv.} \sum t_i \tag{5.24}$$

where $s_{estimated}$ is the computed settlement for the soil profile. This calculation is repeated for each incremental strain in the strain hazard curve. The result is a settlement hazard curve, showing the likelihood of exceedance of a given magnitude of settlement.

5.3 Chapter Summary

Post-liquefaction settlement poses a serious threat to areas affected by seismic events, especially when differential settlement is likely. Differential settlement can cause tilting, cracking, structural damage, and utility line ruptures. While the risk of casualties resulting from settlement is low, the consequences of settlement include costly repairs and disruption of services that can threaten the economic stability of a region following a seismic event. The estimation of risk associated with post-liquefaction settlement is an important step in the seismic design process, facilitating the mitigation of damages during an event and aiding infrastructure survival to assist in the recovery process. This study presents the incorporation of the Cetin et al. (2009) and Ishihara and Yoshimine (1992) methods into the PEER PBEE framework to create fully probabilistic settlement estimation models. The result of these models is a settlement hazard curve presenting the risk of exceeding a range of settlement values.

6 COMPARISON OF PERFORMANCE-BASED, PSEUDO-PROBABILISTIC, AND SEMI-PROBABILISTIC APPROACHES TO SETTLEMENT ANALYSIS

The previous chapter presented a fully probabilistic procedure for predicting post-liquefaction free-field settlements using the PEER framework. The advantages of the PEER framework have been presented in Chapter 4. The incorporation of settlement estimation models into the PBEE framework provides a valuable resource for seismic design. Transitioning design standards from conventional methods to probabilistic methods is the next step in the evolution of seismic design. However, because of the complex nature of probabilistic theory, many engineers are hesitant to make the change. Development of the fully probabilistic method outlined in this study is considered a stepping stone for future work in creating a simplified probabilistic approach for settlement estimation. The goal of a simplified method is to make fully probabilistic methods readily accessible, regardless of an individual's familiarity with the complexity of probabilistic theory. Creating a simple, understandable approach for implementing probabilistic methods will facilitate the progression of seismic design.

As part of the incorporation of settlement estimation models into the PEER framework, additions were made to the analysis tool *PBLiquefY*, originally introduced by Franke, Wright, and Hatch (2014). *PBLiquefY* was used to complete this study and is described in greater detail below. The application of *PBLiquefY* to create a simplified settlement estimation tool is briefly discussed.

Finally, this study will quantify the differences in settlement estimations of the pseudo-probabilistic, semi-probabilistic, and fully-probabilistic methods. While other studies have focused on quantifying and comparing results for different liquefaction effects (i.e., liquefaction triggering, lateral spread, etc.), no comparison of settlement estimations has been performed. By quantifying and comparing the results of conventional and probabilistic settlement estimations, the deficiencies of conventional methods are exposed and the need for a transition to fully-probabilistic design is highlighted.

6.1 Analysis Methods

As described above, the fully-probabilistic procedure is compared to conventional methods. These conventional methods are often referred to as pseudo-probabilistic methods. These methods are described briefly below. Also, the fully-probabilistic procedure is compared to a semi-probabilistic method, which is also described below.

6.1.1 Pseudo-Probabilistic Methods

Conventional design methods involve choosing a "worst-case" seismic event and then computing the effects associated with that event through established correlations. As explained in Chapter 5, both the Ishihara and Yoshimine (1992) method and the Cetin et al. (2009) method involve computing FS_{liq} or CSR and then using those values to compute settlement. Pseudo-probabilistic methods involve obtaining a design earthquake magnitude through probabilistic methods, followed by deterministically computing FS_{liq} or CSR, which is then used to deterministically estimate settlement. The design earthquake magnitude can be specified as either the mean (i.e., average) or modal (i.e., most commonly occurring) magnitude. While pseudo-

probabilistic methods do consider some of the uncertainty in ground motions, they ignore the uncertainty inherent in both the triggering of liquefaction and the severity of the resulting effects.

6.1.2 Semi-Probabilistic Methods

A semi-probabilistic analysis involves computing FS_{liq} using probabilistic methods and then computing settlement using deterministic methods. While this method considers the uncertainty of liquefaction triggering, it ignores the uncertainty of the resulting effects.

6.2 Methodology

An adequate comparison of the various design methods requires an effort to account for the uncertainty of both regional seismicity level and local soil conditions. The methods used to incorporate these variations into the study are described below.

6.2.1 Soil Profiles

Settlements are computed using five theoretical soil profiles. The profiles consist of two m of lean clay underlain by 10 m of silty sand (see Figure 6-1), broken into 1-m-thick sublayers. Soil properties such as fines content, water content, and unit weight for each sublayer are uniform for all sublayers. All soil properties are maintained constant across the five profiles, with the exception of the SPT blow counts (N values) for each sublayer. Each profile exhibits a different trend in N value with depth. The general trends for each profile are presented in Table 6-1. A plot of the trends of each profile with depth is provided in Figure 6-2. An example of a complete soil profile (Soil Profile 1) is shown in Table 6-2.

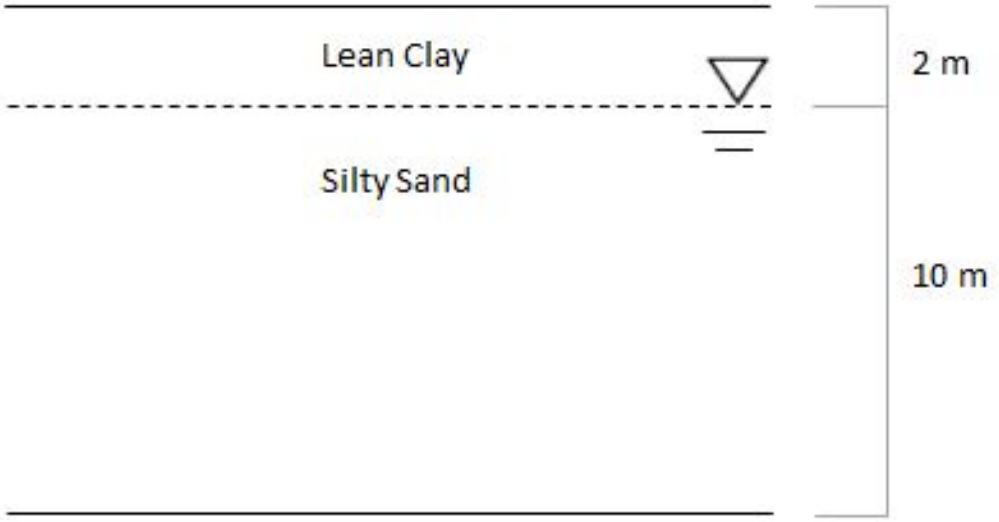

Figure 6-1: Theoretical soil profile used in analyses

Table 6-1: General trends of soil profile N values

Profile	Trend
1	Increasing with depth
2	Decreasing with depth
3	Consistently low
4	Consistently high
5	Random

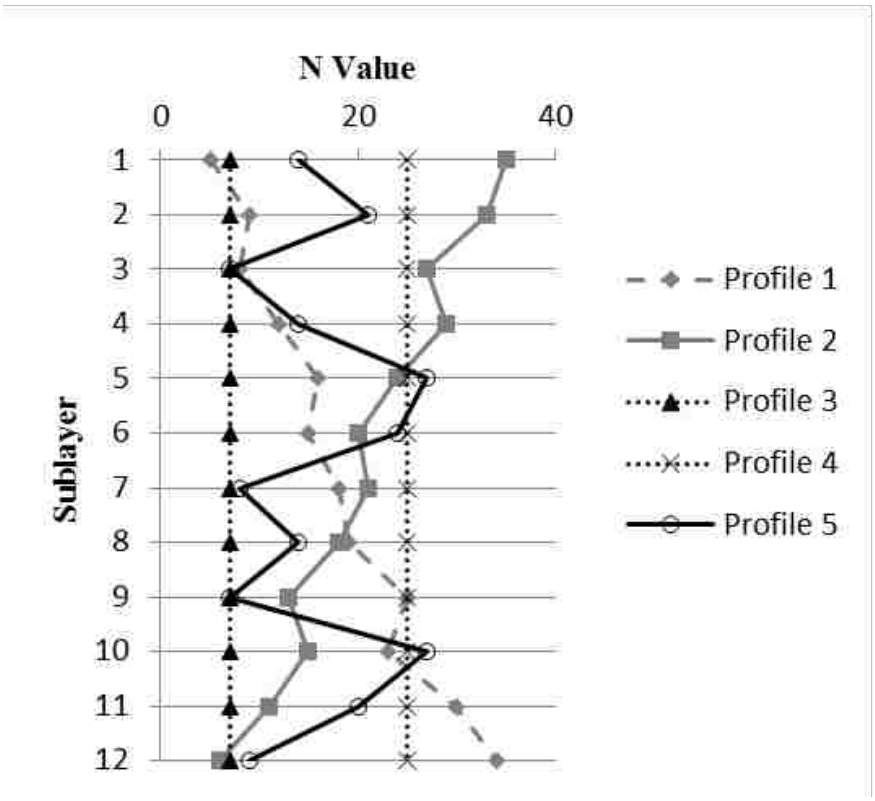

Figure 6-2: Soil profile trends with depth

Table 6-2: Soil profile properties

Sublayer	Bottom Depth (m)	Thickness (m)	Sample Depth (m)	Soil Type	SPT Value	PI(%)	LL(%)	Wc(%)	FC(%)	Unit Weight (kn/m^3)
1	1	1	0.5	Lean Clay	5	0	30	30	10	19.62
2	2	1	1.5	Lean Clay	9	0	30	30	10	19.62
3	3	1	2.5	Silty Sand	8	0	30	30	10	19.62
4	4	1	3.5	Silty Sand	12	0	30	30	10	19.62
5	5	1	4.5	Silty Sand	16	0	30	30	10	19.62
6	6	1	5.5	Silty Sand	15	0	30	30	10	19.62
7	7	1	6.5	Silty Sand	18	0	30	30	10	19.62
8	8	1	7.5	Silty Sand	19	0	30	30	10	19.62
9	9	1	8.5	Silty Sand	25	0	30	30	10	19.62
10	10	1	9.5	Silty Sand	23	0	30	30	10	19.62
11	11	1	10.5	Silty Sand	30	0	30	30	10	19.62
12	12	1	11.5	Silty Sand	34	0	30	30	10	19.62

6.2.2 Site Locations

Ten cities are examined, in part because they represent a wide range of seismicity levels and in part because they have been used in other performance-based studies (Kramer and Mayfield 2007, Franke et al. 2014). A list of the selected cities, their locations, and their corresponding mean/modal magnitudes is presented in Table 6-3.

Table 6-3: Selected cities used in analyses

City	Latitude	Longitude	Mean Magnitude (475 T_R / 2475 T_R)	Modal Magnitude (475 T_R / 2475 T_R)	PGA (g) (475 T_R / 2475 T_R)
Butte	46.003	-112.533	6.03 / 6.05	5.20 / 6.20	0.08344 / 0.1785
Charleston	32.776	-79.931	6.61 / 7.00	7.36 / 7.37	0.1513 / 0.7287
Eureka	40.802	-124.162	7.33 / 7.45	6.99 / 6.99	0.6154 / 1.4004
Memphis	35.149	-90.048	6.98 / 7.24	7.70 / 7.70	0.1604 / 0.5711
Portland	45.523	-122.675	7.24 / 7.31	9.00 / 9.00	0.1990 / 0.4366
Salt Lake City	40.755	-111.898	6.75 / 6.90	6.99 / 6.99	0.2126 / 0.6717
San Francisco	37.775	-122.418	7.31 / 7.44	7.99 / 7.98	0.4394 / 0.7254
San Jose	37.339	-121.893	6.66 / 6.66	6.60 / 6.60	0.4560 / 0.6911
Santa Monica	34.015	-118.492	6.74 / 6.84	7.21 / 7.22	0.3852 / 0.7415
Seattle	47.53	-122.3	6.75 / 6.88	6.60 / 6.80	0.3110 / 0.6432

6.2.3 Return Periods

The seismic event used as the basis for design often depends on the type of structure. Critical structures (e.g. hospitals, nuclear facilities, etc.) are designed to withstand a higher level of loading, represented by an event with a longer return period. This study examines return periods of 475 years and 2475 years, representing relatively low and high levels of seismic loading, respectively.

6.2.4 PBLiquefY

The creation of tools to simplify the procedure of probabilistic analysis is essential in the process of transitioning from conventional design methods. Many practicing engineers simply do not have the time or the resources to immerse themselves in probabilistic theory. Simplified tools can provide the power of fully probabilistic analyses with little required investment, thereby removing the foremost obstacle to the adoption of probabilistic methods in seismic design standards. *PBLiquefY* is a probabilistic analysis tool that has been created to assist engineers unfamiliar with probabilistic theory in completing fully probabilistic analyses. It was originally created by Alexander Wright under the direction of Dr. Kevin Franke (Franke, Wright, and Hatch 2014) and has been updated and expanded for this study.

As mentioned previously, the ultimate goal of this research is to facilitate the creation of simplified tools that provide all engineers with instant access to probabilistic methods. One proven method of accomplishing this goal is through the creation of hazard maps. Hazard maps are generated by batch analyses of a location grid using a tool such as *PBLiquefY*. Analyses are performed with a reference soil profile and contour maps are created showing the hazard for all locations on the map. For a more detailed explanation of hazard maps and their place in probabilistic design, see Ulmer (2015) and Ekstrom (2015). For the purpose of this study, it is sufficient to say that the creation of a fully probabilistic procedure for estimating settlement and the addition of that procedure to an analysis tool, such as *PBLiquefY*, is considered a stepping stone in the process of making probabilistic analyses of settlement more readily available to practicing engineers.

The additions related to the settlement estimation procedure are outlined in Appendix A. For a tutorial on the use of *PBLiquefY* to compute both deterministic and probabilistic settlement estimations, see Appendix B.

6.3 Results and Discussion

In this section, a complete presentation of the results of this study is provided. Results are organized according to the settlement estimation method and soil profile selected for the given analysis. Comments about general trends, patterns, and other notable findings are made. As noted previously, one of the purposes of this study is to provide a quantitative comparison of the settlement estimation methods to demonstrate the deficiencies of conventional design methods.

6.3.1 Cetin et al. (2009) Results

The results of the Cetin et al. (2009) method are summarized in Table 6-4 through Table 6-8. These tables contain results for the pseudo-probabilistic (mean magnitude and modal magnitude), semi-probabilistic, and fully-probabilistic methods for the 475 and 2475 year return periods. All settlements are reported in cm.

Table 6-4: Settlement (cm) computed by Cetin analysis of profile 1

City	475 Mean Magnitude	475 Modal Magnitude	475 Semi-Probabilistic	475 Probabilistic	2475 Mean Magnitude	2475 Modal Magnitude	2475 Semi-Probabilistic	2475 Probabilistic
Butte	0.0	7.0	1.9	0.0	7.0	7.9	11.0	9.9
Charleston	8.1	11.8	8.4	4.6	23.4	24.4	24.4	23.5
Eureka	22.9	21.9	24.8	22.8	29.2	28.2	30.8	35.6
Memphis	10.7	13.9	10.6	6.6	22.0	23.3	23.9	24.8
Portland	14.2	19.9	16.8	15.2	20.3	24.6	24.1	28.7
Salt Lake City	12.6	13.7	14.9	13.0	22.4	22.7	23.9	27.3
San Francisco	20.3	22.2	22.6	23.8	24.6	25.8	26.7	35.4
San Jose	18.3	18.1	21.5	22.5	22.0	21.8	25.2	34.4
Santa Monica	17.5	19.1	20.2	20.9	23.1	24.2	25.0	33.3
Seattle	15.7	15.1	19.1	19.0	22.0	21.8	25.1	30.9

Table 6-5: Settlement (cm) computed by Cetin analysis of profile 2

City	475 Mean Magnitude	475 Modal Magnitude	475 Semi-Probabilistic	475 Probabilistic	2475 Mean Magnitude	2475 Modal Magnitude	2475 Semi-Probabilistic	2475 Probabilistic
Butte	2.6	1.0	4.0	3.6	8.0	8.5	9.7	11.2
Charleston	8.7	10.9	8.1	5.6	21.0	22.0	21.6	21.9
Eureka	20.5	19.5	21.9	20.3	26.8	25.8	28.0	31.3
Memphis	10.2	12.3	9.5	7.2	19.6	20.8	21.0	22.2
Portland	12.5	17.4	13.9	13.2	17.8	22.1	21.2	25.1
Salt Lake City	11.5	12.2	12.5	11.7	20.0	20.3	21.0	24.2
San Francisco	17.8	19.7	19.7	20.5	22.1	23.4	23.9	30.9
San Jose	15.9	15.6	18.5	19.4	19.6	19.4	22.3	29.9
Santa Monica	15.0	16.7	17.3	17.6	20.7	21.8	22.1	28.7
Seattle	13.6	13.1	16.1	15.9	19.6	19.3	22.2	27.7

Table 6-6: Settlement (cm) computed by Cetin analysis of profile 3

City	475 Mean Magnitude	475 Modal Magnitude	475 Semi-Probabilistic	475 Probabilistic	2475 Mean Magnitude	2475 Modal Magnitude	2475 Semi-Probabilistic	2475 Probabilistic
Butte	11.7	3.3	20.4	16.0	26.6	27.5	31.1	38.1
Charleston	27.7	31.3	28.5	21.5	42.1	43.0	43.2	48.5
Eureka	41.6	40.7	43.5	44.0	47.5	46.6	49.2	64.0
Memphis	30.3	33.2	30.6	24.6	40.7	41.9	42.8	49.9
Portland	33.5	38.8	36.2	36.1	39.1	43.1	42.9	57.4
Salt Lake City	32.1	33.1	34.5	34.2	41.1	41.4	42.7	55.6
San Francisco	39.1	40.9	41.5	44.4	43.1	44.3	45.4	64.2
San Jose	37.3	37.1	40.5	44.4	40.7	40.5	43.9	64.0
Santa Monica	36.5	38.0	39.3	42.6	41.8	42.8	43.7	62.6
Seattle	34.9	34.3	38.3	40.8	40.7	40.5	43.8	60.9

Table 6-7: Settlement (cm) computed by Cetin analysis of profile 4

City	475 Mean Magnitude	475 Modal Magnitude	475 Semi-Probabilistic	475 Probabilistic	2475 Mean Magnitude	2475 Modal Magnitude	2475 Semi-Probabilistic	2475 Probabilistic
Butte	0.0	0.0	0.0	0.0	0.6	1.0	2.4	1.4
Charleston	1.1	3.3	0.9	0.0	14.5	15.5	15.3	13.4
Eureka	14.0	13.0	15.7	13.2	20.4	19.4	21.8	21.8
Memphis	2.6	4.9	2.1	0.9	13.0	14.3	14.8	13.9
Portland	5.1	10.9	7.3	5.2	11.2	15.7	14.9	15.7
Salt Lake City	3.9	4.7	5.3	4.0	13.5	13.8	14.7	14.5
San Francisco	11.3	13.3	13.4	13.0	15.7	17.0	17.7	20.7
San Jose	9.2	9.0	12.2	11.6	13.0	12.8	16.1	19.7
Santa Monica	8.3	10.1	10.9	10.0	14.2	15.3	15.9	18.4
Seattle	6.6	5.9	9.7	8.5	13.1	12.8	16.0	17.1

Table 6-8: Settlement (cm) computed by Cetin analysis of profile 5

City	475 Mean Magnitude	475 Modal Magnitude	475 Semi-Probabilistic	475 Probabilistic	2475 Mean Magnitude	2475 Modal Magnitude	2475 Semi-Probabilistic	2475 Probabilistic
Butte	3.7	0.7	7.8	5.2	12.1	12.9	15.9	17.2
Charleston	13.1	16.3	13.6	9.4	27.7	28.6	28.7	30.0
Eureka	27.1	26.2	29.0	28.0	33.3	32.4	34.9	41.7
Memphis	15.4	18.2	15.5	11.1	26.2	27.5	28.2	30.7
Portland	18.5	24.2	21.2	20.0	24.5	28.8	28.3	35.7
Salt Lake City	17.1	18.1	19.3	18.1	26.7	26.9	28.1	33.6
San Francisco	24.5	26.5	26.9	28.1	28.8	30.0	31.0	41.8
San Jose	22.6	22.4	25.8	27.0	26.2	26.0	29.4	40.9
Santa Monica	21.8	23.4	24.5	26.1	27.4	28.4	29.2	39.9
Seattle	20.1	19.4	23.4	24.0	26.2	26.0	29.3	38.5

6.3.2 Ishihara and Yoshimine (1992) Results

The results of the Ishihara and Yoshimine (1992) method are presented in Table 6-9 through Table 6-13. Results are separated by soil profile and all values are reported in units of cm.

Table 6-9: Settlement (cm) computed by Ishihara and Yoshimine analysis of profile 1

City	475 Mean Magnitude	475 Modal Magnitude	475 Semi-Probabilistic	475 Probabilistic	2475 Mean Magnitude	2475 Modal Magnitude	2475 Semi-Probabilistic	2475 Probabilistic
Butte	0.0	0.0	0.0	0.0	2.8	3.4	0.4	1.9
Charleston	3.2	9.8	0.3	0.6	19.8	19.9	19.8	18.8
Eureka	19.8	19.6	19.8	18.2	19.9	19.9	19.9	29.2
Memphis	6.7	13.8	1.7	1.1	19.7	19.8	19.8	20.0
Portland	14.3	19.3	14.3	8.7	19.2	19.9	19.8	23.7
Salt Lake City	11.7	13.7	4.7	5.3	19.7	19.8	19.6	21.9
San Francisco	19.2	19.7	19.5	19.0	19.9	19.9	19.9	29.2
San Jose	18.5	18.4	18.4	18.3	19.6	19.6	19.8	28.7
Santa Monica	18.2	18.9	17.3	16.3	19.8	19.9	19.8	27.7
Seattle	16.6	15.7	15.7	13.3	19.7	19.6	19.8	26.0

Table 6-10: Settlement (cm) computed by Ishihara and Yoshimine analysis of profile 2

City	475 Mean Magnitude	475 Modal Magnitude	475 Semi-Probabilistic	475 Probabilistic	2475 Mean Magnitude	2475 Modal Magnitude	2475 Semi-Probabilistic	2475 Probabilistic
Butte	0.3	0.0	0.1	0.2	6.8	7.5	3.7	5.9
Charleston	7.6	10.2	3.4	1.9	15.7	16.0	15.1	15.8
Eureka	15.4	15.2	15.3	14.9	16.9	16.9	16.9	24.7
Memphis	9.9	11.3	6.2	3.1	15.2	15.5	15.1	16.6
Portland	11.4	14.9	11.5	9.2	14.9	16.0	15.1	19.5
Salt Lake City	10.6	11.2	9.7	7.3	15.3	15.4	15.0	18.7
San Francisco	14.9	15.2	14.9	15.1	16.0	16.4	16.1	23.4
San Jose	13.7	13.6	13.1	15.0	15.2	15.2	15.1	22.7
Santa Monica	13.2	14.2	12.5	13.6	15.6	16.0	15.1	22.0
Seattle	12.3	12.1	12.0	12.0	15.2	15.2	15.1	21.3

Table 6-11: Settlement (cm) computed by Ishihara and Yoshimine analysis of profile 3

City	475 Mean Magnitude	475 Modal Magnitude	475 Semi-Probabilistic	475 Probabilistic	2475 Mean Magnitude	2475 Modal Magnitude	2475 Semi-Probabilistic	2475 Probabilistic
Butte	1.1	0.2	0.2	0.8	31.9	32.3	20.4	25.6
Charleston	32.1	35.3	18.3	8.4	35.3	35.3	35.3	41.1
Eureka	35.3	35.3	35.3	37.9	35.3	35.3	35.3	52.8
Memphis	35.3	35.3	28.5	13.0	35.3	35.3	35.3	42.6
Portland	35.3	35.3	35.3	29.4	35.3	35.3	35.3	49.4
Salt Lake City	35.3	35.3	33.0	25.6	35.3	35.3	35.3	48.0
San Francisco	35.3	35.3	35.3	38.7	35.3	35.3	35.3	52.7
San Jose	35.3	35.3	35.3	38.8	35.3	35.3	35.3	52.8
Santa Monica	35.3	35.3	35.3	37.7	35.3	35.3	35.3	52.4
Seattle	35.3	35.3	35.3	35.6	35.3	35.3	35.3	51.9

Table 6-12: Settlement (cm) computed by Ishihara and Yoshimine analysis of profile 4

City	475 Mean Magnitude	475 Modal Magnitude	475 Semi-Probabilistic	475 Probabilistic	2475 Mean Magnitude	2475 Modal Magnitude	2475 Semi-Probabilistic	2475 Probabilistic
Butte	0.0	0.0	0.0	0.0	0.1	0.1	0.0	0.0
Charleston	0.1	0.9	0.0	0.0	10.1	10.6	8.7	7.8
Eureka	9.7	9.0	9.5	7.7	11.2	11.2	11.2	17.1
Memphis	0.6	1.6	0.1	0.0	9.0	9.9	8.7	7.6
Portland	1.7	7.2	1.9	0.9	6.9	10.7	8.8	9.3
Salt Lake City	1.1	1.5	0.5	0.3	9.5	9.6	7.9	8.2
San Francisco	6.9	9.1	7.5	6.9	10.7	11.0	10.8	15.4
San Jose	4.6	4.4	4.2	5.6	9.2	9.0	8.7	13.4
Santa Monica	3.8	5.5	3.2	4.0	10.0	10.5	8.9	12.4
Seattle	2.5	2.2	2.4	2.6	9.1	8.9	9.0	11.2

Table 6-13: Settlement (cm) computed by Ishihara and Yoshimine analysis of profile 5

City	475 Mean Magnitude	475 Modal Magnitude	475 Semi-Probabilistic	475 Probabilistic	2475 Mean Magnitude	2475 Modal Magnitude	2475 Semi-Probabilistic	2475 Probabilistic
Butte	0.3	0.0	0.1	0.2	11.3	12.1	6.9	9.4
Charleston	11.9	17.3	6.4	2.7	22.5	22.6	22.0	23.7
Eureka	22.3	22.0	22.3	22.4	22.8	22.8	22.8	34.1
Memphis	16.9	18.6	10.3	4.8	22.0	22.4	22.0	24.6
Portland	18.8	21.4	18.8	14.5	21.4	22.6	22.0	29.0
Salt Lake City	17.8	18.5	14.4	11.5	22.2	22.3	21.7	27.8
San Francisco	21.4	22.1	21.6	22.6	22.6	22.8	22.7	33.5
San Jose	20.9	20.9	20.8	22.4	22.1	22.0	22.0	33.0
Santa Monica	20.8	21.1	20.6	20.7	22.4	22.6	22.0	32.1
Seattle	20.5	20.2	19.4	18.6	22.1	22.0	22.1	31.4

6.3.3 Comparison of Pseudo-Probabilistic, Semi-Probabilistic, and Fully-Probabilistic Methods

Several general trends can be observed in the data above. First, pseudo-probabilistic methods generally predict larger settlements than the probabilistic method at the corresponding return period in areas of low to medium seismicity. This trend is logical considering that pseudo-probabilistic methods do not take into account the low probability of a seismic event. Second, pseudo-probabilistic methods seem to correspond fairly well to probabilistic methods for areas of high seismicity when examining the lower return period. Third, in most cases, the pseudo-probabilistic method predicts less settlement than the probabilistic method for the higher return period. To more easily visualize these trends, comparison plots were generated with conventional (pseudo-probabilistic) values plotted vs probabilistic values. The data are separated into three groups, one for each pseudo-probabilistic method. The plots are presented in Figure 6-3, Figure 6-4, and Figure 6-5. The red line represents the best-fit regression line for the data. The black line represents a 1-to-1 ratio for reference.

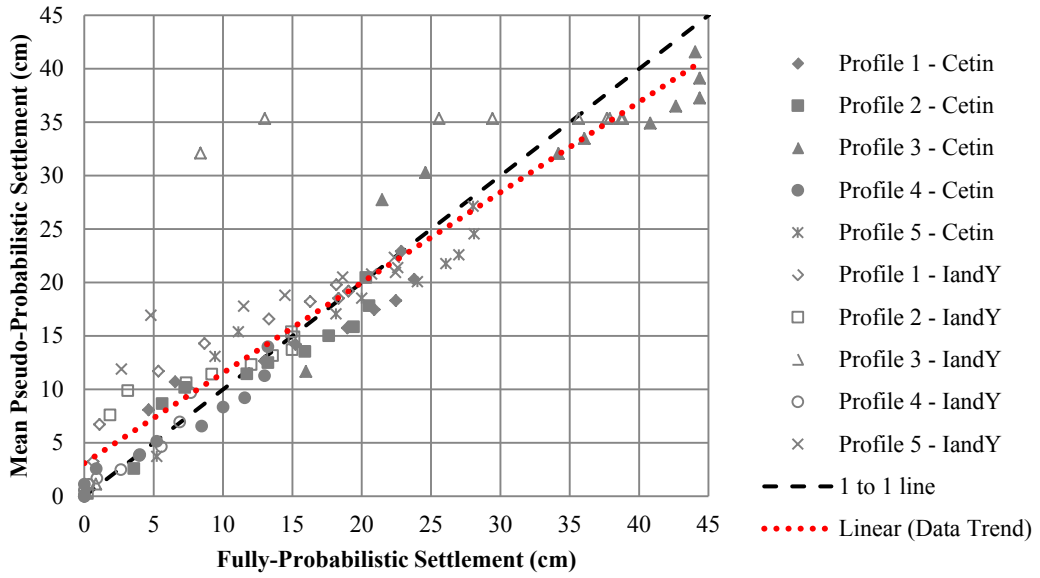

(a)

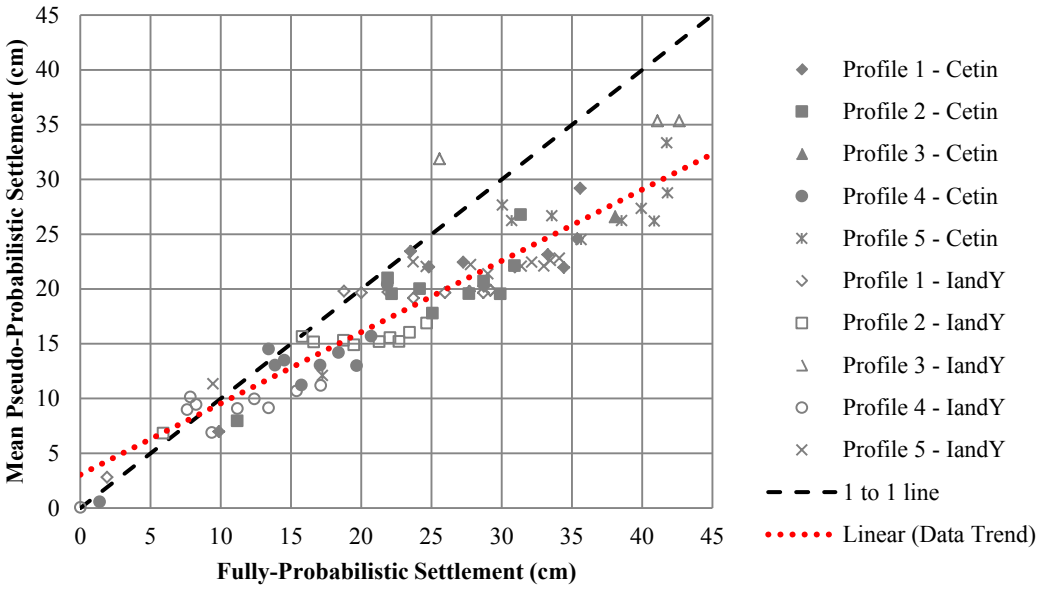

(b)

Figure 6-3: Mean magnitude pseudo-probabilistic versus fully probabilistic analyses for (a) 475 year and (b) 2475 year return periods

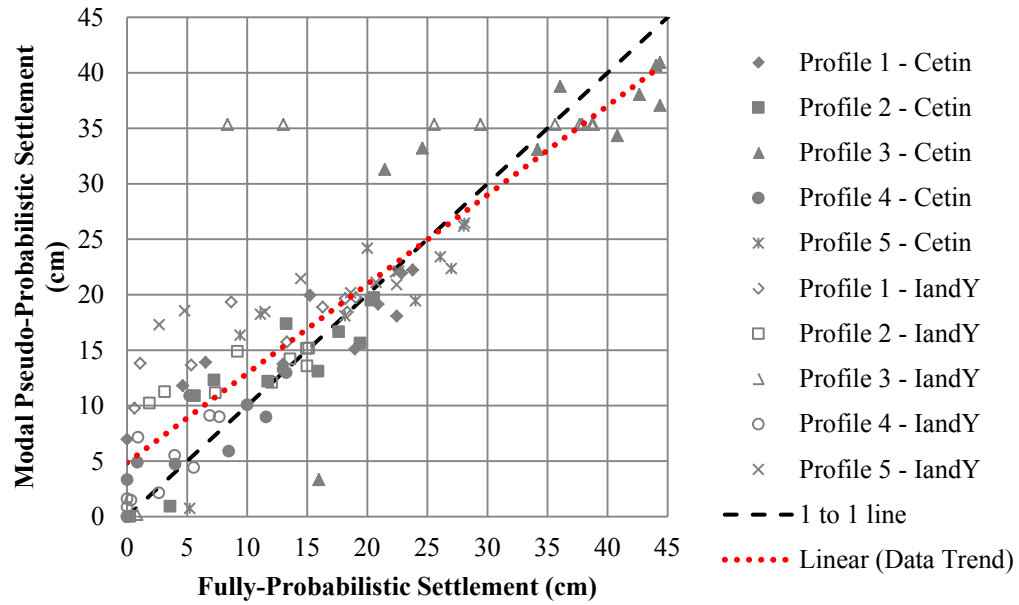

(a)

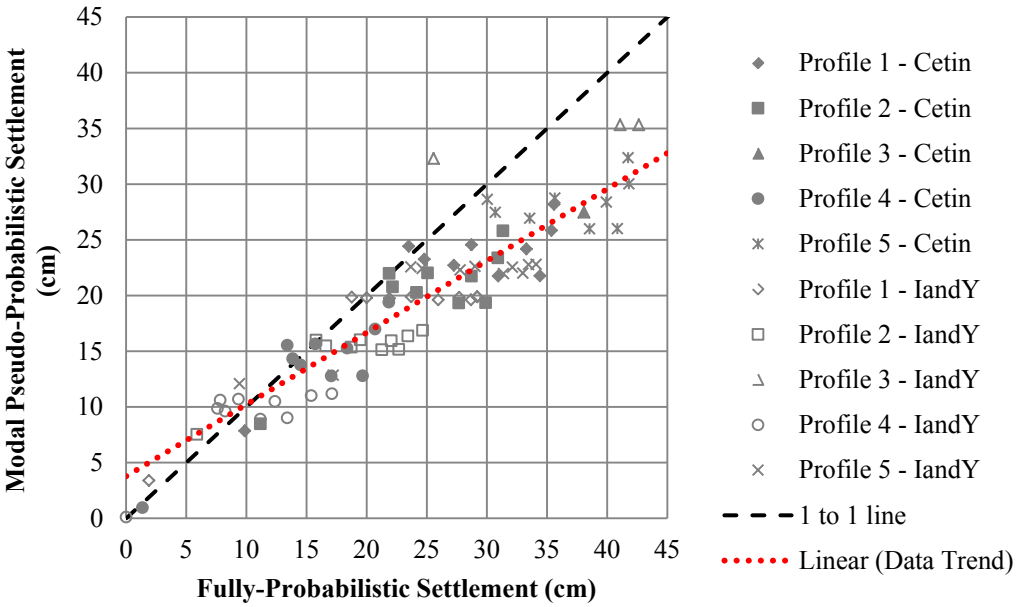

(b)

Figure 6-4: Modal magnitude pseudo-probabilistic versus probabilistic analyses for (a) 475 year and (b) 2475 year return periods

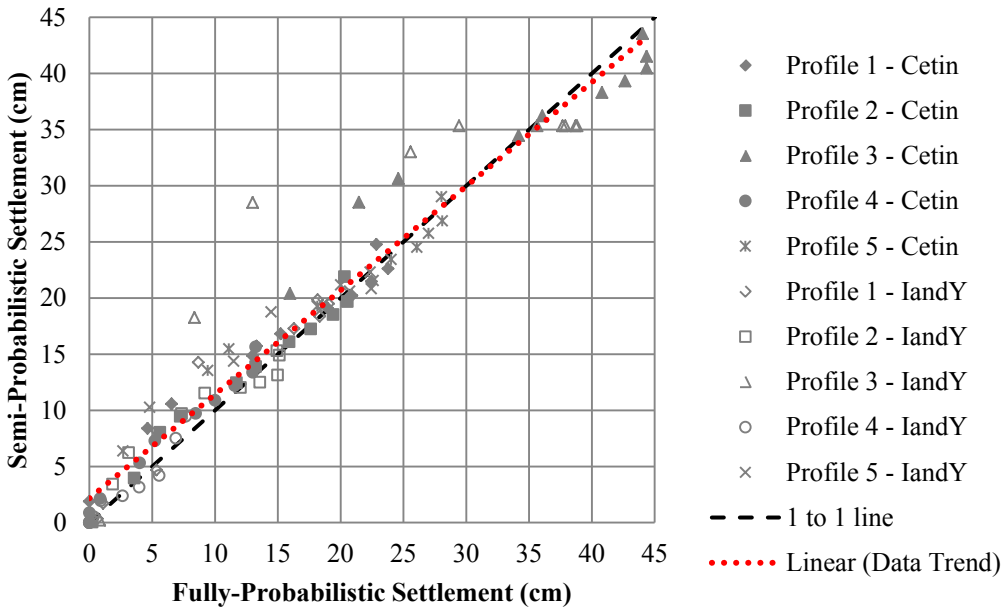

(a)

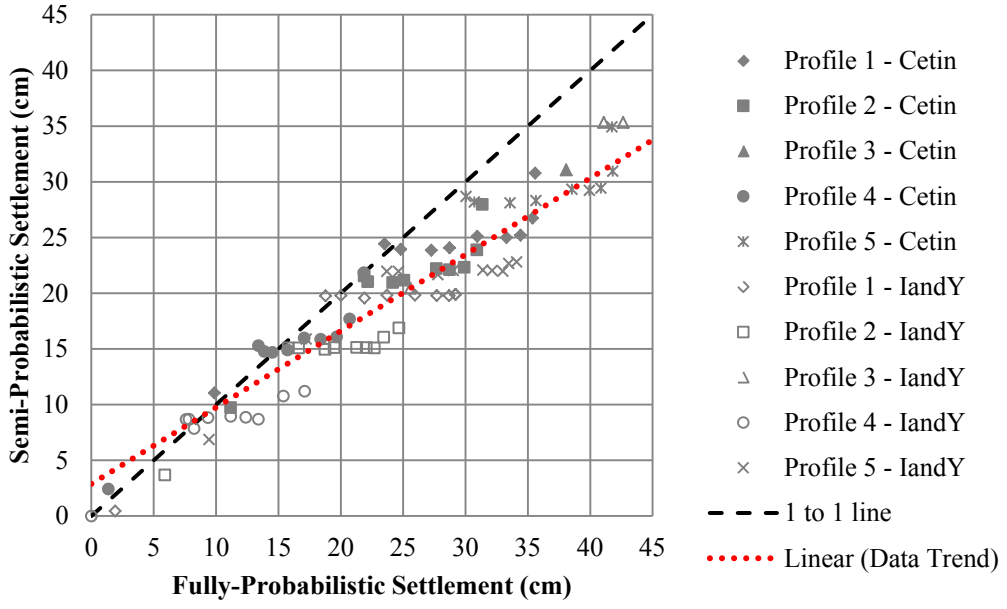

(b)

Figure 6-5: Semi-probabilistic versus probabilistic analyses for (a) 475 year and (b) 2475 year return periods

It is important to note that perfect correlation between the pseudo and semi-probabilistic methods and the fully-probabilistic method would be observed in Figure 6-3 through Figure 6-5 if the data trend line fell exactly on the 1 to 1 line. A data trend line plotting above the 1 to 1 line would demonstrate an over-prediction of settlement by the pseudo and semi-probabilistic methods and, conversely, a data trend line plotting below the 1 to 1 line would demonstrate an under-prediction. It appears that the methods correlate reasonably well for the lower return period event, with the exception of the general trends already mentioned. In each case, however, the correlation deteriorates significantly when analyzing the higher return period. In many cases, pseudo and semi-probabilistic methods are observed to under-predict settlement by up to 15 cm (6 in.).

The correlation of the semi-probabilistic method is especially significant. One criticism of performing fully-probabilistic settlement analysis is that the uncertainty in liquefaction initiation is too high to generate reliable results. The semi-probabilistic method explicitly accounts for the uncertainty in liquefaction initiation, and demonstrates the same deterioration in correlation to fully-probabilistic methods at high return periods. This observation suggests that the deterioration occurs within the settlement calculation, not the liquefaction triggering procedure.

To further examine the source of the trends mentioned above, the settlement estimate values computed from pseudo and semi-probabilistic methods were entered into the probabilistic hazard curve to back-calculate the actual return period associated with that settlement value. The results of this process are presented in Table 6-14 through Table 6-18 and summarized in Figure 6-6 and Figure 6-7.

Table 6-14: Actual return period of settlements estimated for profile 1

		Actual T_R					
		Cetin			IandY		
City	Assumed T_R	Mean	Modal	Semi	Mean	Modal	Semi
Butte	475	475.0	1445.1	625.6	1039.0	1039.0	1039.0
Charleston	475	569.7	714.1	579.6	556.5	974.0	312.3
Eureka	475	454.5	395.7	547.0	546.1	539.3	549.4
Memphis	475	602.1	756.0	597.7	673.9	1240.8	490.7
Portland	475	407.8	777.9	536.1	770.7	1336.5	769.1
Salt Lake City	475	435.9	487.2	531.8	760.8	933.8	416.6
San Francisco	475	308.3	383.4	402.4	481.1	507.3	495.1
San Jose	475	270.6	264.3	405.9	483.9	479.9	476.6
Santa Monica	475	294.9	359.1	417.4	569.2	610.8	519.4
Seattle	475	321.2	301.0	486.3	634.8	583.9	582.6
Butte	2475	1445.1	1655.7	2766.8	2761.8	2984.7	1198.3
Charleston	2475	2153.8	2506.6	2507.6	2728.7	2746.2	2715.4
Eureka	2475	948.0	813.6	1159.4	551.5	551.5	551.5
Memphis	2475	1610.3	1890.4	2084.2	2344.6	2398.4	2389.9
Portland	2475	813.9	1353.2	1287.0	1312.9	1416.9	1407.3
Salt Lake City	2475	1219.5	1254.0	1428.2	1755.3	1764.6	1719.8
San Francisco	2475	511.7	582.7	646.0	514.8	515.1	515.1
San Jose	2475	440.1	426.2	627.8	546.7	545.1	555.1
Santa Monica	2475	579.8	651.9	720.6	679.1	684.5	678.9
Seattle	2475	637.7	621.2	956.6	927.0	922.4	950.4

Table 6-15: Actual return period of settlements estimated for profile 2

		Actual T_R					
		Cetin			IandY		
City	Assumed T_R	Mean	Modal	Semi	Mean	Modal	Semi
Butte	475	339.6	228.3	511.1	481.9	244.3	257.0
Charleston	475	599.5	741.1	569.1	824.2	1140.8	537.3
Eureka	475	482.9	426.6	558.7	498.3	486.5	493.5
Memphis	475	609.2	766.2	570.7	960.4	1131.5	619.4
Portland	475	419.0	767.6	506.0	617.1	1093.5	626.6
Salt Lake City	475	454.4	496.4	508.2	696.2	753.1	616.4
San Francisco	475	328.2	420.7	417.1	456.5	479.0	456.9
San Jose	475	294.8	287.9	413.6	381.1	373.3	349.3
Santa Monica	475	316.1	402.0	444.2	439.5	514.6	392.0
Seattle	475	328.5	310.8	484.5	491.0	479.3	475.3
Butte	2475	1241.1	1355.2	1718.1	2817.3	3135.5	1365.1
Charleston	2475	2165.0	2507.0	2350.8	2407.0	2535.2	2157.0
Eureka	2475	1122.5	978.8	1309.6	588.9	588.9	588.9
Memphis	2475	1684.6	1988.4	2061.1	1872.4	1985.3	1849.7
Portland	2475	815.5	1451.1	1294.8	1095.5	1270.8	1123.6
Salt Lake City	2475	1289.0	1329.3	1447.4	1362.3	1373.8	1303.2
San Francisco	2475	573.8	685.2	744.3	530.1	553.0	530.9
San Jose	2475	482.8	472.8	675.3	489.8	487.3	481.8
Santa Monica	2475	654.4	749.1	789.9	618.6	658.3	580.7
Seattle	2475	702.4	680.8	1055.4	726.2	720.3	719.4

Table 6-16: Actual return period of settlements estimated for profile 3

		Actual T_R					
		Cetin			IandY		
City	Assumed T_R	Mean	Modal	Semi	Mean	Modal	Semi
Butte	475	321.6	168.3	574.2	484.1	252.7	258.1
Charleston	475	608.6	739.8	633.6	1257.1	1527.0	650.2
Eureka	475	387.1	362.4	453.6	389.8	389.8	389.8
Memphis	475	614.0	729.9	626.4	1361.5	1361.5	925.7
Portland	475	370.1	535.0	462.8	657.9	657.9	657.9
Salt Lake City	475	391.6	422.6	475.0	823.0	823.0	700.9
San Francisco	475	303.8	341.7	356.5	366.3	366.3	366.3
San Jose	475	288.1	284.8	349.0	364.3	364.3	364.3
Santa Monica	475	294.9	322.5	349.6	395.3	395.3	395.3
Seattle	475	302.7	292.6	379.1	463.5	463.5	463.5
Butte	2475	889.7	967.7	1235.4	3459.8	3555.8	1711.1
Charleston	2475	1449.3	1543.4	1568.2	1527.0	1527.0	1527.0
Eureka	2475	573.4	542.7	637.1	389.8	389.8	389.8
Memphis	2475	1203.1	1285.8	1353.9	1361.5	1361.5	1361.5
Portland	2475	544.1	704.5	693.0	657.9	657.9	657.9
Salt Lake City	2475	692.1	704.1	774.4	823.0	823.0	823.0
San Francisco	2475	403.1	446.8	484.7	366.3	366.3	366.3
San Jose	2475	353.8	349.6	451.9	364.3	364.3	364.3
Santa Monica	2475	416.4	451.3	485.3	395.3	395.3	395.3
Seattle	2475	461.8	452.4	554.9	463.5	463.5	463.5

Table 6-17: Actual return period of settlements estimated for profile 4

		Actual T_R					
		Cetin			IandY		
City	Assumed T_R	Mean	Modal	Semi	Mean	Modal	Semi
Butte	475	1039.0	1039.0	1039.0	2475.0	2475.0	2475.0
Charleston	475	514.4	626.0	504.2	495.3	626.3	475.0
Eureka	475	507.1	440.4	630.2	619.1	561.5	598.9
Memphis	475	538.3	671.0	518.7	542.2	730.5	480.5
Portland	475	433.7	1052.4	580.4	535.2	1499.0	558.3
Salt Lake City	475	440.1	503.2	537.4	555.4	604.4	494.9
San Francisco	475	328.5	465.5	475.8	479.7	673.9	519.4
San Jose	475	294.7	285.2	494.7	373.7	355.6	338.3
Santa Monica	475	317.3	419.1	485.5	450.0	616.4	369.9
Seattle	475	338.3	305.9	566.6	445.7	390.1	428.4
Butte	2475	1242.5	1435.8	2726.5	3182.5	4327.6	2475.0
Charleston	2475	2780.8	3244.2	3115.3	3456.3	3773.4	2768.0
Eureka	2475	1531.1	1244.0	2265.5	800.5	800.5	800.5
Memphis	2475	1931.9	2497.7	2658.1	2943.1	3343.3	2820.6
Portland	2475	1092.9	2269.8	1913.5	1432.6	3093.1	2146.5
Salt Lake City	2475	1799.2	1893.6	2295.9	2892.4	2961.8	2240.4
San Francisco	2475	675.6	887.6	1052.0	957.0	1042.6	973.8
San Jose	2475	553.1	537.7	1007.2	975.5	940.6	858.4
Santa Monica	2475	860.6	1095.2	1204.2	1450.3	1599.9	1219.5
Seattle	2475	1047.9	993.0	1588.6	1533.3	1483.9	1492.8

Table 6-18: Actual return period of settlements estimated for profile 5

		Actual T_R					
		Cetin			IandY		
City	Assumed T_R	Mean	Modal	Semi	Mean	Modal	Semi
Butte	475	310.3	147.5	594.2	490.8	257.1	267.8
Charleston	475	576.4	709.1	592.4	812.8	1247.4	570.1
Eureka	475	430.5	383.9	516.1	474.6	456.9	472.7
Memphis	475	587.5	724.6	591.3	1092.5	1239.1	641.9
Portland	475	377.6	640.3	493.2	680.8	927.4	678.2
Salt Lake City	475	427.1	479.0	519.0	797.0	860.7	583.5
San Francisco	475	320.1	392.8	413.3	404.7	443.7	413.3
San Jose	475	282.9	278.0	379.1	396.2	394.4	391.3
Santa Monica	475	299.7	349.5	393.8	477.3	490.5	468.5
Seattle	475	312.4	296.0	445.5	550.9	535.2	504.4
Butte	2475	1113.8	1197.2	1720.9	2930.3	3163.7	1614.9
Charleston	2475	1831.4	2056.7	2067.5	2084.2	2114.9	1955.9
Eureka	2475	771.0	693.5	941.6	492.0	492.0	492.0
Memphis	2475	1424.2	1595.2	1711.8	1738.4	1818.7	1721.6
Portland	2475	661.0	1097.3	1059.2	918.0	1073.8	1007.4
Salt Lake City	2475	1069.2	1091.4	1202.9	1251.1	1259.9	1191.0
San Francisco	2475	506.0	559.4	606.2	474.8	482.3	477.2
San Jose	2475	398.1	389.9	550.0	454.2	449.9	447.0
Santa Monica	2475	526.9	576.6	623.8	555.0	561.2	533.6
Seattle	2475	567.2	555.9	765.4	636.1	629.9	635.6

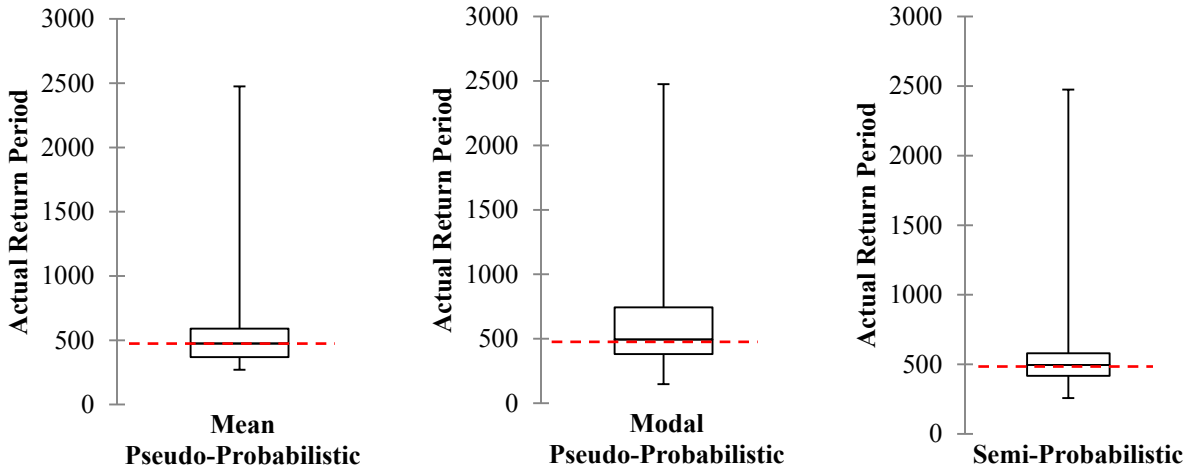

Figure 6-6: Box and whisker plots of actual return periods versus assumed 475 return period

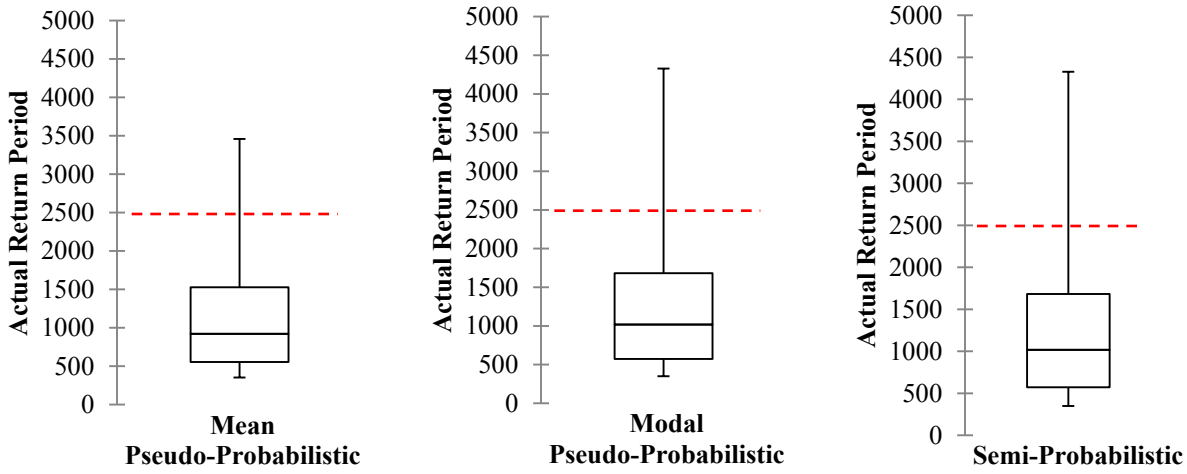

Figure 6-7: Box and whisker plots of actual return periods versus assumed 2475 return period

The box and whisker plots shown in Figure 6-6 and Figure 6-7 illustrate the median, first and third quartiles, and maximum and minimum values of the return periods presented in the tables above. As noted previously, these values represent actual return periods because they are generated from the fully probabilistic hazard curve. The assumed return period is presented as a red dashed line for reference.

The results for the 475 year return period (Figure 6-6) are not surprising. The correlation between the assumed return period and the actual return periods is fairly consistent with what was observed in Figure 6-3 through Figure 6-5, with the deterministic analyses slightly over-predicting the hazard level on average. Deterministic analyses choose a "worst-case" scenario and design for those ground motions, ignoring the likelihood of occurrence of the design event. This approach typically results in an over-prediction of seismic hazard. In other words, it could be said that over-prediction is built within the very framework of deterministic analyses. It is this idea that makes the results of the 2475 return period (Figure 6-7) so disconcerting. The data suggest that, on average, the deterministic analyses underestimate the seismic hazard by more

than half when considering the larger return period. This trend is likely due to the fact that pseudo-probabilistic and semi-probabilistic methods compute volumetric strain of the soil deterministically, ignoring the considerable uncertainty associated with the computation of strain. Fully-probabilistic methods, on the other hand, account for this uncertainty.

It should be noted that the results of the semi-probabilistic method are marginally improved from the pseudo-probabilistic method. This is likely due to the consideration of the uncertainty associated with liquefaction triggering in the semi-probabilistic method. However, the similarities between the pseudo-probabilistic and semi-probabilistic results suggest that the uncertainty associated with liquefaction triggering is less significant than the uncertainty associated with volumetric strain. This data suggests that semi-probabilistic methods are not an improvement to pseudo-probabilistic methods when studying higher return period events.

Deterministic methods are widely accepted because they are believed to produce a conservative prediction of seismic hazard and effects. If, in fact, deterministic methods are predicting settlements that correspond to seismic hazard levels other than those assumed by the designing engineer, then relying on deterministic methods to predict settlement poses a potentially serious risk. This data suggests that while deterministic methods can be appropriate for seismic hazards corresponding to lower return periods, probabilistic methods should be used when examining events with higher return periods.

It should be noted that this study is limited in scope. The focus of this study is settlement, and only two methods of settlement estimation (Cetin et al. and Ishihara and Yoshimine) are examined. Research examining other effects of seismic events (e.g. lateral spread, bearing capacity failure, slope stability, etc.) should be performed to confirm the results of this study.

6.4 Chapter Summary

The fully-probabilistic settlement estimation procedure presented in the previous chapter was compared to deterministic methods for 10 cities of varying seismicity levels using five theoretical soil profiles. The analysis was completed using the tool *PBLiquefY*. Deterministic methods correlate fairly well with probabilistic methods for a low return period event. When examining a high return period event the correlation deteriorates, with deterministic methods consistently predicting less settlement compared to the fully-probabilistic procedure. This data suggests that the used of deterministic methods can result in the computation of settlements that do not correspond to the hazard level assumed by the engineer. It is suggested that probabilistic methods be used when analyzing higher return period events.

7 SUMMARY AND CONCLUSIONS

When a loose soil is subjected to seismic loading, it tends to densify. When the soil is saturated, this densification leads to the buildup of excess pore water pressure that causes the soil to liquefy, a phenomenon known as liquefaction. Once the excess pore water pressure has dissipated, the soil particles tend to settle in a denser configuration, resulting in a volumetric strain of the soil profile. This change in volume is manifested at the ground surface as a change in ground surface elevation. This process of densification is known as liquefaction induced settlement. While settlement rarely results in loss of life, it poses a serious economic threat to regions subjected to seismic activity.

The prediction of settlement effects is an important step in the seismic design process. However, accurately predicting settlement is difficult due to the uncertainty inherent in seismic events. Engineers have traditionally relied on DSHA to mitigate this uncertainty by simply basing seismic design on a "worst-case" scenario. Designs based on DSHA can be expensive, due to the conservative nature of the approach. More recently, PSHA has been developed to directly account for the uncertainty inherent in variables such as location, magnitude, and ground motions, and the associated effects of seismic events. PSHA produces a more accurate representation of seismic hazard but is not widely used due to the complex nature of the analysis. Simplifying PSHA is a central focus of the continued evolution of SHA.

Performance-based earthquake engineering (PBEE) is a newer design approach proposed by the Pacific Earthquake Engineering Research (PEER) Center. The objective of PBEE is to provide a framework that takes full advantage of PSHA while facilitating communication and transparency between all stakeholders involved in seismic design. This study proposes a fully probabilistic procedure for estimating liquefaction-induced settlement by incorporating two commonly accepted settlement estimation models, the Cetin et al. (2009) method and the Ishihara and Yoshimine (1992) method, into the PEER framework.

To assist in the process of performing the probabilistic analyses for this study, an existing SHA tool, known as *PBLiquefY*, was updated to include the fully probabilistic settlement estimation procedure. One of the motivations for the addition of the settlement procedure to *PBLiquefY* is to facilitate the creation of a simplified performance-based procedure for post-liquefaction settlement estimation. Future research will focus on developing the simplified settlement estimation methods.

The results of the fully probabilistic procedure presented in this study were compared to conventional deterministic analyses in 10 cities with varying seismicity levels. Settlements were computed for five theoretical soil profiles in each city. It was observed that deterministic methods produced similar results to probabilistic methods for lower return periods. Deterministic methods did tend to somewhat over-predict seismic hazard, but, due to the conservative nature of deterministic analyses, some over-prediction is to be expected. It was observed that, for larger return periods, deterministic methods seriously underestimated seismic hazard, resulting in under-estimations of settlement. These results suggest that engineers may unintentionally ignore considerable risk when estimating settlements for high seismicity events using deterministic methods.

REFERENCES

Abrahamson, N., and Silva, W. (2008). "Summary of the Abrahamson & Silva NGA Ground-Motion Relations," *Earthquake Spectra*: February 2008, Vol. 24, No. 1, pp. 67-97.

Ambraseys, N.N. (1988). "Engineering seismology," *Earthquake Engineering and Structural Dynamics*, Vol. 17, pp. 1-105

Ancheta, T.D., Darragh, R.B., Stewart, J.P., Seyhan, E., Silva, W.J., Chiou, B. S-J., Wooddell, K.E., Graves, R.W., Kottke, A.R., Boore, D.M., Kishida, T., and Donahue, J.L. (2014). "NGA-West2 Database," *Earthquake Spectra*: Vol. 30, No. 3, pp. 989-1005.

Arias, A. (1970) "A measure of earthquake intensity," in R.J. Hansen, ed. *Seismic Design for Nuclear Power Plants*, MIT Press, Cambridge, Massachusetts, pp. 438-483.

Been, K. and Jeffries, M.G. (1985). "A state parameter for sands," *Geotechnique*, Vol. 35, No. 2, pp. 99-112

Benjamin, J. R. (1988). A Criterion for Determining Exceedances of the Operating Basis Earthquake, EPRI Report NP-5930. Electric Power Research Institute, Palo Alto.

Bertero, R.D., Bertero, V.V. (2002). Performance-based seismic engineering: the needs for a reliable conceptual comprehensive approach. *Earthquake Engineering and Structural Dynamics*, 31, 627-652.

Bilge, H.T., and Cetin, K.O. (2007) "Field performance case histories for the assessment of cyclically-induced reconsolidation (volumetric) settlements." *METU EERC Rep. No. 2007/01*, [http://www.ce.metu.edu.tr/~onder/publications/PUB-NO59.zip] (Jan. 4, 2007).

Boore, D. M. (1989). The Richter scale: its development and use for determining earthquake source parameters. Tectonophysics, 166(1), 1-14.

Boore, D.M., Joyner, W.B., and Fumal, T.E. (1993) Estimation of response spectra and peak accelerations from western North America earthquakes: An interim report, *Open-File-Report 93-509*, U.S. Geological Survey, Reston, Virginia, 72 pp.

Boore, D.M., and Atkinson, G.M. (2008). "Ground-Motion Prediction Equations for the Average Horizontal Component of PGA, PGV, and 5%-Damped PSA at Spectral Periods between 0.01 s and 10.0 s," *Earthquake Spectra*: February 2008, Vol. 24, No. 1, pp. 99-138.

Bouckovalas, G., Dakoulas, P. (2007). Liquefaction performance of shallow foundations in presence of a soil crust. In Earthquake Geotechnical Engineering (pp. 245-276). Springer Netherlands.

Bray, J. D., O'Rourke, J. D., Cubrinovski, M., Zupan, J. D., Jeon, S. S., Taylor, M., ... and Bouziou, D. (2013). Liquefaction impact on critical infrastructure in Christchurch. United States Geological Survey Research Report. Accessed online at http://earthquake. usgs. gov/research/external/reports/G12AP20034. pdf on March, 21, 2014.

Bray, J. D., and Dashti, S. (2014). Liquefaction-induced building movements.Bulletin of Earthquake Engineering, 12(3), 1129-1156.

Campbell, K. W. (1981) "Near source attenuation of peak horizontal acceleration," *Bulletin of the Seismological Society of America*, 71, 2039-2070

Campbell, K.W. and Bozorgnia, Y. (1994) "Near-source attenuation of peak horizontal acceleration from worldwide accelerograms recorded from 1957 to 1993," *Proceedings, Fifth U.S. National Conference on Earthquake Engineering*, Earthquake Engineering Research Institute, Berkeley, California, Vol. 1, pp. 283-292.

Campbell, K.W. and Bozorgnia, Y. (2008). "NGA Ground Motion Model for the Geometric Mean Horizontal Component of PGA, PGV, PGD and 5% Damped Linear Elastic Response Spectra for Periods Ranging from 0.01 to 10 s," *Earthquake Spectra*: February 2008, Vol. 24, No. 1, pp. 139-171.

Casagrande, A. (1936). "Characteristics of cohesionless soils affecting the stability of slopes and earth fills," *Journal of the Boston Society of Civil Engineers, reprinted in Contributions to Soil Mechanics, Boston Society of Civil Engineers,* 1940, pp. 257-276
Castro, G. and Poulos, S.J. (1977). "Factors affecting liquefaction and cyclic mobility," *Journal of the Geotechnical Engineering Division,* ASCE, Vol 106, No. GT6, pp. 501-506

Cetin, K.O.,, et al. (2004) "Standard penetration test-based probabilistic and deterministic assessment of seismic soil liquefaction potential." *J. Geotech. Geoenviron. Eng.*, 10.1061/(ASCE)1090-0241(2004)130:12(1314), 1314-1340

Cetin, K., Bilge, H., Wu, J., Kammerer, A., and Seed, R. (2009) "Probabilistic Model for the Assessment of Cyclically Induced Reconsolidation (Volumetric) Settlements." *J. Geotech. Geoenviron. Eng.*, 135(3), 387-398

Chiou, B. S-J. and Youngs, R.R. (2008). "An NGA Model for the Average Horizontal Component of Peak Ground Motion and Response Spectra," *Earthquake Spectra*: February 2008, Vol. 24, No. 1, pp. 173-215.

Cornell, C. A. (1968). Engineering seismic risk analysis. Bulletin of the Seismological Society of America, 58(5), 1583-1606.

Cornell, C.A., and Krawinkler, H. (2000). "Progress and challenges in seismic performance assessment." *PEER News, April, 1-3.*

Deierlein, G.G., Krawinkler, H., and Cornell, C.A. (2003). "A framework for performance-based earthquake engineering." Proc., 2003 Pacific Conference on Earthquake Engineering, Wellington, New Zealand. Paper No. 140.

Ekstrom, L. T. (2015). A Simplified Performance-Based Procedure for the Prediction of Lateral Spread Displacements.

Fajfar P., Krawinkler, H. (1997). "Seismic Design Methodologies for the Next Generation of Codes," Proceedings of International Conference at Bled, Slovenia. A.A. Balkema, Rotterdam/Brookfield, 1997, pp59-68.

Franke, K. W., Wright, A. D., and Hatch, C. K. (2014). "PBLiquefY: A new analysis tool for the performance-based evaluation of liquefaction triggering." *Proceedings, 10th National Conference on Earthquake Engineering, Paper* (No. 87).

Ghobarah, A. (2001) Performance-based design in earthquake engineering: state of development. *Engineering Structures*, 23, 878-884

Hanzawa, H., Itoh, Y., and Suzuki, K. (1979). "Shear characteristics of a quick sand in the Arabian Gulf," *Soils and Foundations*, Vol. 19, No. 4, pp. 1-15

Housner, G.W. (1959) "Behavior of structures during earthquakes," *Journal of the Engineering Mechanics Division*, ASCE, Vol. 85, No. EM14, 109-129

Huang, Y.M. (2008) "Performance-based design and evaluation for liquefaction-related seismic hazards." *Ph.D. Dissertation*, University of Washington, Seattle, WA.

Hudson, D. E. (1956). "Response spectrum techniques in engineering seismology" Proceedings of the World Conference on Earthquake Engineering (pp. 4-1).

Idriss, I.M. (2008). "An NGA Empirical Model for Estimating the Horizontal Spectral Values Generated By Shallow Crustal Earthquakes," *Earthquake Spectra*: February 2008, Vol. 24, No. 1, pp. 217-242.

Idriss, I. M., & Boulanger, R. W. (2008). *Soil liquefaction during earthquakes*. Earthquake engineering research institute.

Ishihara, K. and Yoshimine, M. (1992). "Evaluation of settlements in sand deposits following liquefaction during earthquakes," *Soils"and Foundations*, Vol. 32, No. 1, p. 173-188.

Jennings, P.C. (1985). "Ground motion parameters that influence structural damage," in R.E. School and J.L. King, eds. *Strong Ground Motion Simulation and Engineering Applications*, EERI Publication 85-02, Earthquake Engineering Research Institute, Berkeley, California.

Jibson, R. (1987). "Summary of research on the effects of topographic amplification of earthquake shaking on slope stability," *Open-File Report 87-286*, U.S. Geological Survey, Menlo Park, California.

Joyner, W.B. and Boore, D.M. (1988) "Measurement, characterization, and prediction of strong ground motion," in *Earthquake Engineering and Soil Dynamics II – Recent Advances in Ground-Motion Evaluation*, Geotechnical Special Publication 20, ASCE, New York, pp. 43-102.

Kanamori, H. (1983). Magnitude scale and quantification of earthquakes.Tectonophysics, 93(3-4), 185-199.

Kawashima, K., and Aizawa, K. (1989). Bracketed and normalized durations of earthquake ground acceleration. Earthquake engineering & structural dynamics, 18(7), 1041-1051.

Kramer, S.L. (1996). *Geotechnical Earthquake Engineering*, Prentice Hall, Inc., Upper Saddle River, NJ, 653 pp.

Kramer, S.L. and Mayfield, R.T. (2007). Return period of soil liquefaction. *J. Geotech. Geoenviron. Eng.* 133(7), 802-813.

Kramer, S.L. (2008). "Evaluation of liquefaction hazards in Washington State." WSDOT Report *WA-RD 668.1*, 152 pp.

Kramer, S.L., Huang, Y.M., and Greenfield, M.W. (2014). Performance-based assessment of liquefaction hazards. *Geotechnics for Catastrophic Flooding Events*, Iai ed., ISBN 978-1-138-02709-1, Taylor and Francis Group, London, 17-26.

Lade, P.V. (1992). "Static instability and liquefaction of loose fine sandy slopes," *Journal of Geotechnical Engineering*, ASCE, Vol. 118, No. 1, pp. 51-71

Lambe, T.W., Garlanger, J.E., & Leifer, S.A. (1974). Prediction and field evaluation of downdrag forces on a single pile (No. Final Rpt.).

Lee, K. and Albaisa, A. (1974). "Earthquake induced settlements in saturated sands," *Journal of ASCE*, Vol. 103, GT6, pp. 565-588.

Mayfield, R. T. (2007). *The return period of soil liquefaction*. Doctoral dissertation, University of Washington.

Mayfield, R.T., Kramer, S.L., and Huang, Y.M. (2010). "Simplified approximation procedure for performance-based evaluation of liquefaction potential." *J. Geotech. Geoenviron. Eng.*, 10.1061/(ASCE) GT.1943-5606.0000191, 140-150

Middlebrooks, T.A. (1942). "Fort Peck Slide", *Transactions*, ASCE, Vol. 107, pp. 723-764

Moehle, J. and Deierlein, G.G. (2004). "A framework methodology for performance-based earthquake engineering." *Proceedings, 13th World Conference on Earthquake Engineering, Vancouver B.C., Canada.* Paper No. 679.

Mogami, T., and Kubo, K. (1953). The behavior of soil during vibration, *Proceedings, 3rd International Conference on Soil Mechanics and Foundation Engineering*, Zurich, Vol. 1, pp. 152-155.

Nagase, H., and Ishihara, K. (1988). "Liquefaction-induced compaction and settlement of sand during earthquakes," *Soils and Foundations*, Vol. 28, No. 1, pp. 66-76.

Poulos, S.J. (1981). "The steady state of deformation," *Journal of the Geotechnical Engineering Division*, ASCE, Vol. 107, No. GT5, pp. 553-562

Roscoe, K.H. and Pooroshasb, H.B. (1963). "A fundamental principle of similarity in model tests for earth pressure problems," *Proceedings, 2nd Asian Regional Conference on Soil Mechanics*, Tokyo, Vol. 1, pp. 134-140

Sanchez-Sesma, F. and Campillo, M. (1993). "Topographic effects for incident P, SV, and Rayleigh waves," *Tectonophysics*, Vol. 218, No. 1-3, pp. 113-125.

Seed, H.B., Murarka, R., Lysmer, J., and Idriss, I.M. (1976). "Relationships of maximum acceleration, maximum velocity, distance from source and local site conditions for moderately strong earthquakes," *Bulletin of the Seismological Society of America*, Vol. 66, No. 4, pp. 1323-1342.

Seed, R.B., Dickenson, S.E., Reimer, M.F., Bray, J.D. , Sitar, N., Mitchell, J.K., Idriss, I.M., Kayen, R.E., Kropp, A., Harder, L.F., and Power, M.S. (1990). "Preliminary report on the principal geotechnical aspects of the October 17, 1989 Loma Prieta earthquake," *Report UCB/EERC-90/05Report UCB/EERC-90/05*, Earthquake Engineering Research Center, University of California, Berkeley, 137 pp.

Shamoto, Y., Zhang, J. M., and Tokimatsu, K. (1998). "Methods for evaluating residual post-liquefaction ground settlement and horizontal displacement." *Soils Found*., 2(2), 69–83.

Somerville, P.G., Smith, N.F., Graves, R.W., and Abrahamson, N.A. (1997) "Modification of empirical strong ground motion attenuation relations to include the amplitude and duration of effects of rupture directivity," *Seismological Research Letters*, January/February 1997, Vol. 68, p. 199-222

Tatsuoka, F., Sasaki, T. and Yamada S. (1984). "Settlement in saturated sand induced by cyclic undrained simple shear," *Eighth World Conference on Earthquake Engineering*, San Francisco, Vol. III, pp. 95-102.

Tokimatsu, K. and Seed, H.B. (1984). "Simplified procedures of the evaluation of settlements in clean sands." *Rep. No. UCB/GT-84/16*, Univ. of California, Berkeley, Calif.

Tokimatsu, K. and Seed, H. (1987). "Evaluation of Settlements in Sands Due to Earthquake Shaking." *J. Geotech. Eng.*, 113(8), 861-878.

Toro, G.R., Abrahamson, N.A., and Schneider, J.F. (1995). "Engineering model of strong ground motions from earthquakes in the central and eastern United States," *Earthquake Spectra*, in press.

Tsukamoto, Y., Ishihara, K. (2010) "Analysis on settlement of soil deposits following liquefaction during earthquakes," *Soils and Foundations*, Vol. 50, No. 3, pp. 399-411

Ulmer, K. J. (2015). Development of a Simplified Performance-Based Procedure for Assessment of Liquefaction Triggering Using Liquefaction Loading Maps.

Ulmer, K. and Franke, K. (2015). "Modified Performance-Based Liquefaction Triggering Procedure Using Liquefaction Loading Parameter Maps." J. Geotech. Geoenviron. Eng., 10.1061/(ASCE)GT.1943-5606.0001421, 04015089.
Vaid, Y.P. and Chern, J.C. (1983). "Effect of static shear on resistance of liquefaction," *Soils and Foundations*, Vol. 23, No. 1, pp. 47-60

Vidale, J.E. and Helmberger, D.V. (1988). "Elastic finite difference of the 1971 San Fernando earthquake," *Bulletin of the Seismological Society of America*, Vol. 78, No. 1, pp. 122-141.

Watson JT, Gayer M, Connolly MA. (2007) "Epidemics after natural disasters," *Emerging Infectious Diseases*, Vol. 1, No. 1, pp. 1-5

Wu, J., and Seed, R. B. (2004). "Estimation of liquefaction-induced ground settlement (case studies)." *Proc., 5th Int. Conf. on Case Histories in Geotechnical Engineering*, Paper 3.09, New York.

Youd, T. L., and Perkins, D. M. (1978)." Mapping liquefaction-induced ground failure potential." Journal of the Geotechnical Engineering Division, 104(4), pp. 433-446.

Youd, T.L. (1984). "Recurrence of liquefaction at the same site," *Proceedings, 8th World Conference on Earthquake Engineering*, Vol. 3, pp. 231-238

Youd, T.L. (1991). "Mapping of earthquake-induced liquefaction for seismic zonation," *Proceedings, 4th International Conference on Seismic Zonation*, Earthquake Engineering Research Institute, Stanford University, Vol. 1, pp. 111-147

Youngs, R.R., Day, S.M., and Stevens, J.L. (1988). "Near field ground motions on rock for large subduction earthquakes," *Proceedings, Earthquake Engineering and Soil Dynamics II: Recent Advances in Ground Motion Evaluation*, Geotechnical Special Publication 20, ASCE, New York, pp. 445-462

APPENDIX A: ADDITIONS TO PBLIQUEFY

To use *PBLiquefY* to perform the analyses for this study, additions needed to be made to the code of *PBLiquefY* to incorporate the fully-probabilistic settlement estimation procedure presented in this study. The complete code, beginning on the next page, is provided in this section to facilitate recreation of this study.

```
Sub cetin_settlement_code()

''''''''''''''''''''''''''''''''''''''''''''''''''''''''''''''''''''''''''''''''
''''''''''''''''''''''''''''''''''''''''''''''''''''''''''''''''''''''''''''''''
        'create array of lamda and CSRss,20,1D,1atm values
''''''''''''''''''''''''''''''''''''''''''''''''''''''''''''''''''''''''''''''''
''''''''''''''''''''''''''''''''''''''''''''''''''''''''''''''''''''''''''''''''

ReDim settle_array(1 To 49, 1 To 3, 1 To 1) '(nreq, 1-nreq 2-lambda 3-csr,
sublayer)

Dim i As Integer
Dim j As Integer
Dim layercount As Integer
Dim slrange As Range
Dim slrow As Integer

Dim slcol As Integer
Dim offsetrow As Integer
Dim offsetcol As Integer
Dim fc As Double
Dim Mw As Double
Dim effstress As Double
Dim atmpress As Double
Dim Dr As Double
Dim progvals As Double
Dim theta2 As Double
Dim theta3 As Double
Dim theta6 As Double
Dim PLexp As Double
Dim rng As Range

layercount =
Worksheets("Hidden_Prob_results_cetin").Range("B:B").Cells.SpecialCells(xl
TextValues).count

ProgressBar.Show vbModeless
ProgressBar.Caption = "Probabilistic Settlement Calculation"
ProgressBar.Label1.Caption = "Calculation Progress:"
ProgressBar.ParameterEstType.Caption = "Creating Sublayer Arrays..."
ProgressBar.AdvancedPest.Visible = False
ProgressBar.Ksigmalimit_TF.Visible = False
ProgressBar.PB_MSFused.Visible = False
ProgressBar.NumberRuns.Visible = False
ProgressBar.minmax 1, 6
progvals = 0

progvals = progvals + 1
ProgressBar.values progvals
ProgressBar.ParameterEstType.Caption = "Creating Sublayer Arrays..."
DoEvents

ReDim nsitearray(1 To layercount) 'used for PL equation
ReDim settle_array(1 To 49, 1 To 3, 1 To layercount)
```

```
ReDim csr_array(1 To 49, 1 To 1, 1 To layercount)

'loop through nreq values in Hidden_Prob_results_cetin, find aggregate
lambda, generate table of nreq and lambda
    'find first sub layer
        'loop through nreq (49)
            'store lambda value in an array with the nreq (save room for
the csr value)
            'next nreq
        'next sub layer

For i = 1 To layercount

    nsitearray(i) = Sheet2.Range("Nvalue").Offset(i - 1, 0).value

    Set slrange = Worksheets("Hidden_Prob_results_cetin").Cells.Find("Sub
Layer " & i & "")

    slrow = slrange.Row
    slcol = slrange.Column

    'find the row totalling the lambda values
    offsetrow = 0
    Do Until InStr(Worksheets("Hidden_Prob_results_cetin").Cells(slrow,
slcol).Offset(offsetrow, 4), "TOTAL") <> 0
        offsetrow = offsetrow + 1
    Loop

    fc = Worksheets("Cetin_et_al_Deterministic").Range("cetinFC").Offset(i
- 1, 0)
    Mw = Worksheets("Cetin_et_al_Deterministic").Range("cetinMw").Offset(i
- 1, 0)
    effstress =
Worksheets("Cetin_et_al_Deterministic").Range("cetineffectivestress").Offs
et(i - 1, 0)
    atmpress =
Worksheets("Cetin_et_al_Deterministic").Range("cetinatmpressure").Offset(i
- 1, 0)

    For j = 1 To 49 'each possible value of Nreq

        offsetcol = 5 + (j - 1) * 3

        settle_array(j, 1, i) = j
        settle_array(j, 2, i) =
Worksheets("Hidden_Prob_results_cetin").Cells(slrow,
slcol).Offset(offsetrow, offsetcol)

        'take nreq value and plug into CSR = CRR(nreq) equation ****(see
Cetin 2004 paper, eq. 20, Mayfield Kramer 2010, eq. 2 w/table)****
        'add csr value to array of nreq and lambda
```

```
        If Sheet3.settle_exclude_par_uncertainty.value = True Then
'****after Mayfield (2010), Table 1****

            theta2 = 13.32
            theta3 = 29.53
            theta6 = 16.85
            PLexp = 2.7

        Else

            theta2 = 13.79
            theta3 = 29.06
            theta6 = 15.25
            PLexp = 4.21

        End If

        csr_array(j, 1, i) = Exp((j - theta3 * LN(7.5) + theta6) / theta2)
'****after Mayfield (2010) eq. 28****

        'adjust CSRfield to account for multidirectional shaking effects
(to create CSRss,20,1D,1atm)
        Dr = Worksheets("Soil_Profile_Info").Range("RelDensity").Offset(i
- 1, 0)
        settle_array(j, 3, i) = csr_array(j, 1, i) / (0.361 * LN(Dr) -
0.579) '****after Cetin et al (2009) eq. 2 and eq. 3****

    Next j

Next i

''''''''''''''''''''''''''''''''''''''''''''''''''''''''''''''''''''''''
            'create table to show values      (this is useful, but not
completely necessary. if code is running slow, consider deleting)
''''''''''''''''''''''''''''''''''''''''''''''''''''''''''''''''''''''''

'With Worksheets("Hidden_1")
'
'    .Range(Range("Probsettlementtable").Offset(1, 0),
Range("Probsettlementtable").Offset(60, 101)).ClearContents
'
'
'    For i = 1 To layercount
'
'        .Range("Probsettlementtable").Offset(4 * (i - 1) + 1, 0) = "Sub
Layer " & i
'        .Range("Probsettlementtable").Offset(4 * (i - 1) + 2, 0) = "Nreq"
'        .Range("Probsettlementtable").Offset(4 * (i - 1) + 3, 0) =
"lambda"
'        .Range("Probsettlementtable").Offset(4 * (i - 1) + 4, 0) =
"CSRss,20..."
'
'        For j = 1 To 49
'
```

```
'            .Range("Probsettlementtable").Offset(4 * (i - 1) + 2, j) = j
'            .Range("Probsettlementtable").Offset(4 * (i - 1) + 3, j) =
settle_array(j, 2, i)
'            .Range("Probsettlementtable").Offset(4 * (i - 1) + 4, j) =
settle_array(j, 3, i)
'
'        Next j
'
'    Next i

'End With

''''''''''''''''''''''''''''''''''''''''''''''''''''''''''''''''''''''''''''
''''''''''''''''''''''''''''''''''''''''''''''''''''''''''''''''''''''''''''
                'Compute strain for each layer
''''''''''''''''''''''''''''''''''''''''''''''''''''''''''''''''''''''''''''
''''''''''''''''''''''''''''''''''''''''''''''''''''''''''''''''''''''''''''

Dim currentstrain As Double
Dim maxstrain As Double
Dim deltalambda As Double
Dim n160cs As Double
Dim csr As Double
Dim incrementlambda As Double
Dim stack As Double
Dim Ev As Double
Dim lnEv As Double
Dim z As Double
Dim straincounter As Integer
Dim emax As Double
Dim PL As Double
Dim delta_emax As Double

Dim strain_array(1 To 50, 1 To 150) As Double
Dim lambda_array(1 To 50, 1 To 150) As Double
Dim final_lambda_array(1 To 50, 1 To 150) As Double

progvals = progvals + 1
ProgressBar.values progvals
ProgressBar.ParameterEstType.Caption = "Computing Strain..."
DoEvents

For i = 1 To layercount 'each sublayer

    'check if layer is susceptible to liquefaction
    If Sheets("Cetin_et_al_Deterministic").Range("CetinFSliq").Offset(i -
1, 0) = "Not_Susc." Then GoTo nxt

    n160cs =
Sheets("Cetin_et_al_Deterministic").Range("cetinN160cs").Offset(i - 1, 0)

    maxstrain = -2.24 * LN(n160cs) + 9.2081 '****after Huang (2008)
(equation regressed by Brian Peterson)****
    delta_emax = 0.02
```

```
    For e = 1 To 51 'emax of 0.5*emax to 1.5*emax in increments of
0.02*emax

        emax = (0.5 + (e - 1) * delta_emax) * maxstrain

        currentstrain = 0.1
        straincounter = 1

        Do Until currentstrain > 15 '****to capture the 1.5*10% strain
accounted for in Huang (2008)****

            stack = 0

            'add check for maximum strain (if maxstrain is exceeded,
Probability of exceedance is 0)
            If currentstrain > emax Then
                GoTo emaxexceed
            End If

            For j = 1 To 49 'each CSR

                csr = settle_array(j, 3, i)

                'compute current strain value ****after Cetin et al (2009)
eq. 1****
                'make sure equation does not return a negative value (LN
will not compute)
                'if value is undefined, it means the value is very small
and does not contribute to settlement
                If (780.416 * LN(csr) - n160cs + 2442.465) / (636.613 *
n160cs + 306.732) <= 0 Then 'inside LN value

                    Ev = 0.00001
                    GoTo computez

                ElseIf 1.879 * LN((780.416 * LN(csr) - n160cs + 2442.465)
/ (636.613 * n160cs + 306.732)) + 5.583 <= 0 Then 'outside LN value

                    Ev = 0.00001
                    GoTo computez

                Else

                    Ev = (1.879 * LN((780.416 * LN(csr) - n160cs +
2442.465) / (636.613 * n160cs + 306.732)) + 5.583)

                End If

                'consider Probability of Liquefaction
                If Sheet3.settle_consider_PL.value = True Then
                    PL = Application.WorksheetFunction.Norm_S_Dist(-
(n160cs - settle_array(j, 1, i)) / PLexp, True) '****after Ulmer et al
(2015)****
                    Ev = Ev * PL
```

```
                End If

computez:
                'compute probability of exceedance(lambda)
                z = (LN(Ev) - LN(currentstrain)) / 0.61

                incrementlambda =
Application.WorksheetFunction.Norm_S_Dist(z, True)

                'compute deltalambda and multiply by incrementlambda
                If j = 1 Then
                    deltalambda = settle_array(j, 2, i) - (settle_array(j
+ 1, 2, i) + settle_array(j, 2, i)) / 2
                ElseIf j = 49 Then
                    deltalambda = (settle_array(j - 1, 2, i) +
settle_array(j, 2, i)) / 2 - settle_array(j, 2, i)
                Else
                    deltalambda = (settle_array(j - 1, 2, i) +
settle_array(j, 2, i)) / 2 - (settle_array(j + 1, 2, i) + settle_array(j,
2, i)) / 2
                End If

                incrementlambda = incrementlambda * deltalambda / 51

                stack = stack + incrementlambda


            Next j 'next csr

emaxexceed:
            'assign aggregate lambda value and strain value to arrays for
creating graph
            strain_array(i, straincounter) = currentstrain

            lambda_array(i, straincounter) = stack

            straincounter = straincounter + 1
            currentstrain = currentstrain + 0.1

        Loop

        straincounter = straincounter - 1

        'take the lambdas and strains from the emax loop and store them in
final array
        For s = 1 To straincounter

            final_lambda_array(i, s) = final_lambda_array(i, s) +
lambda_array(i, s)

        Next s

    Next e 'next emax increment
```

```
nxt:
Next i 'next sublayer


''''''''''''''''''''''''''''''''''''''''''''''''''''''''''''''''''''
''''''''''''''''''''''''''''''''''''''''''''''''''''''''''''''''''''
            'show values in Hidden_Cetin_Prob_Settlement tab
''''''''''''''''''''''''''''''''''''''''''''''''''''''''''''''''''''
''''''''''''''''''''''''''''''''''''''''''''''''''''''''''''''''''''

With Sheets("Hidden_Cetin_Prob_Settlement")
    .Range(.Cells(1, 1), .Cells(152, 150)).ClearContents
End With

Dim mycol As Integer
Dim xarray(1 To 150) As Double
Dim yarray(1 To 150) As Double

mycol = 2

progvals = progvals + 1
ProgressBar.values progvals
ProgressBar.ParameterEstType.Caption = "Writing Data..."
DoEvents

For i = 1 To layercount

    With Sheets("Hidden_Cetin_Prob_Settlement")

        .Range("A1").Offset(0, mycol - 1) = "Sublayer " & i
        .Range("A1").Offset(1, mycol - 1) = "Strain"
        .Range("A1").Offset(1, mycol) = "Lambda"

        For j = 1 To 150

            xarray(j) = strain_array(i, j)
            yarray(j) = final_lambda_array(i, j)

        Next j

        .Range(.Cells(3, mycol), .Cells(152, mycol)) =
Application.Transpose(xarray)
        .Range(.Cells(3, mycol + 1), .Cells(152, mycol + 1)) =
Application.Transpose(yarray)

        mycol = mycol + 3

    End With


Next i
```

```
'prepare to tell compute_settlement and createchart modules which sheets
to reference (cetin=1,IandY = 2)

Dim analysistype As Integer
analysistype = 1

progvals = progvals + 1
ProgressBar.values progvals
ProgressBar.ParameterEstType.Caption = "Calculating Settlement..."
DoEvents

compute_settlement layercount, analysistype

progvals = progvals + 1
ProgressBar.values progvals
ProgressBar.ParameterEstType.Caption = "Creating Charts..."
DoEvents

createhazardcurvechart layercount, analysistype

'createsettlementchart layercount, analysistype

progvals = progvals + 1
ProgressBar.values progvals
ProgressBar.ParameterEstType.Caption = "Done"
DoEvents

ProgressBar.Hide


End Sub

Sub IandY_settlement_code()

''''''''''''''''''''''''''''''''''''''''''''''''''''''''''''''''''''''''''''''
''''''''''''''''''''''''''''''''''''''''''''''''''''''''''''''''''''''''''''''
        'create array of lamda and CSRss,20,1D,1atm values
''''''''''''''''''''''''''''''''''''''''''''''''''''''''''''''''''''''''''''''
''''''''''''''''''''''''''''''''''''''''''''''''''''''''''''''''''''''''''''''


Dim i As Integer
Dim j As Integer
Dim layercount As Integer
Dim slrange As Range
Dim slrow As Integer

Dim slcol As Integer
Dim offsetrow As Integer
Dim offsetcol As Integer
Dim Dr As Double
Dim progvals As Double
Dim n160cs As Double
```

```
layercount =
Worksheets("Hidden_Prob_results_IandB").Range("B:B").Cells.SpecialCells(xl
TextValues).count

ProgressBar.Show vbModeless
ProgressBar.Caption = "Probabilistic Settlement Calculation"
ProgressBar.Label1.Caption = "Calculation Progress:"
ProgressBar.ParameterEstType.Caption = "Creating Sublayer Arrays..."
ProgressBar.AdvancedPest.Visible = False
ProgressBar.Ksigmalimit_TF.Visible = False
ProgressBar.PB_MSFused.Visible = False
ProgressBar.NumberRuns.Visible = False
ProgressBar.minmax 1, 6
progvals = 0

progvals = progvals + 1
ProgressBar.values progvals
ProgressBar.ParameterEstType.Caption = "Creating Sublayer Arrays..."
DoEvents

ReDim settle_array(1 To 49, 1 To 3, 1 To layercount) '(nreq, 1-nreq 2-
lambda 3-FSliq, sublayer)

'loop through nreq values in Hidden_Prob_results_IandB, find aggregate
lambda, generate table of nreq and lambda
    'find first sub layer
        'loop through nreq (49)
            'store lambda value in an array with the nreq (save room for
the FSliq value)
            'next nreq
        'next sub layer

For i = 1 To layercount

    Set slrange = Worksheets("Hidden_Prob_results_IandB").Cells.Find("Sub
Layer " & i & "")

    slrow = slrange.Row
    slcol = slrange.Column
    n160cs = Sheets("IandB_Deterministic").Range("IandBN160cs").Offset(i -
1, 0).value

    'find the row totalling the lambda values
    offsetrow = 0
    Do Until InStr(Worksheets("Hidden_Prob_results_IandB").Cells(slrow,
slcol).Offset(offsetrow, 4), "TOTAL") <> 0
        offsetrow = offsetrow + 1
    Loop

    For j = 1 To 49 'each possible value of Nreq

        offsetcol = 5 + (j - 1) * 3

        settle_array(j, 1, i) = j
```

```
        settle_array(j, 2, i) =
Worksheets("Hidden_Prob_results_IandB").Cells(slrow,
slcol).Offset(offsetrow, offsetcol)
        settle_array(j, 3, i) = Exp((n160cs - j) / 14.1 + (n160cs ^ 2 - j
^ 2) / 126 ^ 2 - (n160cs ^ 3 - j ^ 3) / 23.6 ^ 3 + (n160cs ^ 4 - j ^ 4) /
25.4 ^ 4) '****after Ulmer (2015)****

    Next j

Next i

''''''''''''''''''''''''''''''''''''''''''''''''''''''''
            'create table to show values      (this is useful, but not
necessary. Written to visually check accuracy of arrays
''''''''''''''''''''''''''''''''''''''''''''''''''''''''

'With Worksheets("Hidden_1")
'
'    .Range(Range("Probsettlementtable").offset(1, 0),
Range("Probsettlementtable").offset(60, 101)).ClearContents
'
'
'    For i = 1 To layercount
'
'        .Range("Probsettlementtable").offset(4 * (i - 1) + 1, 0) = "Sub
Layer " & i
'        .Range("Probsettlementtable").offset(4 * (i - 1) + 2, 0) = "Nreq"
'        .Range("Probsettlementtable").offset(4 * (i - 1) + 3, 0) =
"lambda"
'        .Range("Probsettlementtable").offset(4 * (i - 1) + 4, 0) =
"FSliq"
'
'        For j = 1 To 49
'
'            .Range("Probsettlementtable").offset(4 * (i - 1) + 2, j) = j
'            .Range("Probsettlementtable").offset(4 * (i - 1) + 3, j) =
settle_array(j, 2, i)
'            .Range("Probsettlementtable").offset(4 * (i - 1) + 4, j) =
settle_array(j, 3, i)
'
'        Next j
'
'    Next i
'
'End With

''''''''''''''''''''''''''''''''''''''''''''''''''''''''''''''''''''''
''''''''''''''''''''''''''''''''''''''''''''''''''''''''''''''''''''''
                'Compute strain for each layer
''''''''''''''''''''''''''''''''''''''''''''''''''''''''''''''''''''''
''''''''''''''''''''''''''''''''''''''''''''''''''''''''''''''''''''''

Dim currentstrain As Double
Dim maxstrain As Double
```

```
Dim n160 As Double
Dim deltalambda As Double
Dim csr As Double
Dim incrementlambda As Double
Dim stack As Double
Dim Ev As Double
Dim lnEv As Double
Dim z As Double
Dim straincounter As Integer
Dim gammalim As Double
Dim falpha As Double
Dim gammamax As Double
Dim gammacheck As Double 'used in the gammamax equation to compare against
gammalim
Dim min As Double
Dim PLexp As Double
Dim emax As Double

Dim strain_array(1 To 50, 1 To 150) As Double
Dim lambda_array(1 To 50, 1 To 150) As Double
Dim final_lambda_array(1 To 50, 1 To 150) As Double

progvals = progvals + 1
ProgressBar.values progvals
ProgressBar.ParameterEstType.Caption = "Computing Strain..."
DoEvents

'check uncertainty option for PL equation
If Sheet3.settle_exclude_par_uncertainty.value = True Then
    PLexp = -7.69
Else
    PLexp = -3.61
End If

For i = 1 To layercount 'each sublayer

    'check if layer is susceptible to liquefaction
    If Sheets("IandB_Deterministic").Range("IandBFSliq").Offset(i - 1, 0)
= "Not_Susc." Then GoTo nxt

    'compute values needed for strain equation
    n160cs = Sheets("IandB_Deterministic").Range("IandBN160cs").Offset(i -
1, 0)

    Dr = Sheets("Soil_Profile_Info").Range("RelDensity").Offset(i - 1, 0)
/ 100

    gammalim = 1.859 * (1.1 - (n160cs / 46) ^ 0.5) ^ 3 '****after IandY
(1992)****

    If gammalim < 0 Then gammalim = 0

    falpha = 0.032 + 4.7 * Dr - 6 * Dr ^ 2 '****after IandY (1992)****
```

```
    maxstrain = -2.24 * LN(n160cs) + 9.2081 '****after Huang (2008),
equation regressed by Brian Peterson****
    delta_emax = 0.02

    For e = 1 To 51 'emax from 0.5*emax to 1.5*emax in increments of
0.02*emax '****after Mayfield (2010)****

        emax = (0.5 + (e - 1) * delta_emax) * maxstrain

        currentstrain = 0.1
        straincounter = 1

        Do Until currentstrain > 15

            stack = 0

            'add check for maximum strain (if maxstrain is exceeded,
Probability of exceedance is 0)
            If currentstrain > emax Then
                GoTo emaxexceed
            End If

            For j = 1 To 49 'each FSliq

                    FSliq = settle_array(j, 3, i) '****per IandY
(1992)****

                    gammacheck = 0.035 * (2 - FSliq) * ((1 - falpha) /
(FSliq - falpha))

                    'assign gammamax
                    If FSliq >= 2 Then
                        gammamax = 0
                        GoTo nextj
                    ElseIf 2 > FSliq And FSliq > falpha Then
                        If gammalim < gammacheck Then
                            gammamax = gammalim
                        Else
                            gammamax = gammacheck
                        End If
                    ElseIf FSliq <= falpha Then
                        gammamax = gammalim
                    End If

                    'compute min(0.08,gammamax)
                    If gammamax > 0.08 Then
                        min = 0.08
                    Else
                        min = gammamax
                    End If

                    'compute current lambda value

                    Ev = (1.5 * Exp(-0.369 * n160cs ^ 0.5) * min) * 100
```

```
                    'check PL option
                    If Sheet3.settle_consider_PL.value = True Then
                        PL =
Application.WorksheetFunction.Norm_S_Dist(LN(FSliq ^ PLexp), True)
                        Ev = Ev * PL
                    End If

                    z = (LN(Ev) - LN(currentstrain)) / 1.12

                    incrementlambda =
Application.WorksheetFunction.Norm_S_Dist(z, True)

                    'compute delta lambda and multiply by increment lambda
                    If j = 1 Then
                        deltalambda = settle_array(j, 2, i) -
(settle_array(j + 1, 2, i) + settle_array(j, 2, i)) / 2
                    ElseIf j = 49 Then
                        deltalambda = (settle_array(j - 1, 2, i) +
settle_array(j, 2, i)) / 2 - settle_array(j, 2, i)
                    Else
                        deltalambda = (settle_array(j - 1, 2, i) +
settle_array(j, 2, i)) / 2 - (settle_array(j + 1, 2, i) + settle_array(j,
2, i)) / 2
                    End If

                    incrementlambda = incrementlambda * deltalambda / 51

                    stack = stack + incrementlambda
nextj:
            Next j 'next FSliq

emaxexceed:
            'assign aggregate lambda value and strain value to arrays for
creating graph

            strain_array(i, straincounter) = currentstrain

            lambda_array(i, straincounter) = stack

            straincounter = straincounter + 1
            currentstrain = currentstrain + 0.1

        Loop 'next strain

        straincounter = straincounter - 1

        For s = 1 To straincounter

            final_lambda_array(i, s) = final_lambda_array(i, s) +
lambda_array(i, s)

        Next s
```

```
    Next e 'next emax increment

nxt:
Next i 'next sublayer


''''''''''''''''''''''''''''''''''''''''''''''''''''''''''''''''''''''''''''''''
''''''''''''''''''''''''''''''''''''''''''''''''''''''''''''''''''''''''''''''''
            'show values in Hidden_IandY_Prob_Settlement tab
''''''''''''''''''''''''''''''''''''''''''''''''''''''''''''''''''''''''''''''''
''''''''''''''''''''''''''''''''''''''''''''''''''''''''''''''''''''''''''''''''

With Sheets("Hidden_IandY_Prob_Settlement")

    .Range(.Cells(1, 1), .Cells(152, 150)).ClearContents
    .Range(.Cells(155, 1), .Cells(300, 150)).ClearContents

End With

Dim mycol As Integer
Dim xarray(1 To 150) As Double
Dim yarray(1 To 150) As Double

mycol = 2

progvals = progvals + 1
ProgressBar.values progvals
ProgressBar.ParameterEstType.Caption = "Writing Data..."
DoEvents

For i = 1 To layercount

    With Sheets("Hidden_IandY_Prob_Settlement")

        .Range("A1").Offset(0, mycol - 1) = "Sublayer " & i
        .Range("A1").Offset(1, mycol - 1) = "Strain"
        .Range("A1").Offset(1, mycol) = "Lambda"

        For j = 1 To 150

            xarray(j) = strain_array(i, j)
            yarray(j) = final_lambda_array(i, j)

        Next j

        .Range(.Cells(3, mycol), .Cells(152, mycol)) =
Application.Transpose(xarray)
        .Range(.Cells(3, mycol + 1), .Cells(152, mycol + 1)) =
Application.Transpose(yarray)

        mycol = mycol + 3

    End With
```

```
Next i

'prepare to tell compute_settlement and createchart modules which sheets
to reference (cetin=1,IandY = 2)

Dim analysistype As Integer
analysistype = 2

progvals = progvals + 1
ProgressBar.values progvals
ProgressBar.ParameterEstType.Caption = "Calculating Settlement..."
DoEvents

compute_settlement layercount, analysistype

progvals = progvals + 1
ProgressBar.values progvals
ProgressBar.ParameterEstType.Caption = "Creating Charts..."
DoEvents

createhazardcurvechart layercount, analysistype

'createsettlementchart layercount, analysistype

progvals = progvals + 1
ProgressBar.values progvals
ProgressBar.ParameterEstType.Caption = "Done"
DoEvents

ProgressBar.Hide


End Sub

Sub compute_settlement(layercount As Integer, analysistype As Integer)

ReDim DF_array(1 To layercount) 'depth factor
ReDim strain_array(1 To layercount)
ReDim t_array(1 To layercount) 'thickness
Dim hiddensheetname As String
Dim determsheetname As String
Dim FSrange As Range
Dim lambda_array(1 To 8) As Double

Dim num As Double
Dim den As Double
Dim sumt As Double
Dim equivstrain As Double
Dim s As Double 'settlement
Dim d As Double 'mid-depth of layer
Dim lambda As Double
Dim myrow As Integer
Dim mycol As Integer
```

```
Dim ymax As Double 'interpolation values
Dim ymin As Double '
Dim yfind As Double '
Dim xmax As Double '
Dim xmin As Double '
Dim theta As Double 'field calibration coefficient

Dim lambdacount As Integer
Dim columnoffset As Integer
Dim finished As Boolean
ReDim my_strain_max(1 To layercount) As Double
Dim q As Integer
Dim my_lambda_value As Double

'assign correct reference worksheets for the analysis type
If analysistype = 1 Then
    hiddensheetname = "Hidden_Cetin_Prob_Settlement"
    determsheetname = "Cetin_et_al_Deterministic"
    theta = 1.15
    Set FSrange = Sheets("Cetin_et_al_Deterministic").Range("CetinFSliq")
ElseIf analysistype = 2 Then
    hiddensheetname = "Hidden_IandY_Prob_Settlement"
    determsheetname = "IandB_Deterministic"
    theta = 0.9
    Set FSrange = Sheets("IandB_Deterministic").Range("IandBFSliq")
End If

With Sheets(hiddensheetname)
    .Range(.Cells(155, 1), .Cells(205, 3)).ClearContents
End With

columnoffset = 0

mycol = 5

lambdacount = 1

'retrieves lambda value for each return period
Do While lambdacount <= 8

     lambda_array(lambdacount) = 1 / Sheet15.Range("Return" &
lambdacount).Offset(1, 1)

     lambdacount = lambdacount + 1

Loop

lambdacount = 1

'performs calculations for each return period
Do While lambdacount <= 8

    lambda = lambda_array(lambdacount)
```

```
    For i = 1 To layercount

            'check if layer is susceptible to liquefaction
        If FSrange.Offset(i - 1, 0) = "Not_Susc." Then
            strain_array(i) = 0
            GoTo nxt
        End If

             'assign DF_array
        d = Sheets("Soil_Profile_Info").Range("BottomDepth").Offset(i - 1,
0) - (0.5 * Sheets("Soil_Profile_Info").Range("Thickness").Offset(i - 1,
0))

        DF_array(i) = 1 - (d / 18)

        If DF_array(i) < 0 Then DF_array(i) = 0

            'assign t_array
        t_array(i) =
Sheets("Soil_Profile_Info").Range("Thickness").Offset(i - 1, 0)

            'assign strain_array
        With Sheets(hiddensheetname)

            myrow = 3

            If .Cells(myrow, 3 * i) < lambda Then

                strain_array(i) = 0
                GoTo nxt

            End If

            Do Until .Cells(myrow, 3 * i) < lambda

                myrow = myrow + 1

            Loop

            If .Cells(myrow, 3 * i) = 0 Then

                strain_array(i) = my_strain_max(i) / 100
                GoTo nxt

            Else

                ymin = .Cells(myrow, 3 * i).value
                ymax = .Cells(myrow - 1, 3 * i).value
                xmin = .Cells(myrow - 1, 3 * i - 1).value
                xmax = .Cells(myrow, 3 * i - 1).value

            End If

        End With
```

```
        ymin = 10 ^ ymin
        ymax = 10 ^ ymax
        yfind = 10 ^ lambda

        strain_array(i) = (Linear_interpolation(yfind, ymin, ymax, xmin,
xmax)) / 100


nxt:
    Next i

    num = 0
    den = 0
    sumt = 0

    For i = 1 To layercount

            'check if layer is susceptible to liquefaction
        If FSrange.Offset(i - 1, 0) = "Not_Susc." Then GoTo nxt2

        num = num + strain_array(i) * t_array(i) * DF_array(i)
        den = den + t_array(i) * DF_array(i)
        sumt = sumt + t_array(i)

nxt2:
    Next i

    equivstrain = num / den

    s = equivstrain * sumt * theta

    ''''''''''''''''''''''''''''''''''''''''''''''''''''''''''''''''''''''''
    ''''''''''''''''''''''''''''''''''''''''''''''''''''''''''''''''''''''''
    '              show values in Hidden_Prob_Settlement tabs
    ''''''''''''''''''''''''''''''''''''''''''''''''''''''''''''''''''''''''
    ''''''''''''''''''''''''''''''''''''''''''''''''''''''''''''''''''''''''

    With Sheets(hiddensheetname)

        .Range("A155") = "Return Period"
        .Range("A155").Offset(0, 1) = "Strain"
        .Range("A155").Offset(0, 2) = "Settlement [m]"
        .Range("A155").Offset(lambdacount, 0) = Sheet15.Range("Return" &
lambdacount).Offset(1, 1)
        .Range("A155").Offset(lambdacount, 1) = equivstrain
        .Range("A155").Offset(lambdacount, 2) = s

        'individual sublayer strains
        .Range("E156").Offset(-1, columnoffset) = "RP: " &
Sheet15.Range("Return" & lambdacount).Offset(1, 1)
        .Range("E156").Offset(0, columnoffset) = "Sublayer"
        .Range("E156").Offset(0, columnoffset + 1) = "Depth"
        .Range("E156").Offset(0, columnoffset + 2) = "Strain"
```

```
    End With

        myrow = 157

    For i = 1 To layercount

       Sheets(hiddensheetname).Cells(myrow, mycol + 1).value =
Sheets("Soil_Profile_Info").Range("B43").Offset(i, 0).value

        myrow = myrow + 1

    Next i

    'populate sublayer, strain, and settlement columns
    ReDim layercountarray(1 To layercount) As Integer

    For i = 1 To layercount

        layercountarray(i) = i

    Next i

    myrow = 157

    For i = 1 To layercount

        With Sheets(hiddensheetname)

            .Cells(myrow, mycol) = layercountarray(i)
            .Cells(myrow, mycol + 2) = strain_array(i)

        End With

        myrow = myrow + 1

    Next i

    mycol = mycol + 4
    columnoffset = columnoffset + 4

    lambdacount = lambdacount + 1

Loop

End Sub

Sub createhazardcurvechart(layercount As Integer, analysistype As Integer)

    Dim hiddensheetname As String
    Dim determsheetname As String
    Dim FSrange As Range
    Dim hazardcurvechart As String
    Dim settlementhazardcurvechart As String
```

```
    Dim settlementhazardcurverange As String

    'assign correct reference worksheets for the analysis type
    If analysistype = 1 Then
        hiddensheetname = "Hidden_Cetin_Prob_Settlement"
        determsheetname = "Cetin_et_al_Deterministic"
        Set FSrange =
Sheets("Cetin_et_al_Deterministic").Range("CetinFSliq")
        hazardcurvechart = "cetin strain hazard curve"
        settlementhazardcurvechart = "Cetin settlement hazard curve"
        settlementhazardcurverange = "cetinsettlehazcurve"
    ElseIf analysistype = 2 Then
        hiddensheetname = "Hidden_IandY_Prob_Settlement"
        determsheetname = "IandB_Deterministic"
        Set FSrange = Sheets("IandB_Deterministic").Range("IandBFSliq")
        hazardcurvechart = "IandY strain hazard curve"
        settlementhazardcurvechart = "IandY settlement hazard curve"
        settlementhazardcurverange = "IandYsettlehazcurve"
    End If


Sheets("Performance_Based_Settlement").ChartObjects(hazardcurvechart).Acti
vate

    For Each s In ActiveChart.SeriesCollection
    s.Delete
    Next s

    Dim datarow As Integer
    Dim datacol As Integer
    Dim xrange As Range
    Dim yrange As Range
    Dim seriesnum As Integer

    datacol = 2
    seriesnum = 1

    For i = 1 To layercount

    If FSrange.Offset(i - 1, 0) = "Not_Susc." Then
        datacol = datacol + 3
        GoTo nxt
    End If

    'loop to find end of data in series

    datarow = 3

    Do Until Sheets(hiddensheetname).Cells(datarow, datacol) = 0
       datarow = datarow + 1
    Loop

    With Sheets(hiddensheetname)
```

```
        Set xrange = .Range(.Cells(3, datacol), .Cells(datarow - 1,
datacol))
        datacol = datacol + 1
        Set yrange = .Range(.Cells(3, datacol), .Cells(datarow - 1,
datacol))

        ActiveChart.SeriesCollection.NewSeries
        ActiveChart.SeriesCollection(seriesnum).Name = "=""Sublayer " & i
& """"
        ActiveChart.SeriesCollection(seriesnum).XValues = xrange
        ActiveChart.SeriesCollection(seriesnum).values = yrange

        datacol = datacol + 2
        seriesnum = seriesnum + 1

    End With
nxt:
    Next i

'create settlement hazard curve

seriesnum = 1

Sheets("Performance_Based_Settlement").ChartObjects(settlementhazardcurvec
hart).Activate

For Each s In ActiveChart.SeriesCollection
s.Delete
Next s

'create and store array of total settlement for each return period
Dim settlehazcurve_array(1 To 8) As Double

For i = 1 To 8
    settlehazcurve_array(i) =
Sheets(hiddensheetname).Range("A155").Offset(i, 2) * 100
    Sheets("Hidden_1").Range(settlementhazardcurverange).Offset(i, 1) =
settlehazcurve_array(i)
Next i

With Sheets("Hidden_1")

    Set xrange = .Range(.Range(settlementhazardcurverange).Offset(1, 1),
.Range(settlementhazardcurverange).Offset(8, 1))
    Set yrange = .Range(.Range(settlementhazardcurverange).Offset(1, 0),
.Range(settlementhazardcurverange).Offset(8, 0))

End With

ActiveChart.SeriesCollection.NewSeries
ActiveChart.SeriesCollection(seriesnum).Name = "Settlement Hazard Curve"
ActiveChart.SeriesCollection(seriesnum).XValues = xrange
ActiveChart.SeriesCollection(seriesnum).values = yrange
```

```
End Sub
Sub Number_Cruncher()

Dim numlayers As Integer
Dim settlement_array(1 To 2, 1 To 6) As Double '(1-cetin 2-IandY, 1-mean
475 2-mean 2475 3-modal 475 4-modal 2475 5-semi 475 6-semi 2475)
Dim city As Integer
Dim casetype As Integer
Dim i As Integer
Dim j As Integer
Dim cityname As String
Dim profilename As String
Dim counter As Integer
Dim strainrowcounter As Integer
Dim settlementrowcounter As Integer
Dim CSRoffsetcounter As Integer

Unprotect_All

counter = 0
CSRoffsetcounter = 3
numlayers = Sheet2.Range("Numlayers").value

ReDim strain_array(1 To 2, 1 To 6, 1 To numlayers) As Double '(1-cetin 2-
IandY, 1-mean 475 2-mean 2475 3-modal 475 4-modal 2475 5-semi 475 6-semi
2475, each sublayer)

ReDim copypaste_array(1 To numlayers) As Variant

cityname = Sheet15.Range("Site_ID_1")
profilename = Sheet15.Range("Site_ID_2")

'find offset of csr data for semi-prob calcs
Do Until Sheet15.Range("CSR_for_semi_calcs").Offset(0, counter * 2) =
cityname
    counter = counter + 1
Loop

Do Until Sheet15.Range("CSR_for_semi_calcs").Offset(CSRoffsetcounter, -1)
= profilename
    CSRoffsetcounter = CSRoffsetcounter + 1
Loop

For casetype = 1 To 4 'each case

'select case
    If casetype = 1 Then 'mean 475
        Sheet3.Deterministic_MeanModal_ComboBox = "Mean Magnitude -
Specify Return Period"
        Return_Period_select.MagSelector.value = "Return Period 475
years."
    ElseIf casetype = 2 Then 'mean 2475
        Sheet3.Deterministic_MeanModal_ComboBox = "Mean Magnitude -
Specify Return Period"
```

```
        Return_Period_select.MagSelector.value = "Return Period 2475
years."
    ElseIf casetype = 3 Then 'modal 475
        Sheet3.Deterministic_MeanModal_ComboBox = "Modal Magnitude -
Specify Return Period"
        Return_Period_select.MagSelector.value = "Return Period 475
years."
    ElseIf casetype = 4 Then 'modal 2475
        Sheet3.Deterministic_MeanModal_ComboBox = "Modal Magnitude -
Specify Return Period"
        Return_Period_select.MagSelector.value = "Return Period 2475
years."
    End If

    i = 1

'update info on Sheet3 ************ taken from mag_update ************
        Do While i <= 8

                'finds data user specified

                If Return_Period_select.MagSelector.value = "Return Period
" & Sheet15.Range("Return" & i).Offset(1, 1) & " years." Then

                        j = i

                    End If

                i = i + 1

            Loop

        'updates user defined Mw and amax and RP boxes

        Sheet3.Select

        If Sheet3.Deterministic_MeanModal_ComboBox = "Mean Magnitude -
Specify Return Period" Then

                Sheet3.Range("detRP").Offset(0, -1).Style = "normal"

                Application.ScreenUpdating = False

                Sheet3.Activate

                Sheet3.Range("detRP").Offset(0, -1).HorizontalAlignment =
xlRight

                Application.ScreenUpdating = True

                Sheet3.Range("detRP") = Sheet15.Range("Return" &
j).Offset(1, 1)

                Sheet3.Range("detRP").Style = "Border_black"
```

```
                Sheet3.Range("detMw") = Sheet15.Range("Return" &
j).Offset(3, 2)

                Sheet3.Range("detMw").Style = "Border_black"

                Sheet3.Range("det_amax") = Sheet15.Range("Return" &
j).Offset(1, 4)

                Sheet3.Range("det_amax").Style = "Border_black"

            ElseIf Sheet3.Deterministic_MeanModal_ComboBox = "Modal
Magnitude - Specify Return Period" Then

                Sheet3.Range("detRP").Offset(0, -1).Style = "normal"

                Application.ScreenUpdating = False

                Sheet3.Activate

                Sheet3.Range("detRP").Offset(0, -1).HorizontalAlignment =
xlRight

                Application.ScreenUpdating = True

                Sheet3.Range("detRP") = Sheet15.Range("Return" &
j).Offset(1, 1)

                Sheet3.Range("detRP").Style = "Border_black"

                Sheet3.Range("detMw") = Sheet15.Range("Return" &
j).Offset(4, 2)

                Sheet3.Range("detMw").Style = "Border_black"

                Sheet3.Range("det_amax") = Sheet15.Range("Return" &
j).Offset(1, 4)

                Sheet3.Range("det_amax").Style = "Border_black"

            Else

                MsgBox "Error - select mean or modal magnitude for use in
deterministic calculations."

            End If

            Deterministic_options_box.Summaryamax.Caption = "amax = " &
Sheet3.Range("det_amax").value

            Deterministic_options_box.SummaryTR.Caption = "Return Period =
" & Sheet3.Range("detRP").value
```

```
            Deterministic_options_box.SummaryMw.Caption = "Mw = " &
Sheet3.Range("detMw").value
'************ end of portion taken from mag_update ************

'run calculations
    DeterministicRun

    settlement_array(1, casetype) =
Sheet4.Range("cetincumulativesettlement")
    settlement_array(2, casetype) =
Sheet5.Range("IandYcumulativesettlement")

    For i = 1 To numlayers
        strain_array(1, casetype, i) =
Sheet4.Range("cetinsettlestrain").Offset(i - 1, 0)
        strain_array(2, casetype, i) =
Sheet5.Range("IandYstrain").Offset(i - 1, 0)
    Next i

'compute semi probabilistic strain/settlement
    If casetype = 1 Then

        For i = 1 To numlayers

            copypaste_array(i) =
Sheet15.Range("CSR_for_semi_calcs").Offset(CSRoffsetcounter + i - 1,
counter * 2)
            Sheet4.Range("cetinCSR").Offset(i - 1, 0).value =
copypaste_array(i)
            Sheet5.Range("IandBCSR").Offset(i - 1, 0).value =
copypaste_array(i)

        Next i

        settlement_array(1, casetype + 4) =
Sheet4.Range("cetincumulativesettlement")
        settlement_array(2, casetype + 4) =
Sheet5.Range("IandYcumulativesettlement")

        For i = 1 To numlayers
            strain_array(1, casetype + 4, i) =
Sheet4.Range("cetinsettlestrain").Offset(i - 1, 0)
            strain_array(2, casetype + 4, i) =
Sheet5.Range("IandYstrain").Offset(i - 1, 0)
        Next i

    ElseIf casetype = 2 Then

        For i = 1 To numlayers

            copypaste_array(i) =
Sheet15.Range("CSR_for_semi_calcs").Offset(CSRoffsetcounter + i - 1,
(counter * 2) + 1)
```

```
            Sheet4.Range("cetinCSR").Offset(i - 1, 0).value =
copypaste_array(i)
            Sheet5.Range("IandBCSR").Offset(i - 1, 0).value =
copypaste_array(i)

        Next i

        settlement_array(1, casetype + 4) =
Sheet4.Range("cetincumulativesettlement")
        settlement_array(2, casetype + 4) =
Sheet5.Range("IandYcumulativesettlement")

        For i = 1 To numlayers
            strain_array(1, casetype + 4, i) =
Sheet4.Range("cetinsettlestrain").Offset(i - 1, 0)
            strain_array(2, casetype + 4, i) =
Sheet5.Range("IandYstrain").Offset(i - 1, 0)
        Next i

    End If

Next casetype

strainrowcounter = 1
settlementrowcounter = 1

Do Until Sheet15.Range("Psuedo_strain_outputs").Offset(strainrowcounter,
0) = ""
    strainrowcounter = strainrowcounter + 1
Loop

Do Until
Sheet15.Range("Psuedo_settlement_outputs").Offset(settlementrowcounter, 0)
= ""
    settlementrowcounter = settlementrowcounter + 1
Loop

'print data on sheets
For i = 1 To numlayers

    Sheet15.Range("Psuedo_strain_outputs").Offset(strainrowcounter, 0) =
cityname
    Sheet15.Range("Psuedo_strain_outputs").Offset(strainrowcounter, 1) =
profilename


    'input strain data
    For j = 1 To 6
        Sheet15.Range("Psuedo_strain_outputs").Offset(strainrowcounter, j
+ 1) = strain_array(1, j, i)
        Sheet15.Range("Psuedo_strain_outputs").Offset(strainrowcounter, j
+ 7) = strain_array(2, j, i)
    Next j
```

```
    strainrowcounter = strainrowcounter + 1

Next i

Sheet15.Range("Psuedo_settlement_outputs").Offset(settlementrowcounter, 0)
= cityname
Sheet15.Range("Psuedo_settlement_outputs").Offset(settlementrowcounter, 1)
= profilename

For j = 1 To 6
    'input settlement data

Sheet15.Range("Psuedo_settlement_outputs").Offset(settlementrowcounter, j
+ 1) = settlement_array(1, j)

Sheet15.Range("Psuedo_settlement_outputs").Offset(settlementrowcounter, j
+ 7) = settlement_array(2, j)
Next j

Protect_All

End Sub

'Sub createsettlementchart(layercount As Integer, analysistype As Integer)
'
'Dim hiddensheetname As String
'Dim determsheetname As String
'Dim settlementchart As String
'
''assign correct reference worksheets for the analysis type
'If analysistype = 1 Then
'    hiddensheetname = "Hidden_Cetin_Prob_Settlement"
'    determsheetname = "Cetin_et_al_Deterministic"
'    settlementchart = "cetin settlement chart"
'ElseIf analysistype = 2 Then
'    hiddensheetname = "Hidden_IandY_Prob_Settlement"
'    determsheetname = "IandB_Deterministic"
'    settlementchart = "IandY settlement chart"
'ElseIf analysistype = 3 Then
'    hiddensheetname = "Hidden_Juang_Prob_Settlement"
'    determsheetname = "Youd_et_al_Deterministic"
'    settlementchart = "Juang settlement chart"
'End If
'
'Dim xrange As Range
'Dim yrange As Range
'Dim offsetcolumn As Integer
'
''count number of series to be graphed (number of return periods analyzed)
'Dim seriescount As Integer
'
'seriescount =
Application.WorksheetFunction.CountA(Sheet14.Range("A155:AY155"))
```

```
'Sheets("Performance_Based_Settlement").ChartObjects(settlementchart).Acti
vate
'
'For Each s In ActiveChart.SeriesCollection
'    s.Delete
'Next s
'
'offsetcolumn = 0
'
'For i = 1 To seriescount
'
'    With Sheets(hiddensheetname)
'        Set xrange = .Range(.Cells(157, offsetcolumn + 5), .Cells(157 +
layercount - 1, offsetcolumn + 5))
'        Set yrange = .Range(.Cells(157, offsetcolumn + 2), .Cells(157 +
layercount - 1, offsetcolumn + 2))
'    End With
'
'    ActiveChart.SeriesCollection.NewSeries
'    ActiveChart.SeriesCollection(i).Name =
Sheet14.Range("settlementinfo").Offset(-1, offsetcolumn).value
'    ActiveChart.SeriesCollection(i).XValues = xrange
'    ActiveChart.SeriesCollection(i).values = yrange
'
'    offsetcolumn = offsetcolumn + 6
'
'Next i
'
'End Sub
```

APPENDIX B: PBLIQUEFY TUTORIAL

PBLiquefY is designed to be user friendly, but because of the complex nature of probabilistic methods, a tutorial is provided to ensure all users are comfortable throughout the analysis process. It should be noted that the instructions included below are also included within *PBLiquefY* itself. When *PBLiquefY* is opened, a title page is shown, along with a flow chart of a typical analysis process. The instructions provided below will generally follow the same process as shown in the program flowchart. Namely, that a user will navigate to the page of interest (in the specified order) and then follow the outlined steps.

Soil Profile Info Page

1. Provide required input in the cells listed on the page. Cells requiring user input are shown in red, while values listed in black should not be changed by the user.
2. Press the "Generate Sub Layers" button. This will generate a table at the bottom of the page.
3. Specify the type of additional loading (embankment, uniform, or none) under Applied Loads and Fills at the bottom of the page. Follow directions in the pop up box to apply loading and Ka factors.
4. Provide the required input in the soil profile table below the applied loads section. (Required Input shown in Red; if copying and pasting data, make sure to type in data for

at least one cell and press enter to trigger auto calculations.) NOTE: C1 is a value for sampler type.

- Optional: Allow *PBLiquefY* to calculate relative density and shear wave velocity based on SPT correlations. To do this, simply check the corresponding boxes and press the "Update Table and Stresses" button. This study estimated shear wave velocity and relative density based on the SPT blow counts.

5. When finished, select the "Loading Info" hyperlink at top of page to advance to the next page or RETURN TO FLOW CHART.

Loading Info Page

1. Select Amplification Factor type.

- Optional: Decide whether to account for uncertainty when amplifying ground motions by checking the appropriate box.

2. Specify the type of file to upload.
3. Press the "Auto Download" button to begin uploading of files.
    a. Choose the deaggregation of interest
    b. Enter the latitude and longitude of the site of interest.
4. Select the magnitude bin size using the drop box located next to the "Generate Plots and Data" button.
5. Press "Generate Plots and Data".
6. Check that the data was uploaded correctly by reviewing the plots located at the bottom of the page.

7. To advance to the next page select the "Analysis Options" hyperlink at the top of the page (shown in blue).

NOTES:

- If values or options are changed by the user at any time, the plots and data MUST be regenerated using the "Generate Plots and Data" button.
- EZ-Frisk files and other large files take more time to analyze.

Liquefaction Analysis Options Page

Deterministic Options

1. Select deterministic data type (mean, modal, user specified).
2. Select Return Period from pop up box (or enter user defined scenario).

- Optional: Turn on Ksigma limit of 1.1 for Idriss and Boulanger calculations. (this option was selected for this study)
- Optional: Select to use Performance Based Magnitude Scaling Factors and enter required values in the associated pop up box.
- Optional: Select to use probability of 15% (after Cetin et al., 2004) (this option was selected for this study)

3. Press "Run Deterministic Analysis".

Performance Based Options

1. Select performance based analysis type.
2. Enter the number of runs to use in the analysis. Number of runs must be large enough to include at least one amax bin per set of data points on the magnitude specific hazard curves. This study used a value of 250.

- Optional: Select to use Performance Based Magnitude Scaling Factors and enter required values in the corresponding pop up box.
- Optional: Select to use Ksigma for Idriss and Boulanger calculations used by Idriss and Boulanger and Juang et al.
- Optional: Select to include or exclude parameter estimation error; for the Idriss and Boulanger analysis, advanced options are available.
- Optional: Select to include or exclude probability of liquefaction

3. Press "Run Performance Based Analysis".

Results

1. To view deterministic analysis results, select the page you wish to view. For example, the Cetin and Ishihara and Yoshimine settlement results can be viewed by selecting the "Cetin_et_al_Deterministic" and "IandB_Deterministic" pages, respectively. The Idriss and Boulanger deterministic model used the Ishihara and Yoshimine settlement procedure, which is why the results are found on the Idriss and Boulanger results page.
2. To view probabilistic analysis results, select the "Performance_Based_Summary" tab, and scroll down to the "Soil Profile Data and Details" table. Settlement estimations can be viewed for the return period listed in the header of column K. Notice that this value is red, meaning it can be modified by the user. Changing the return period in this cell will update the values shown in the table.